UNIVERSITÀ DEGLI STUDI DI PADOVA
Dipartimento di Salute della Donna e del Bambino (SDB)

CORSO DI DOTTORATO DI RICERCA IN
Medicina Dello Sviluppo E Scienze Della Programmazione Sanitaria
CURRICULUM: Emato-oncologia, Genetica, Malattie rare e Medicina predittiva
CICLO: XXIX

IN VITRO AND *IN VIVO* ANTITUMOR ACTIVITY OF NEW CHOLINE KINASE INHIBITOR: A PHARMACOLOGICAL STRATEGY FOR BREAST CANCER AND LEUKEMIA TREATMENT

Tesi redatta con il contributo finanziario della Fondazione Città della Speranza

Coordinatore: Ch.mo Prof. Carlo Giaquinto

Supervisore: Ch.mo Prof. Giuseppe Basso

Tutor: Dr. Giampietro Viola

Dottorando: ELENA MARIOTTO

TABLE OF CONTENTS

SUMMARY

Aberrant choline metabolism is a feature shared by many tumors. It is predominantly caused by elevated expression and activation of choline kinase alpha (ChoKα), which catalyzes the phosphorylation of choline to phosphocholine in the Kennedy's pathway for membrane lipids synthesis. In this PhD thesis, the most promising symmetrical ChoKα inhibitor has been identified from the novel series of choline kinase inhibitors, designed and synthesized by Prof. Lopez-Cara's group, University of Granada, Spain. The therapeutic potential of the selected lead compound was compared to previously reported symmetrical ChoKα inhibitors and evaluated in two different tumoral contexts. Furthermore, the new ChoKα inhibitor was used to investigate for the first time choline metabolism deregulation in hematological tumors.

The ChoKα inhibitor **EB-3D** (also known as compound **10a**) was selected as lead compound. The crystal structure of ChoKα1 in complex with compound **EB-3D** (PDB ID: 5FTG) reveals that the compound effectively binds to the choline-binding site and inhibits ChoKα1 with IC_{50} of 1.00 ± 0.01 μM. **EB-3D** strongly inhibits cell growth in a panel of cancer cell lines with GI_{50} ranging from 27 to 110 nM for solid tumors and from 0.9 to 479 nM for hematological tumors. **EB-3D** inhibits also the formation of phosphocholine and reduces the content of choline-containg metabolites in treated cells.

In triple-negative MDA-MB-231 breast cancer cells, **EB-3D** arrests cells in the G0/G1 phase of the cell cycle triggering irreversible cellular senescence. Moreover, **EB-3D** potentiates the antitumoral effect of cisplatin and impairs migration and invasiveness of the higly metastatic MDA-MB-231 cell line. Lastly, treatment of syngeneic orthotopic EO771-C57BL/6 mouse model with 1mg/kg of **EB-3D** i.p. resulted in strong tumour growth inhibition and reduction of metastasis formation. Altogether, these data reveal the antitumorigenic and antimetastatic potential of **EB-3D** in triple-negative breast cancer.

T acute lymphoblastic leukemia (T-ALL) cell lines exhibit increased levels of ChoKα compared to healthy lymphocytes and higher ChoKα/β ratio. **EB-3D** induces G0/G1 cell cycle arrest in T-ALL and, in contrast to breast cancer cells, induces cell death by apoptosis. The effect is rapidly triggered and cannot be rescued by compound withdrawal. **EB-3D** modulates the AMPK-mTOR pathway leading to the inactivation of final effectors required for protein synthesis and cell cycle progression. On the contrary, the effect appears attenuated in normal lymphocytes where other signaling pathways are involved.

Finally, **EB-3D** strongly synergizes with L-asparaginase lowering the GI_{50} and increasing cell death. Taken together, these data validate ChoKα as a novel attractive therapeutic target in T-ALL and justify the further development of **EB-3D** inhibitor.

PUBLICATIONS

The following publications are associated with this dissertation:

Castro-Navas, F. F., Schiaffino-Ortega, S., Carrasco-Jimenez, M. P. P., Ríos-Marco, P., Marco, C., Espinosa, A., Gallo, M. A., **Mariotto, E.**, Basso, G., Viola, G., *et al.* (2015). *New more polar symmetrical bipyridinic compounds: new strategy for the inhibition of choline kinase α1*. Future medicinal chemistry *7*, 417-436.

Schiaffino-Ortega, S.*, Baglioni, E.*, **Mariotto, E.**, Bortolozzi, R., Serrán-Aguilera, L., Ríos-Marco, P., Carrasco-Jimenez, P. M., Gallo, M. A., Hurtado-Guerrero, R., Marco, C., *et al.* (2016). *Design, synthesis, crystallization and biological evaluation of new symmetrical biscationic compounds as selective inhibitors of human Choline Kinase α1 (ChoKα1)*. Scientific Reports *6*, 23793.

Mariotto, E., Bortolozzi, R., Ronca, R., Carta, D., Serafin, V., Accordi, B., Basso, G., Lopez-Cara, L., Viola, G. *The novel choline kinase alpha inhibitor EB-3D induces cellular senescence in triple-negative breast cancer and reduces tumor growth and metastatic dissemination.*

The following publications have been contributed to during the course of this degree, but are not included in this work:

Romagnoli, R., Baraldi, P., Prencipe, F., Oliva, P., Baraldi, S., Tabrizi, M., Lopez-Cara, L., Ferla, S., Brancale, A., Hamel, E., Ronca, R., Bortolozzi, R., **Mariotto E.**, Basso, G., Viola G. (2016). *Design and Synthesis of Potent in Vitro and in Vivo Anticancer Agents Based on 1-(3',4',5'-Trimethoxyphenyl)-2-Aryl-1H-Imidazole.* Scientific Reports *6*, 26602.

Romagnoli, R., Baraldi, P., Prencipe, F., Oliva, P., Baraldi, S., Lopez-Cara, L., Brancale, A., Ferla, S., Hamel, E., Ronca, R., Bortolozzi, R., **Mariotto E.**, Porcù, E., Basso, G., Viola G. *Synthesis and Biological Evaluation of 2-Methyl-4,5-Disubstituted Oxazoles as a Novel Class of Highly Potent Antitubulin Agents.* Submitted.

Bortolozzi, R., Bresolin, S., Rampazzo, E., Paganin, M., Maule, F., **Mariotto, E.**, Boso, D., Minuzzo, S., Viola, G., Indraccolo, S., Cazzaniga, G., Basso G., Persano, L. *AKR1C enzymes sustain therapy resistance in pediatric T-ALL.* Submitted.

1. INTRODUCTION

1.1 Lipid Metabolism: a new hallmark of cancer

The reprogramming of cellular energy metabolism is required to support exacerbate cell growth and proliferation, replacing the metabolic program that operates in physiological counterpart. In fact, the "metabolic reprogramming" has been introduced as one of the new hallmarks of cancer (Hanahan and Weinberg, 2011). This is especially true for solid tumors where cancer cells are surrounded by a totally different microenvironment than that of normal cells, and tumor cells must exhibit rapidly adaptive responses to hypoxia and hypo-nutrient conditions. Metabolic reprogramming is also required for both tumor invasion and metastasis since cells must adapt to new microenvironment condition and different challenges. Also in non-solid tumors mechanism of metabolic switch have been described (Kishton et al., 2016).

Changes in lipid metabolism during tumorigenesis have long been described but the molecular mechanisms underlying these alterations are still being unraveled (Santos and Schulze, 2012). Beyond their important role in delimiting cell structure and organelles, lipids are also fundamental for cell shape and motility, membrane protein localization and generation of bioactive signaling molecules. Because the uncontrolled proliferation of cancerous cells requires sustained lipids synthesis, many oncogenes directly or indirectly regulate lipids turnover (Menendez and Lupu, 2007; Ricoult et al., 2016). However, the overexpression of lipid enzymes generally is not sufficient to drive malignant transformation. A notable exception is represented by choline kinase α (ChoKα; E.C. 2.7.1.32).

1.2 The Kennedy's Pathway

Choline kinase (ChoK) is one of the most important enzymes for the generation of two major membrane phospholipids, phosphatidylcholine (PtdCho) and sphingomyelin (SM), and subsequently for the cell division. Free choline (Cho) is transported inside cells by different classes of choline transporters (ChoT). The choline kinase catalyses the Mg^{2+}-ATP-dependent phosphorylation of choline to phosphocholine (PCho) as the first step in the CDP-choline branch of Kennedy's pathway (Kennedy, 1957) (Figure 1). As a matter of fact, ChoK could also phosphorylate ethanolamine in the parallel CDP-ethanolamine branch. The succesive PCho conversion to CDP-choline is the rate-limiting step catalyzed

by the phosphocholine cytidylyltransferase (CCT) that becomes active only when recruited to the nuclear membrane. The final step of the pathway involves the transfer of phosphocholine headgroup from CDP-choline to diacylglycerol (DAG) backbone to form PtdCho, catalyzed by choline phosphotransferase (CPT), located predominantly in endoplasmic reticulum (ER) and Golgi membranes.

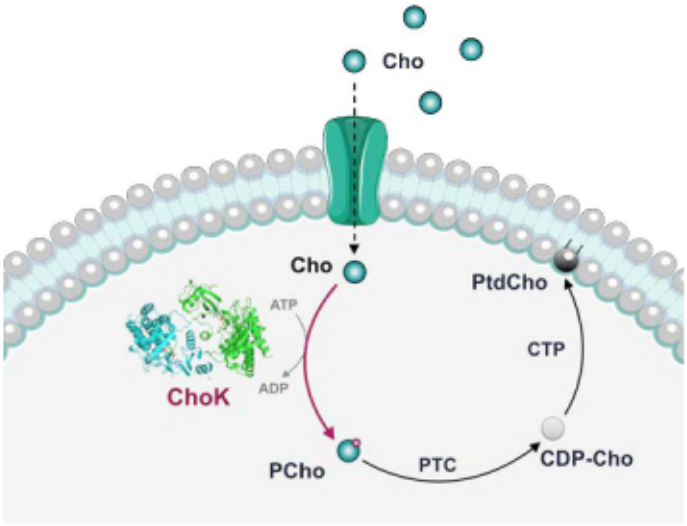

Figure 1: The Kennedy's pathway

Simplified scheme of the CDP-choline branch of Kennedy's pathway.
Cho, choline. ChoK, choline kinase. PCho, phosphocholine. PtdCho, phosphatidylcholine.

Various phospholipase enzymes can break down PtdCho: phospholipases A1 and A2 (PLA1 and PLA2) generate fatty acids and lyso-phosphatidylcholine (Lyso-PtdCho), which is further metabolized by lysophospholipase (LPL) into fatty acids and glycerophosphocholine (GPC); phospholipase C (PLC) generates PCho and DAG; and phospholipase D (PLD) generates choline and phospahtidic acid (PA). GPC can be further metabolized by glycerophosphocholine phosphodiesterase (GDPD) into choline.

1.3 Choline Kinase (ChoK)

In humans, ChoK is encoded by two different genes, *CHKA* and *CHKB*, located in chromosomes 11q13.1 and 22q13.33 respectively. Because of the high sequence similarity (~60%) it seems reasonable that the two genes arise from a process of gene duplication from a common ancestor. *CHKA* generates two isoforms by alternative splicing ChoKα1 (457 aa) and ChoKα2 (439 aa) while *CHKB* encodes ChoKβ isoform (395 aa). The functional form of the enzyme is homodimeric or heterodimeric with different activity

levels: α/α dimers have the highest activity, α/β intermediate and β/β the lowest activity. The three isoforms are ubiquitously expressed but their ratio varies widely between tissues. Each isozyme can phosphorylate both choline and the structurally similar ethanolamine, but ChoKα has higher affinity for choline whereas ChoKβ is more selective for ethanolamine substrate.

The crystal structures of human ChoKα in its apo form, ADP and phosphocholine-bound complexes reveal the molecular details of the substrate binding sites (Figure 2). ATP binds in a cleft formed by residues from both N and C-terminal lobes, while the choline-binding site constitutes a deep hydrophobic groove in the C-terminal domain with a rim composed of negatively charged residues.

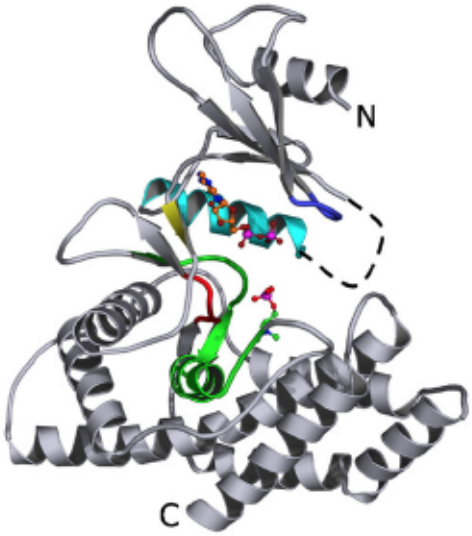

Figure 2: Crystal structures of human ChoKα monomer with PCho and ADP

Ribbon diagram of ChoKα monomer with ADP and PCho molecules concomitantly present. Key structural elements are colored: the ATP-binding loop in blue, the dimer interface α-helix in cyan, the short β-strand that links the N and C-terminal domains in yellow, the Brenner's motif in red, and the choline kinase motif in green. Ball-and-stick representation of ADP and PChol molecules are shown with their carbon atoms colored in orange and green, respectively. Oxygen, nitrogen and phosphate atoms are shown in red, blue and magenta, respectively. Adapted from Malito et al., 2006.

ChoK can be considered an atypical kinase because it works by a two-steps mechanism, without the formation of a ternary complex (Figure 3). First, ATP transfers a phosphate group directly to the enzyme at Asp306 residue and then, only the phosphorylated enzyme is able to bind the choline substrate. Choline binding causes a conformational change that favours the transfer of phosphate group from the enzyme to choline and the following release of PCho.

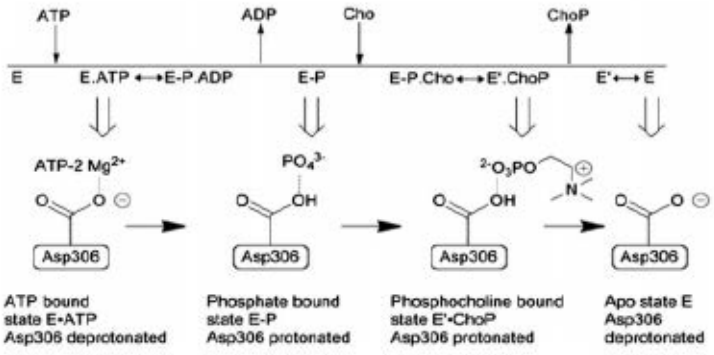

Figure 3: ChoKα phosphorylates choline via an unusual two-steps mechanism

Unprotonated Asp306 residue in the active site of human ChoKα can accept a phosphate group by a Mg^{2+} coordinated reaction resulting in protonation of the amino acid and subsequent ejection of ADP. The phosphate-primed enzyme can accept Cho, which induces a conformational shift in the enzyme resulting in PCho exit. The deprotonated ChoKα enzyme reverts to its original conformation and is again ready for ATP binding. Adapted from Arlauckas et al., 2016.

In mammalian cells, only the ChoKα isoforms play a central role in sustaining PCho biosynthesis. Knock-out experiments in mouse model revealed that only *CHKA* deletion leads to embryonic lethal phenotype indicating that ChoKβ isoform cannot compensate to ChoKα absence (Wu et al., 2008). Therefore, ChoKα is essential for cell viabily and proliferation.

Most importantly, the overexpression of ChoKα isoform alone is sufficient to drive tumorigenesis, while ChoKβ is not (Gallego-Ortega et al., 2009). To reinforce the importance of ChoKα isoform and its involvement in pathogenesis, several studies revealed that ChoKα, but not ChoKβ, protein expression in inducible by carcinogenic substances, by oncogenes overexpression or mutation and by treatment with other kinase inhibitors. In fact, both *CHKA* and *CHKB* genes are controlled by a constitutive promoter but, in *CHKA* regulatory regions the presence of inducible promoters have been described. The hepatotoxin CCl_4 increases the expression of ChoKα through the upregulation of c-jun transcription factor that binds to the activator protein 1 (AP1) consensus site located in a distal promoter of CHKA gene (Aoyama et al., 2007). The induction of c-myc proto-oncogene increases ChoKα expression (Morrish et al., 2008) and the consequent increase in PCho levels (Morrish et al., 2009). Low oxigen condition also regulates uniquely ChoKα expression due to the presence of hypoxia-inducible factor 1α (HIF-1α) binding sites in its promoter region (Bansal et al., 2011; Glunde et al., 2008).

1.4 The "Cholinic Phenotype" in tumorigenesis

Alteration in the choline metabolism, characterized by ChoKα overexpression and/or hyperactivation and the resulting increase of phosphocholine (PCho) and total choline-containing compounds (tCho) in general, is referred to as "cholinic phenotype" and it has been associate to tumorigenesis. Indeed, high levels of ChoKα were first reported for colon cancer and since then for breast, lung, prostate and ovarian tumors.

PCho metabolite levels and ChoKα activity were higher in colon cancer than in normal colon tissue (Nakagami et al., 1999). Ramírez de Molina *et al*. described increased ChoKα protein expression in lung, breast and prostate cancer compared to their normal counterparts (Ramírez de Molina et al., 2002d). Toghether with enzymatic expression, it has also been reported the augmented ChoKα activity in tumoral biopsies of patients with breast cancer and a clear correlation between ChoKα activity and histologic tumor grade (Ramírez de Molina et al., 2002a). This work highlighted for the first time that ChoKα activation could be considered as a marker of malignancy and worst prognosis in breast tumors. mRNA and protein expression of ChoKα were found upregulated in primary as well as metastatic prostate tumors with an assciation with tumor grade and poor recurrence-free survival (Asim et al., 2016) and the immunohystochemical detection of ChoKα has been proposed for diagnostic purpose (Challapalli et al., 2015). A retrospective study indicated the overexpression of ChoKα as an independent predictor factor of relapse-free survival in early-stage non-small-cell lung cancer (Ramírez de Molina et al., 2007). Abnormal choline metabolism was extensively described also in ovarian cancer with the overexpression of PCho in tumor cell lines (Iorio et al., 2005) and the overexpression and hyperactivation of ChoKα in both cell lines and patient's tumor sample (Iorio et al., 2010). Recently, a serum metabolomic profile analysis revealed dysregulation of choline metabolism in patients with T cell lymphoma along with ChoKα protein overexpression (Xiong et al., 2015).

1.5 Diagnostic and prognostic value in cancer

Tumor imaging plays a significant role in diagnosis, treatment planning, and follow-up in a variety of tumors. The search for biomarkers non-invasive cancer detection and to monitor the response to treatment has led to several clinical studies evaluating the level of choline-

containing metabolites in many tumors, including breast, ovarian, lung, colon, prostate and brain tumors.

While magnetic resonance imaging (MRI) identifies the anatomical location of a tumor, MR spectroscopy (MRS) compares the different metabolic profile between tumor tissue and normal tissue. Specifically, ^{1}H-MR spectra allow the visualization of tCho peak (consisting of the sum of Cho, PCho and GPC) that is higher in tumoral lesion compared to surrounding tissues (Figure 4). The increasing resolution obtained by ^{1}H-NMR allows to discriminate choline (Cho), phosphocholine (PC) and glycerophosphocholine (GPC) peaks from cancer cell extracts.

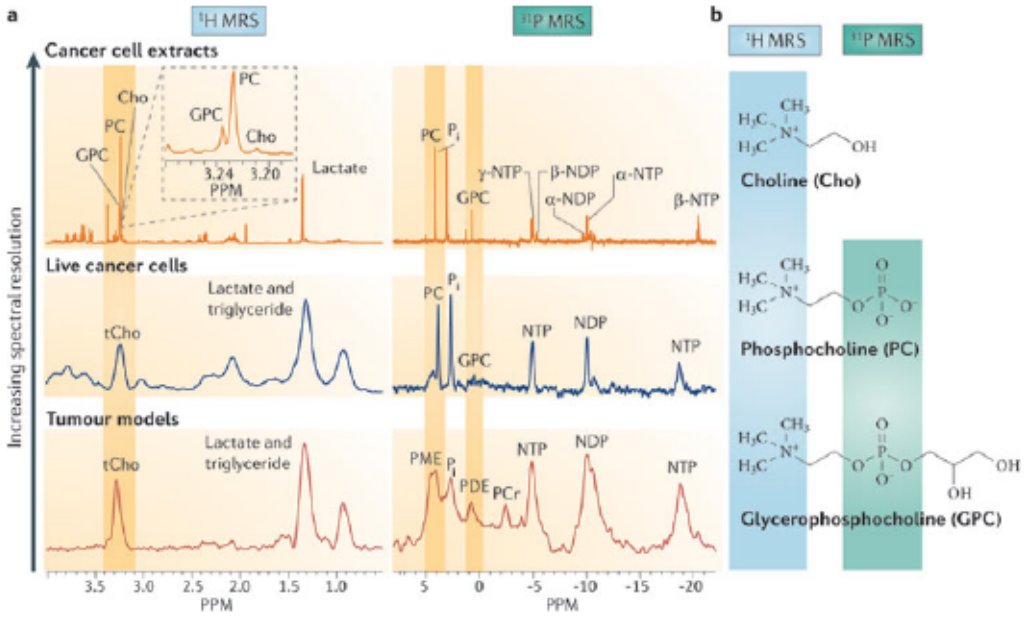

Figure 4: Metabolite analysis by ^{1}H and ^{31}P-MRS.

a) Typical MRS spectra obtained from *in vivo* tumour models and live cancer cells where total choline-containing compounds (tCho) signal in is detected as a single peak. In cancer cell extracts, the increasing resolution allows to discriminate choline (Cho), phosphocholine (PC) and glycerophosphocholine (GPC) peaks. b) Structures of the choline-containing metabolites detected by MRS analysis. Adapted from Glunde et al., 2011.

To date, MRS is considered the current clinical gold standard for some tumor (e.g. brain) however, despite providing superior structural detail, it features poor specificity in identifying residual tumors, especially after treatments (Figure 5). The introduction of positron emission tomography (PET), and its combination with computed tomography (PET/CT), that employs molecular tracers involved in cellular metabolism significantly improved patients management. [^{18}F] 2-fluoro-2-deoxy-D-glucose (^{18}F-FDG) is the most common radiotracer, unfortunately ^{18}F-FDG PET/CT presents poor specificity such as the

high glucose uptake of certain normal tissue (e.g. brain cortex), low tumor/background signal ratio, and the high accumulation also in inflammatory sites. Indeed, the recent introduction of ^{11}C-choline PET/CT imaging improved the diagnosis of some borderline cases. A comparison study between ^{18}F-FDG and ^{11}C-choline PET in different tumors revealed that the two technique are comparable in all cases except for brain tumor where choline uptake result more specific (Tian et al., 2004). Indeed ^{11}C-choline PET/CT shows higher sensitivity and specificity than ^{18}F-FDG and MRI in brain tumor diagnosis (Tan et al., 2011) and higher accuracy for differentiating radiation necrosis and tumour recurrence (Giovannini et al., 2015) but also to distinguish tumor lesion from pulmonary tuberculosis nodule (Hara et al., 2003). Collectively these studies support the relevance of choline metabolism in tumors and that ^{11}C-choline PET/CT is a compelling alternative to the widely used MRI and ^{18}F-FDG PET/CT.

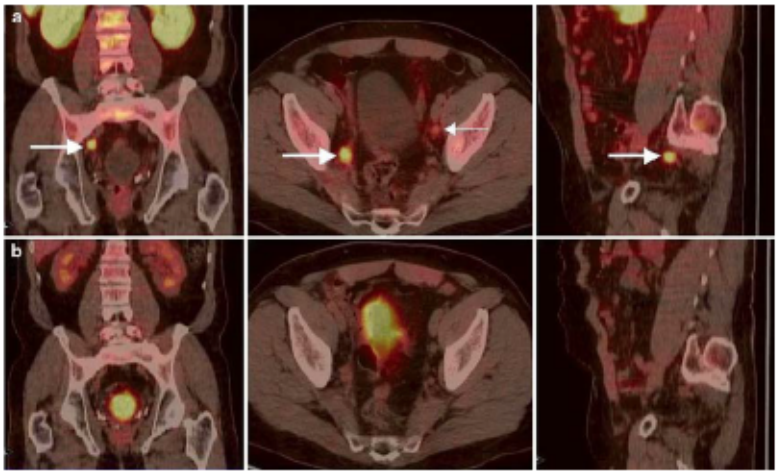

Figure 5: Comparison between ^{11}C-choline PET/CT and ^{18}F-FDG PET/CT scans

PET/CT scans of a 55-year-old patient with suspected recurrence, >2 years after radical prostatectomy. Focal ^{11}C-choline uptake (a) in right (bold arrow) and left (thin arrow) iliac region revealed lymph node involvement, not observed with ^{18}F-FDG PET (b). Coronal (left), axial (middle), and sagittal (right) fused image projections of PET/CT scans. Adapted from Richter et al., 2010.

1.6 Choline Kinase α as therapeutic target

Altogether, the studies reporting ChoKα overexpression and hyperactivation in tumors, suggest ChoKα as prognostic marker for cancer progression and as a novel therapeutic target to improve cancer treatments.

siRNA-mediated knockdown of ChoKα induces apostosis in HeLa cells, while single ChoKβ or simultaneous ChoKα/ChoKβ silencing have no effect on cell viability (Gruber et al., 2012), suggesting that the balance between α and β isoforms is important for cell

viability. This finding also emphasizes the concept that ChoKα is the only relevant isoenzyme for tumor cell survival, although no evidence suggests a differential role for ChoKα1 or ChoKα2. Indeed, downregualtion of *CHKA* by RNA interference has been demonstrated to reduce cell proliferation and tumor growth (Glunde et al., 2005; Krishnamachary et al., 2009), prevent mitotic entry (Gruber et al., 2012), induce apoptosis (Falcon et al., 2013), sensitize cancer cells to chemotherapeutics (Granata et al., 2014; Mori et al., 2007) and suppress migration and invasion (Asim et al., 2016; Granata et al., 2015).

CHKA silencing has been reported to reduce *in vitro* cell proliferation in breast cancer (Glunde et al., 2005) and ovarian cancer due to the accumulation of cells in the G1 phase of the cell cycle (Granata et al., 2014). On the contrary, ChoKα overexpression is sufficient to promote cell proliferation of quiescent human mammary epithelial cells (HMEC) promoting entry into S phase of cell cycle (Ramírez de Molina et al., 2004a). According to these data, mitotic defects were observed after *CHKA* silencing (Gruber et al., 2012), reinforcing the idea that ChoKα is required for cell cycle progression.

Some researches recently gave insight in signaling pathway modulated by ChoKα specific inhibition. ChoKα downregulation in ovarian cancer inhibits cell proliferation without affecting cell viability, as shown by the absence of changes in the phosphorylation levels of AKT, also known as protein kinase B (PKB), and the mitogen-activated protein kinase (MAPK) survival signaling pathways (Granata et al., 2014). On the other hand, several authors have reported the induction of cell death in *CHKA*-silenced HeLa (Falcon et al., 2013; Yalcin et al., 2010) and Jurkat cells (Xiong et al., 2015) along with the dephosphorylation of AKT and the extracellular signal–regulated kinases (ERK). The apoptotic effect of *CHKA* silencing has been described also for breast cancer model, where it seems to be specific for tumoral cells wherease it is not lethal for the quiescent human mammary epithelial cells (HMEC) (Bañez-Coronel et al., 2008).

Although it has been reported that mitogenic and growth factors (such as oestrogens, insulin, epidermal growth factor (EGF), platelet-derived growth factor (PDGF) as well as Ras protein family members, enhance ChoKα activity, the exact mechanisms still remain unclear. In fact, nowadays little is known about interaction with other proteins and possible phosphorylation sites on human ChoKα. The fact that EGF or insulin stimulation enhances choline uptake and PCho production has been described for quite some time ago (Uchida, 1996) but only recently, the interaction between EGF receptor (EGFR) and ChoKα through

c-Src kinase was shown. Indeed EGFR forms a complex with c-Scr, which recruits ChoKα to the cell membrane and phosphorylates the enzyme at Tyr197 and Tyr333 residues causing ChoKα activation (Miyake and Parsons, 2012). These data reveal for the first time an activating phosphorylation in human ChoKα and demonstrate a link between ChoKα and growth factor stimulation. On the other hand, members of the Ras oncogenes family are frequently mutated in human cancers, and the overexpression of either of the *RAS* genes in fibroblasts results in ChoKα activation and sensitizes cells to ChoKα inhibitors (Ramírez de Molina et al., 2001). The exact mechanism of Ras-induced ChoKα activation remains unclear but it has been proposed that Ral-GDS and PI3K contribute in ChoKα activation in the Ras-mutated background (Ramírez De Molina et al., 2002c).

1.7 Choline Kinase α Inhibitors (ChoKαIs)

In the past three decades, there has been growing interest in the "cholinic phenotype", identifying ChoKα as a new attractive therapeutic target. Despite ChoKα knock-down through RNA interference has largely contributed to our knowledge in the oncogenic role of ChoK isoforms, the use of small molecules as ChoK inhibitors remains the more feasible approach for clinical trials. Thus, the last ten years have witnessed a frantic activity in the synthesis of new ChoKα inhibitors by several research groups. The determination of the crystal structures of ChoK proteins (Malito et al., 2006; Peisach et al., 2003) and the localization of ATP and choline binding sites into the crystal structure of human ChoKα have enabled the design and the synthesis of a series of small molecules as potential ChoKα inhibitors and antiproliferative compounds.

1.7.1 Symmetric ChoKα inhibitors

The majority of ChoKα inhibitors are derived from the Hemicolinium-3 (HC-3) (Figure 6-7), the first known ChoKα inhibitor that unfortunately presented high neurotoxicity *in vivo* because its off-target inhibition of the high-affinity choline transporter interfering with the cholinergic neurotransmission (Lloveras et al., 1985).

However, the inhibitory effect of HC-3 was extremely higher toward the ChoKα isoforms compared to ChoKβ, indicating that HC-3 is a more potent and selective inhibitor for ChoKα, showing similar activity toward α1 and α2 isoforms (Hong et al., 2010).

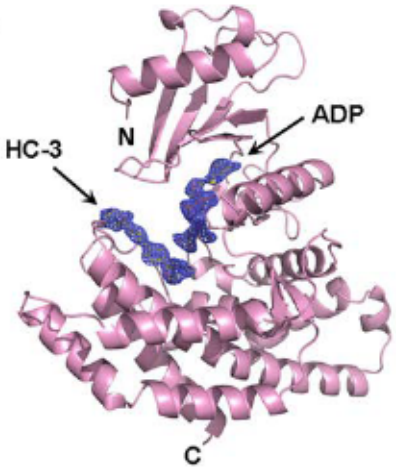

Figure 6: Crystal structures of ChoKα1 monomer with HC-3 and ADP
Adapted from Hong et al., 2010.

The HC-3-based inhibitors present a symmetric biscationic structure composed by a hydrofobical spacer (linker) whose lenght is critical for the proper distance between the two cationic heads. Quantitative structure-activity relationship (QSAR) analyses suggest that the inhibitor-binding site of ChoKα is highly specific for predominantly hydrophobic molecules carrying positively charged nitrogens. Depending on their head-groups, that always include a positively charged quaternary ammonium, symmetric inhibitors are divided in two main classes, bis-pyridinium or bis-quinolinium ChoKα inhibitors.

The most promising bis-pyridinium compounds is **MN58b** (Figure 7) designed by Prof. Lacal's group, with a strong improvement in ChoKα inhibition compared to its ancestor HC-3. The compound resulted effective *in vitro* against multiple cancer cell lines being highly selective in tumoral cells killing through the induction of cytotoxic ceramides and endoplasmic reticulum (ER) stress (Al-Saffar et al., 2006; Rodríguez-González et al., 2004; Rodríguez-González et al., 2003). **MN58b** also reduced *in vivo* tumor growth (Hernández-Alcoceba et al., 1999).

QSAR studies of bis-pyridinium ChoKα inhibitors and the analysis of their interaction with the active site, led to the substitution of the pyridine moiety with a quinolinium group, increasing compound hydrophobicity. In this category, **RSM-932A** (named also **TCD-717**, Figure 7) resulted the most important candidate, with further improvement of ChoKα inhibition and greater antiproliferative activity *in vitro* (Sanchez-Lopez et al., 2013). This compound presented also good *in vivo* antitumoral activity (Lacal and Campos, 2014) and notably it has recently completed Phase I clinical trial for solid tumor treatment

(NTC01215864) but preclinical data are undisclosed. As described for **MN58b**, also **RSM-932A** induces ER stress response along with the activation of the transcription factors CCAAT-enhancer-binding protein (C/EBP) and its homologous protein (CHOP), causing a pronounced apoptotic response restricted to cancer cells and not observed in normal counterparts (Sanchez-Lopez et al., 2013).

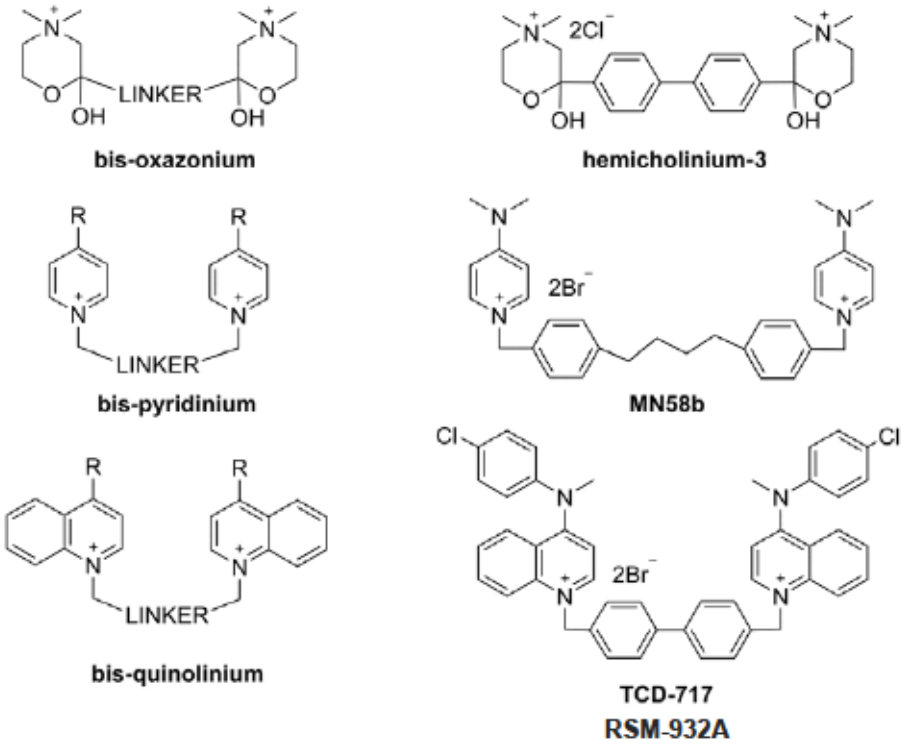

Figure 7: Symmetric ChoKα inhibitors

General structure of each symmetric inhibitor class (left column) and their most representative compound (right column). Adapted from Arlauckas *et al*., 2016.

1.7.2 Non-symmetric ChoKα inhibitors

Generations of half-inhibitor fragment were right after tested to understand if the symmetry was a necessary feature for ChoKα inhibition, but the first results were disappointing, with lower inhibitory property and higher toxicity. These data, togheter with the crystal structure of inhibitors docked at the ChoKα active site, discredited the hypothesis that each cationic head of symmetric compounds interacts with the active site of one of the two monomers (Lacal, 2001). In fact, it is now clear that the two choline-binding sites are too far for the symmetric inhibitors to span between the ChoKα dimers (Hong et al., 2010). What remained to be elucidated is the possibility that the un-bound head interacts with the

ATP-binding site. Pursuing this conjecture, researchers lately attempted to design dual inhibitors composed by one choline-like group while the other mimics the ATP structure (Schiaffino-Ortega et al., 2013; Trousil et al., 2013). The results unfortunately suggested that the asymmetrical conformation of inhibitors potentially interferes with the interaction between the second molecule of inhibitor and the coupled monomer (Sahún-Roncero et al., 2013).

Recently, based on the crystal structure of ChoKα, Clem *et al.* conducted an *in silico* screening of small molecules identifying **CK37** (Figure 8) as new potential ChoKα inhibitor. Despite the novelty of lacking the quaternary ammonium that certainly improve compound hydrophobicity, **CK37** resulted in lower affinity for ChoKα compared to the symmetrical inhibitor while displaying antiproliferative activity both *in vitro* (Clem et al., 2011) and *in vivo* (Xiong et al., 2015).

Finally, compound **V-11-0711** (Figure 8) is the only ATP competitive ChoKα inhibitor developed to date by a structure-directed optimisation approach (Falcon et al., 2013). The compound resulted a potent ChoKα inhibitor causing a strong dose-dependent reduction of PCho levels. **V-11-0711** shows good antiproliferative activity but failed to induce cell death in MDA-MB-231 triple-negative breast cancer cell line (Mori et al., 2015).

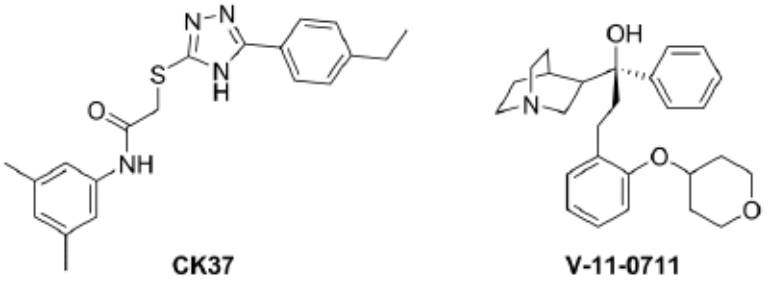

CK37 **V-11-0711**

Figure 8: Non-symmetric ChoKα inhibitors

Structure of the two most relevant asymmetric ChoKα inhibitors. Adapted from Arlauckas *et al.*, 2016.

2. AIM OF THE STUDY

Given the extensively characterised deregulation of choline metabolism in cancers, the main goal of this project is to identify a novel choline kinase α inhibitor, developed by the group of Prof. Lopez-Cara (University of Granada, Spain) for cancer treatment.

The following milestones were set:

1. Preliminar biological evaluation of a novel series of symmetrical ChoKα inhibitors in a panel of different tumor cell lines, in order to identify one lead compound for further studies.

2. Comprehensive *in vitro* and *in vivo* pharmacological evaluation of the most promising compound **EB-3D** (named also **10a**, Figure 9) in triple-negative breast cancer (TNBC) model, including data on antiproliferative, antitumour and antimetastatic effects.

3. Elucidation of the mechanisms leading to cell proliferation arrest induced by **EB-3D**.

4. To investigate for the first time the choline metabolism in pediatric T cell acute lymphoblastic leukemia (T-ALL) and the possibility to use ChoKα inhibitor **EB-3D** to reduce lymphoblasts viability.

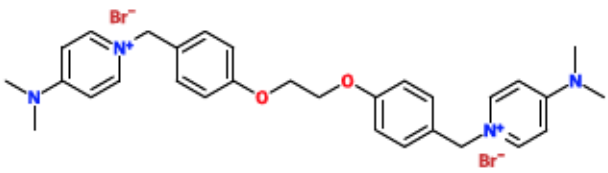

Figure 9: EB-3D structure

Structure of **EB-3D (10a)**, the most promising compound selected from the new series of symmetrical biscationic ChoKα inhibitors synthesized by Prof. Lopez-Cara's group.

3. RESULTS

3.1 Design, synthesis, crystallization and biological evaluation of new symmetrical biscationic compounds as selective inhibitors of human Choline Kinase α1 (ChoKα1)

Santiago Schiaffino-Ortega*, Eleonora Baglioni*, **Elena Mariotto**, Roberta Bortolozzi, Lucía Serrán-Aguilera, Pablo Ríos-Marco, M. Paz Carrasco-Jimenez, Miguel A. Gallo, Ramon Hurtado-Guerrero, Carmen Marco, Giuseppe Basso, Giampietro Viola, Antonio Entrena, Luisa Carlota López-Cara

* *Equal contributing authors*

Scientific reports. 2016, 6: p. 23793. DOI: 10.1038/srep23793, PMID: 27029499

3.1.1 ABSTRACT

A novel family of compounds derivative of 1,1'-(((ethane-1,2-diylbis(oxy))bis(4,1-phenylene))bis(methylene))-bispyridinium or –bisquinolinium bromide (**10a-l**) containing a pair of oxygen atoms in the spacer of the linker between the biscationic moieties, were synthesized and evaluated as inhibitors of choline kinase against a panel of cancer-cell lines. The most promising compounds in this series were 1,1'-(((ethane-1,2-diylbis (oxy))bis(4,1-phenylene))bis(methylene))bis(4-(dimethylamino)pyridinium)bromide (**10a**) and 1,1'-(((ethane-1,2-diylbis(oxy))bis(4,1-phenylene))bis(methylene))- bis(7-chloro-4-(pyrrolidin-1-yl)quinolinium) bromide (**10l**), which inhibit human choline kinase (ChoKα1) with IC_{50} of 1.0 and 0.92 μM, respectively, in a range similar to that of the previously reported biscationic compounds **MN58b** and **RSM932A**. Our compounds show greater antiproliferative activities than do the reference compounds, with unprecedented values of GI_{50} in the nanomolar range for several of the cancer-cell lines assayed, and more importantly they present low toxicity in non-tumoral cell lines, suggesting a cancer-cell-selective antiproliferative activity. Docking studies predict that the compounds interact with the choline-binding site in agreement with the binding mode of most previously reported biscationic compounds. Moreover, the crystal structure of ChoKα1 with compound **10a** reveals that this compound binds to the choline-binding site and mimics **HC-3** binding mode as never before.

3.1.2 INTRODUCTION

Cancer is a worldwide health threat and the second leading cause of mortality in developed countries (Adjei and Rowinsky, 2003; Neidle and Thurston, 2005). Since many of the current treatments still prove toxic and/or lead to drug resistance, there is a strong demand for the discovery and development of effective new cancer therapies (Kamb et al., 2007).

Protein kinases have emerged as one of the most important types of targets in cancer- drug discovery due to their major roles in regulating cell growth and survival and many other cell functions (Brognard and Hunter, 2011; Reimand et al., 2013). An abnormal kinase signaling network underlies the development and progression of tumors, and thus the targeted inhibition of protein kinases has become an attractive strategy in cancer treatment (for a recent review see Gross et al. (Gross et al., 2015)) and in the last decade the intense development in the field has led to different kinase inhibitors that have been approved for use in clinical therapy.

Choline kinase (ChoK) (EC 2.7.1.32) catalyzes the phosphorylation of choline by ATP in the presence of Mg^{2+} to yield phosphocholine (PCho) and ADP (Aoyama et al., 2004; Ishidate, 1997). This step introduces choline to the so-called Kennedy or CDP-choline pathway for the biosynthesis of phosphatidylcholine, which represents the most abundant class of phospholipids in eukaryotic cells, constituting 40–60% of the phospholipids content in cell membranes (Kent, 1990). In addition to forming the major structural component of the membrane bilayer, phosphatidylcholine also serves as a precursor for the production of lipid second messengers (Exton, 2000).

Mammalian ChoK exists as three isoforms, encoded by two separate genes (Aoyama et al., 1998a; Aoyama et al., 1998b). In humans, ChoKα1 (457 amino acids) and ChoKα2 (439 amino acids) derive from a single gene (*CHKA*) by alternative splicing, while ChoKβ (395 amino acids) is the product of a different gene (*CHKB*). The amino acid sequence identity is 56% between ChoKα and ChoKβ, and both *CHKB* and *CHKB* mRNAs, as well as their encoded protein 3 isoforms, are ubiquitously expressed in diverse tissues (Aoyama et al., 2002). Each isoform is present as either dimers (homo- or hetero-) or as tetramers in solution and is not active in monomeric form (Ishidate, 1997), suggesting that, for higher eukaryotes, dimeric ChoK is the minimum functional form.

Choline kinase is overexpressed in many tumors such as breast, lung, bladder, colon, prostate, ovary, and liver carcinomas (Granata et al., 2014; Hernández-Alcoceba et al., 1999; Ramírez de Molina et al., 2002d) and recently elevated enzymatic activity has also

been shown in T-lymphoma (Xiong et al., 2015). This increasing expression leads to abnormal choline metabolism, resulting in higher phosphocholine levels, which refer to a cholinic phenotype associated with oncogenesis and tumor progression (Glunde et al., 2011). As a result, ChoKα, has become an attractive target for novel anticancer therapies.

The determination of the crystal structures of ChoK proteins from Caenorhabditis elegans and human, in which two monomers were dimerized in each asymmetric unit (Malito et al., 2006; Peisach et al., 2003) and the correct identification of ATP and choline binding sites into crystal structure of human ChoKα2 isoform, have enabled the design and the synthesis of a series of asymmetrical molecules as potential ChoK inhibitors and antiproliferative compounds (Rubio-Ruíz et al., 2012; Schiaffino-Ortega et al., 2013). Figure 1 shows **HC-3**, the first inhibitor of choline kinase described, **MN58b** and **RSM923A**, which belong to the first generation of ChoK inhibitors (Al-Saffar et al., 2006; Hernández-Alcoceba et al., 1999; Lloveras et al., 1985; Ramírez de Molina et al., 2004a; Ramírez de Molina et al., 2004b; Rodríguez-González et al., 2003), and the most promising compounds developed by our group. Note that **RSM932A** (also called **TCD-717**) has evidenced a low-toxicity profile with improved tolerability in mice (Lacal and Campos, 2014) and a Phase I clinical trial has just been completed for the treatment of advanced solid tumors (http://clinicaltrials.gov/ct2/show/NCT01215864).

For compounds **1** and **2**, we identified the adenine and 1-benzyl-4-(dimethylamino)pyridinium as the most efficient fragments of these molecules by the deconvolution approach based on the ChoKα1/**1** (PDB ID: 3ZM9) (Sahún-Roncero et al., 2013) and ChoKα1/**2** (PDB ID: 4BR3) (Sahún-Roncero et al., 2013) crystal structures, demonstrating that the adenine fragment occupies the ATP binding site and that the pyridinium fragment, through its positive charge delocalized over the nitrogen atom, mimics the positive charge present in choline or in **HC-3**.

The second generation of inhibitors (compounds **3** and **4**), asymmetrical bispyridinium compounds, proved to be good inhibitors and provide the discovery of a new inhibitory binding site on ChoKα1 Compound **4** (Figure 10), which induced the opening of new adjacent binding site where the 4-Chloro-N-methylaniline fragment is located, adopting an unprecedented modality of binding to ChoKα1 (ChoKα1/**4** PDB ID: 4CG8) (Rubio-Ruiz et al., 2014), while compound **3** (with biphenyl group as a linker) adopts a binding mode similar to the one observed for compound **2**.

In an effort to produce additional highly active compounds, we focused on longer spacers between biphenilic or bipyridinic rings, which have electron donor or acceptor groups

necessary to increase the binding to the enzyme through of hydrogen bonds and the solubility, while retaining some inhibition properties.

Deep modeling and virtual screening studies (Serrán-Aguilera et al., 2015) have suggested the interaction with the choline binding site in the ChoKα1/**4** complex while keeping the biscationic structure unchanged. Thus a classical bioisosteric exchange between carbon and oxygen atoms could increase, on one hand, the polarity and the solubility of these compounds and, on the other hand, the affinity for the enzyme due to the synclinal conformation of the linker of these molecules. In this way, in the present study, we reconfigured the substitution pattern around linker moiety by the preparation of 1,1'-(((ethane-1,2-diylbis(oxy))bis(4,1-phenylene))bis(methylene))-bis[4-pyridinium or quinolinium] bromide derivatives with general structures **10a-l**. **MN58b**, **RSM932A**, **1**, **2**, **3**, **4**, our recently published compound **5** (Castro-Navas et al., 2015) (Figure 10) and the most active compounds described by S. Trousil (Trousil et al., 2013), were taken as patterns to improve the polarity and solubility, while also improving inhibition by the enzyme and consequently enhancing the antiproliferative effect. This series was obtained by interchanging the substitution pattern of linker by the introduction of two oxygen atoms in the linker, in order to determine the influence of these groups on the antiproliferative and inhibitory activity of ChoKα1, using various cationic heads previously synthesized by our group in similar compounds. We fixed the most successful cationic heads described previously (pyridinium and quinolinium salts) (Campos et al., 2002; Castro-Navas et al., 2015; Conejo-García et al., 2003b; Gomez-Perez et al., 2012; Rubio-Ruiz et al., 2014; Sánchez-Martín et al., 2005; Trousil et al., 2013) and examined several 4-substitutions with alkylamines or phenylamines on the arylmoiety. Also, we introduced a quinuclidinium salt, which mimics the trimethylammonium of the choline, but potentially prevents interactions with the cholinergic system.

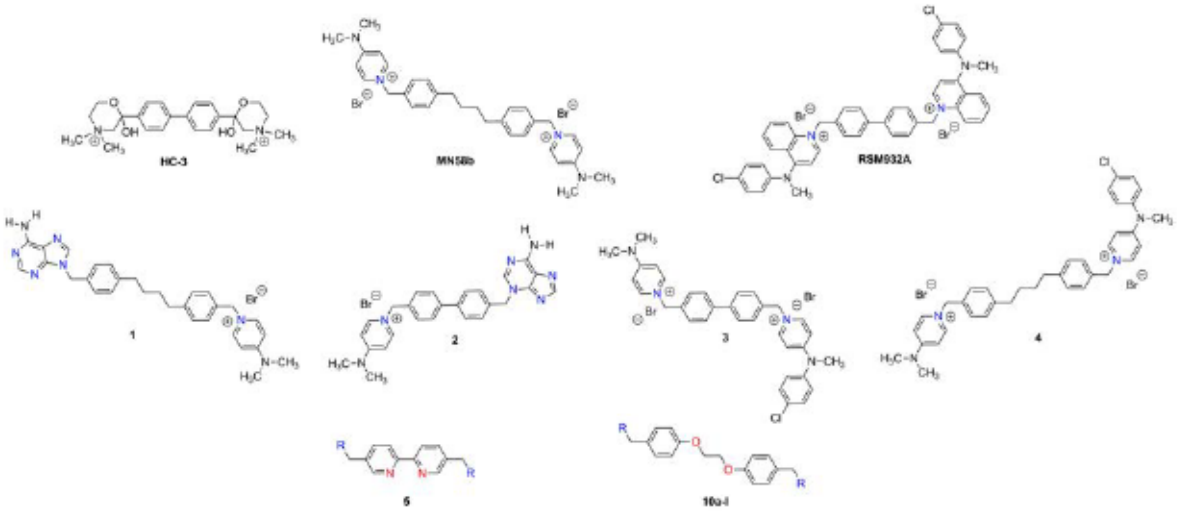

Figure 10. Structure of choline kinase α inhibitors

Structures of symmetrical and non- symmetrical inhibitors of choline kinase previously published (**HC-3**, **MN58b**, **RSM-932A** and compounds **1–5**) and the general structure of compounds **10a-l** described in this paper.

3.1.3 RESULTS

Chemistry

Microwave-assisted (MW) reactions present several advantages, such as a remarkable reduction in reaction times compared to those of the conventionally heated reactions and often lead to improved yields (Kappe, 2004). In the present work, we describe the use of microwave irradiation as an energy source for the synthesis of the intermediate (**7** and **8**) of twelve 1,2-bis(p-methylphenoxy)ethane derivatives **10a-l**, substituted in the methylphenoxy group with different cationic heads as moieties. These compounds can be also considered as more polar analogues of choline kinase inhibitor derivatives than those previously synthesized.

The synthesis of compounds **10a-l** is shown in Figure 11, and follows three easy steps. The first is the treatment of the 4-methylphenol (**6**) in ethanol with NaOH (1.1 equiv) stirring at room temperature for 30 min, followed by the addition of 1,2-dibromoethane (0.5 equiv), under microwave irradiation (130°C, 28 min) to provide the 1,2-bis(p-methylphenoy)ethane (**7**) (Cantrill et al., 2000; Xiao et al., 2007). Then, bromination in the methylene of **7** with NBS and dibenzoylperoxide in CCl_4 also under microwave irradiation (120°C, 21 min), to give the 1,2-bis(4-bromomethylphenoy)ethane (**8**) (Cabezon et al., 2000). In comparison with conventional (thermal) heating, the microwave heating reduced the reaction time in both reactions (30 min vs. 8 h and 21 min vs. 5 h, respectively), but we also noted some yield improvement (35% vs. 21% and 65% vs. 39%, respectively). We conducted different experiments to achieve these successful results with MW. Although in the second step, we were restricted by the quantity to use, since using only 100 mg of derivative **7** gave the best yields, while more quantity of **7** led to diminished yields. This result was due to the volume of the reactor, which allows only 5 mL of the mixture, while more than 100 mg of **7** derivative would need more solvent to dissolve it. Finally, the last step is the introduction of cationic heads (previously synthesized using the procedure reported (Campos et al., 2002; Castro-Navas et al., 2015; Conejo-García et al., 2003b; Gomez-Perez et al., 2012; Rubio-Ruiz et al., 2014; Sánchez-Martín et al., 2005; Trousil et al., 2013), by means of a simple S_N2 reaction in acetonitrile under argon atmosphere for 72 h at reflux of 1,2-bis(4-bromomethylphenoxy)ethane (**8**) and the 4-substituted pyridine derivative (**9a-c**), quinuclidine derivative (**9d-e**) or 4-substituted quinoline or 7-Chloro-4-substituted quinoline (**9f-l**) to afford **10a-l** (Figure 11 and Table 1) with moderate or good

yields.

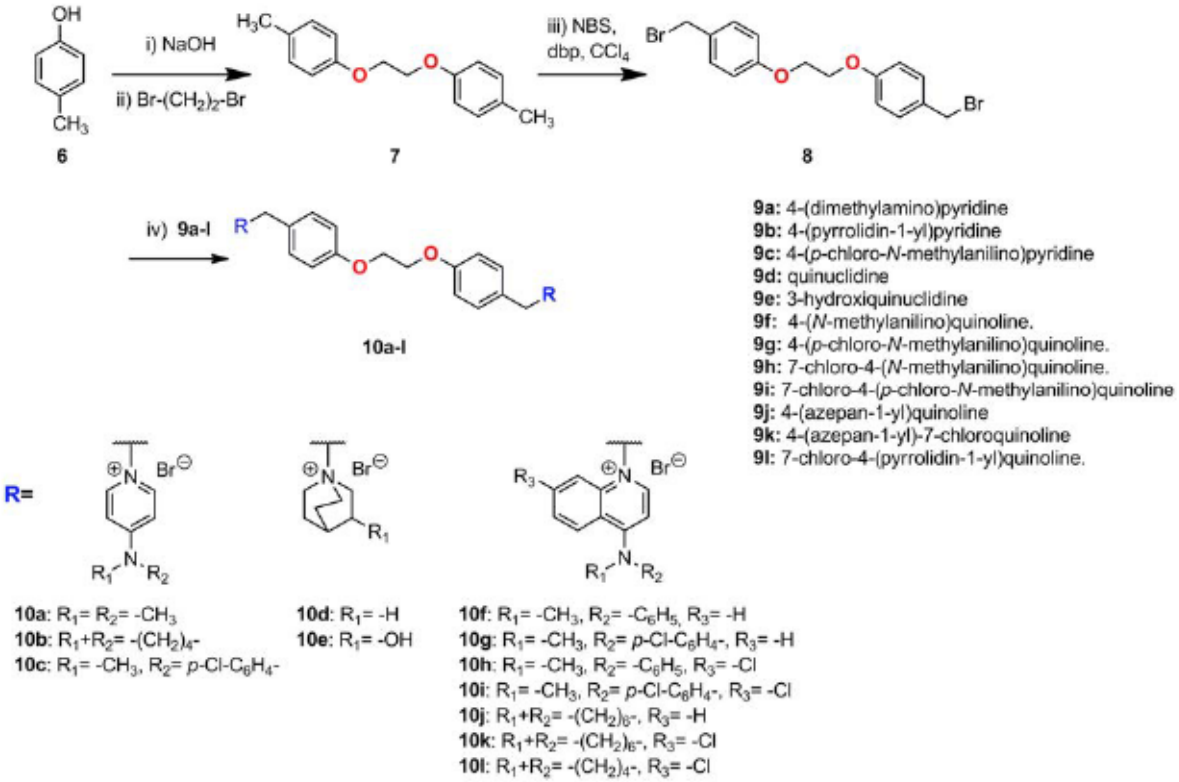

Figure 11: General synthetic pathway followed in the preparation of compounds 10a-l

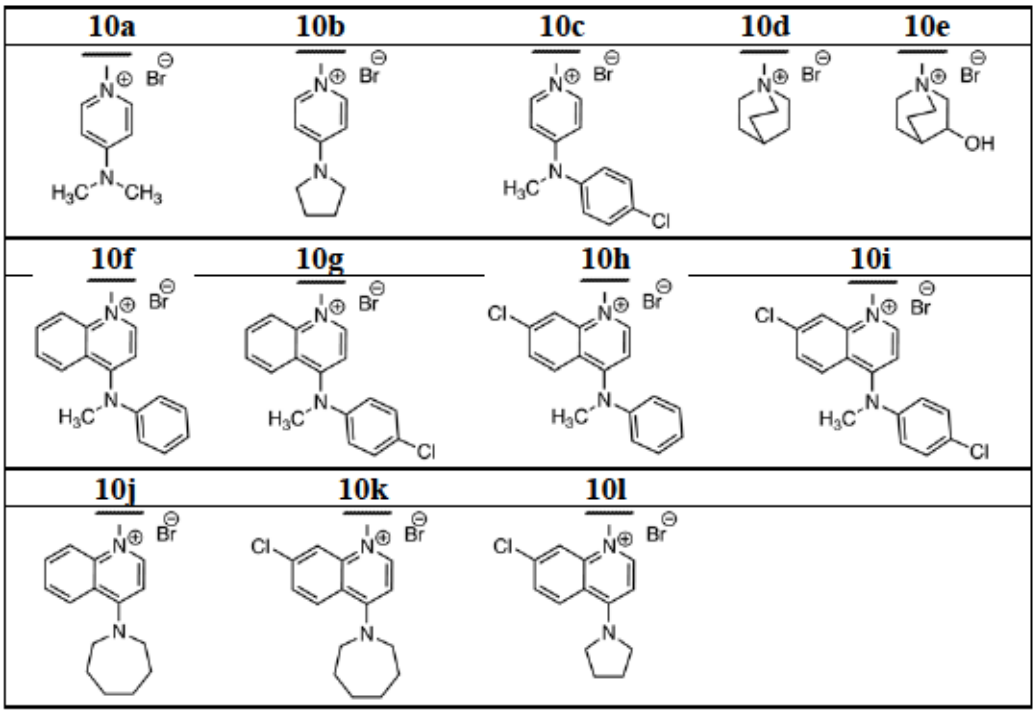

Table 1: Cationic head residues (R) of compounds 10a-l

Docking studies

Docking studies were made in order to design the new ChoK inhibitors. The crystal structures of greatest interest for docking studies are those of ChoKα1 isoenzyme in complex with compounds **2** (PDB ID: 4BR3) (Sahún-Roncero et al., 2013) and **4** (PDB ID: 4CG8) (Rubio-Ruiz et al., 2014), since the cationic heads of compounds described in this paper are similar to those of compounds **2** and **4**.

Figure 12A shows compound **2** (carbon atoms in yellow color) inserted into the Cho binding site, being stabilized by cation-π interactions with Tyr333, Tyr354, Tyr440, Trp420, Trp423, and Phe435 (carbon atoms in cyan color). In particular, the biphenyl group shows optimal parallel hydrophobic stacking interactions with Tyr354, and the 4-(dimethylamino)pyridinium moiety interacts through parallel cation-π interaction with Trp420. The orientation of this compound inside the Cho binding site was accommodated by a conformational change of Tyr333, which moved back to create an extra space (Sahún-Roncero et al., 2013; Sahún-Roncero et al., 2013). The adenine fragment of compound **2** inserted into the Cho binding site was outside the enzyme and showed no interaction with the protein, 1-(biphenyl-4-ylmethyl)-4-(dimethylamino)pyridinium being the key fragment of this compound for the interaction at the Cho binding site. Figure 13A shows compound **4** (carbon atoms in orange color) inserted into the ChoKα1 crystal structure. This compound adopts a new different binding mode, inducing a conformational change in some amino acids. Tyr256, Tyr333, and Trp420 are the residues that undergo the major changes, and the rotation of these side chains is critical to allow the insertion of the 4-chloro-N-methylaniline fragment into an additional binding site (carbon atoms in magenta color), being stabilized by hydrophobic interactions with Trp248, Tyr256, Tyr333, Leu419, Trp420, and Trp423. The rest of the molecule is located inside the Cho binding site (carbon atoms in cyan color), the pyridinium moieties being stabilized through cation-π interactions with Tyr333, Tyr354, Trp420, and Tyr440 (Rubio-Ruiz et al., 2014). Compound **4** is more inserted into the Cho binding site in comparison to compound **2** since this compound makes the complete opening of this site.

Docking studies have been performed in both crystal structures and the analysis of the resulting poses indicates which compounds could be similar to compound **2** or to compound **4**. In fact, compounds **10a**, **10b**, **10d**, and **10e** have shown good poses in the crystal structure of compound **2** (Figure 12), while the correct poses of compounds **10c**,

10f, **10g**, **10h**, **10i**, **10j**, **10k**, and **10l** resulted in the crystal structure of compound **4** (Figure 13).

Figure 12 shows the resulting pose of compounds **10a**, **10b**, **10d**, and **10e**. Compound **10a** (carbon atoms in green color) has two 4-(dimethylamino)pyridinium cationic heads, similarly to compound **2** (Figure 12B). One 1-benzyl-4-(dimethylamino)pyridinium fragment is inserted in a way very similar to that of compound **2**: i) the cationic head is situated close to Trp420, being stabilized by π-cation interactions with Trp420, Tyr333, and Trp423; and: ii) the benzyl fragment is also optimized by hydrophobic stacking interactions with Tyr354. The linker of compound **10a** is extremely long, and the second 1-benzyl-4- (dimethylamino)pyridinium fragment is situated outside of the enzyme, an additional hydrophobic interaction occurring between the second phenyl fragment and Ile433. The pose of compound **10b** is very similar to that of compound **10a**, the pyridinium moiety being slightly more separated from Tyr333 due to the higher volume of the pyrrolidine fragment, but the interaction of the whole molecule with the Cho binding site is very similar to that of compound **10a**. Compound **10d** shows also a similar pose to that of compound **10a**, though slightly more inserted into the Cho binding site due to the smaller volume of the quinuclidine cationic head. The resulting pose of compound **10e** is also similar, being slightly outside compound **10a** due to the establishment of two H-bond between the 3-OH groups and Asn305 and Glu434, respectively.

Figure 13 shows the resulting pose of compounds **10c** and **10f-l**. Compound **10l** (carbon atoms in orange color) has two 7-chloro-4-(pyrrolidin-1-yl)quinolinium) cationic heads, one of which is inserted very similarly to compound **4** (Figure 13I): the 4-pyrrolidin fragment is inserted into the additional binding site and stabilized by hydrophobic interactions, while the 7-chloroquinolinium moiety is situated into the Cho binding site and stabilized by cation-π interactions. The second cationic head is also inserted into the protein and stabilized by hydrophobic interactions with Ile433 and Arg117, and the phenyl group connected to this cationic head is also stabilized by cation-π interaction with Phe435. The most notable effect in these molecules is the conformation of the linker, since the 1,2-dioxoethane fragment adopts a synclinal conformation due to the gauche effect of the O-C-C-O bonds. This conformation of the linker allows the total insertion of compound **10l** inside the Cho binding site, and also favors the insertion of compound **10a**.

Compounds **10f-k** have shown a pose very similar to that of compound **10l** (Figure 13D), one of the cationic heads being inserted inside the additional binding site and into the Cho

binding site. The second cationic head is also inserted into the protein being stabilized by hydrophobic interactions with Arg117 and Ile433, and the phenyl group of this cationic head is also stabilized by π-cation interaction with Phe435. The resulting pose of compound **10c** shows a slight difference. This compound has two 4-((4-chlorophenyl)(methyl)amino)pyridinium cationic heads. One cationic head is also inserted into the additional binding site and into the choline binding site, as in compound 4, and the second cationic head is also inserted into the enzyme, but with a different orientation. Nevertheless, the most noteworthy effect is that in the resulting pose of these compounds the 1,2-dioxoethane fragment also adopted a synclinal conformation and, for this reason, all these compounds should be completely inserted into the enzyme and probably will show good ChoKα1 inhibition.

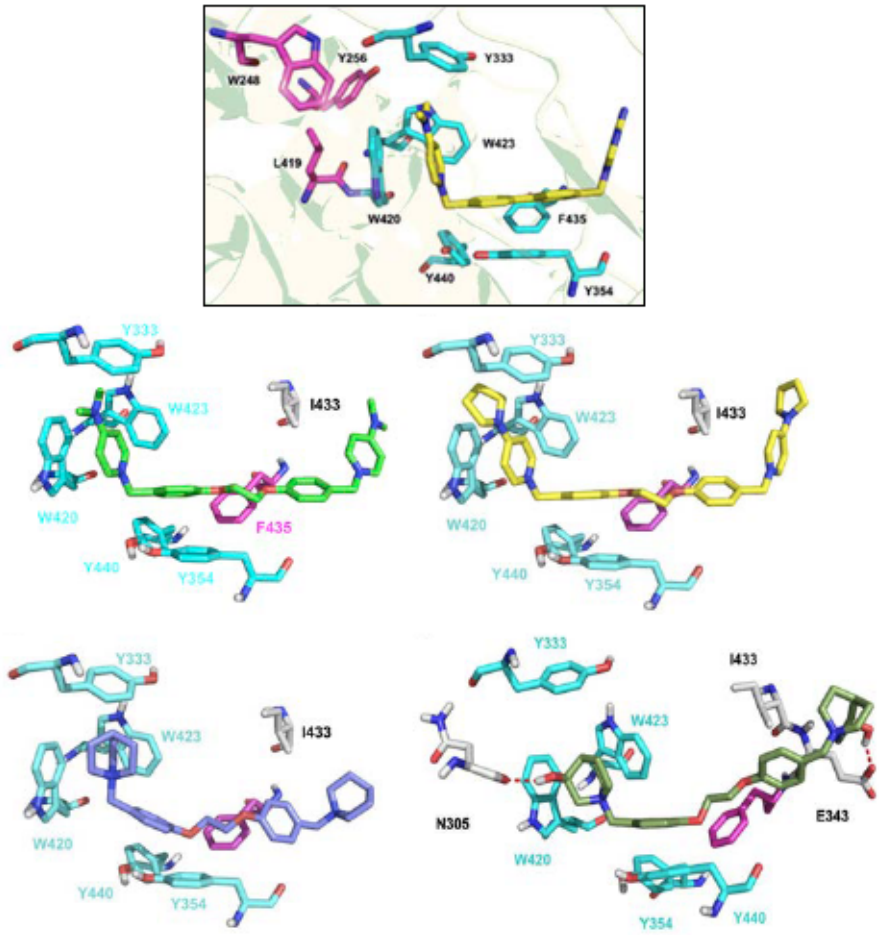

Figure 12: Resulting pose of compounds 10a-b and 10d-e in the crystal structure of ChoKα1/2 complex

(**A**) Crystal structure of ChoKα1/**2** complex (PDB ID: 4BR3). Compound **2** (carbon atoms in yellow color) is inserted into the Cho binding site (carbon atoms in cyan color). Resulting pose of compound **10a** (**B**, carbon atoms in light green color), **10b** (**C**, carbon atoms in yellow color), **10d** (**D**, carbon atoms in purple color) and **10e** (**E**, carbon atoms in green color) inside the Cho binding site of ChoKα1/**2** complex.

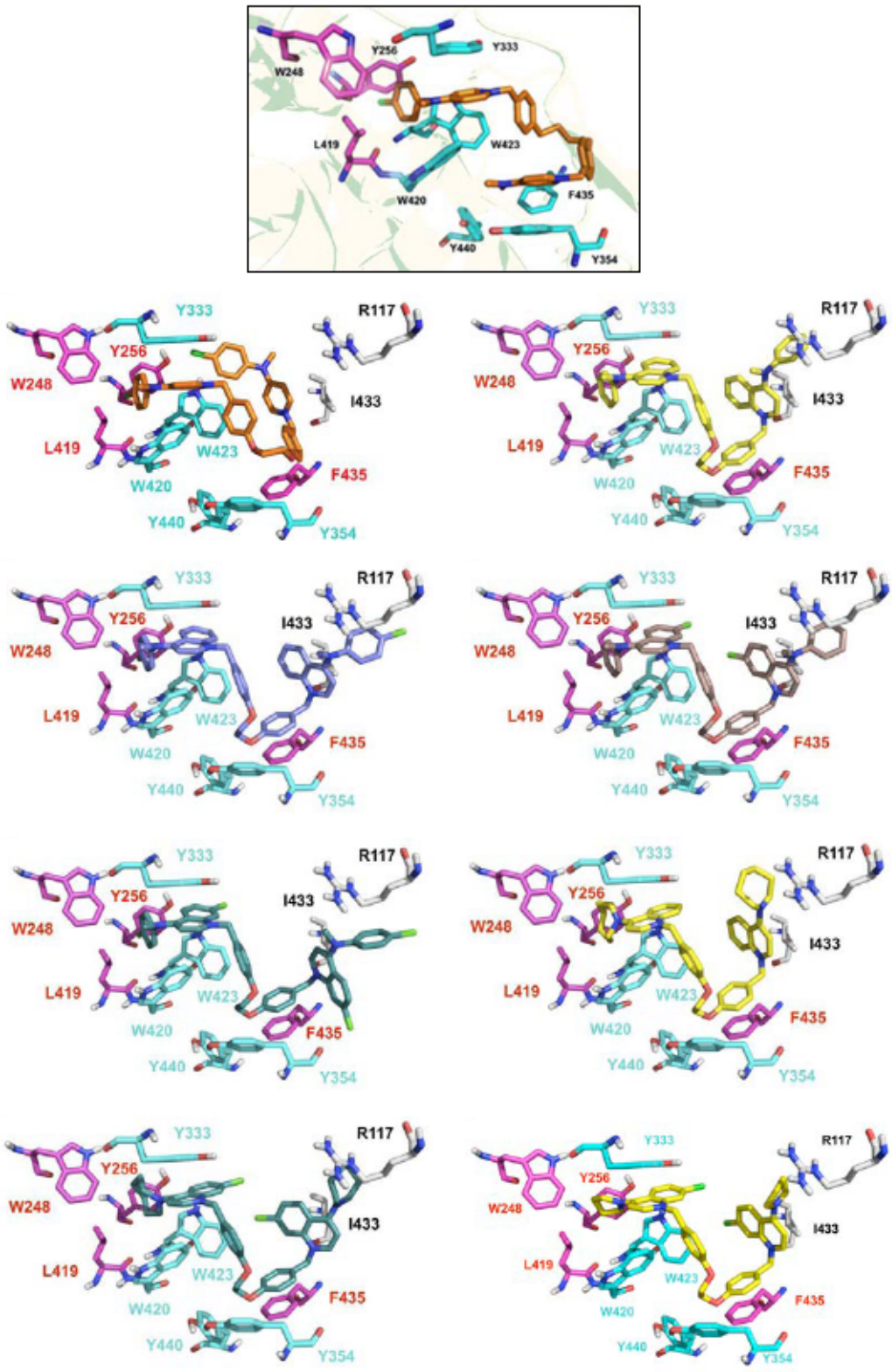

Figure 13: Resulting pose of compounds 10c and 10f-l in the crystal structure of ChoKα1/4 complex

(**A**) Crystal structure of ChoKα1/4 complex (PDB ID: 4CG8). Compound **4** (carbon atoms in orange color) is inserted into the Cho binding site (carbon atoms in cyan color) and in an additional binding site (carbon atoms in magenta color). Resulting pose of compound **10c** (**B**, carbon atoms in orange color), **10f** (**C**, carbon atoms in yellow color), **10g** (**D**, carbon atoms in purple color), **10h** (**E**, carbon atoms in brown color), **10i** (**F**, carbon atoms in dark green color), **10j** (**G**, carbon atoms in yellow color), **10k** (**H**, carbon atoms in dark green color) and **10l** (**I**, carbon atoms in yellow color) inside the Cho binding site of ChoKα1/4 complex.

Inhibition of ChoKα1 enzymatic activity

It has been reported that a potent anticancer effect inducing maximal apoptosis is achieved only when ChoKα1 expression is specifically knocked down, without affecting ChoKβ levels (Gruber et al., 2012). Thus, in an initial step we evaluated whether these compounds have a selective behaviour on ChoKα1.

We selected the most representative compounds of each family, (**10a** for pyridinium compounds and **10f**, **10g**, **10k**, and **10l** for quinolinium compounds) and, since selectivity may be explained by a reduced flexibility of Trp353 in ChoKβ compared to its homologue Trp420 in ChoKα1, as proposed for **HC-3** (Sahún-Roncero et al., 2013), tryptophan fluorescence assays were performed. As expected from their chemical structures similar to that of compound **4**, the results of the spectroscopy analysis, depicted in Table 2, showed that the Kd values of these compounds for ChoKα1 were in the low μM range (0.241-0.700 μM), indicating high affinity for the enzyme. These results agree with the first experimental validation of the docking studies described above.

Compound	HsChoKα1 Kd (μM)[a]
10a	0.700 ± 0.080
10f	0.295 ± 0.127
10g	0.517 ± 0.099
10k	0.241 ± 0.03
10l	0.357 ± 0.039
4	0.110 ± 0.01
HC-3	0.18 ± 0.03

Table 2: Kd values of selected compounds evaluated by tryptophan fluorescence quenching

[a]Kd values of indicated compounds for ChoKα1 are expressed as mean ± SD of at least three independent experiments.

Of all tested compounds, the ones that present an alkylamine or a cycloalkylamine substituted at position 4 of the pyridinium or quinolinium system, **10a-b** and **10j-l**, offer the best results in terms of enzyme inhibition and antiproliferative assays.

Regarding ChoKα1 inhibitory effect, all compounds showed a micromolar activity, comparable to that of the two reference compounds **RSM932A** and **MN58b**. The docking studies indicated that all compounds could be inserted into the choline binding site and could be grouped into two families on the basis of their different insertion modes. Compounds **10a**, **10b**, **10d**, and **10e** could be inserted similarly to compound **2**. Compound **10a** showed good ChoKα1 inhibition (IC_{50} = 1.0 μM), thanks to the presence of the 1-

benzyl-4-(dimethylamino)pyridinium fragment, which performs a strong π-cation interaction with the Cho binding site (Figure 12B), this having been described as one of the most efficient moieties for ChoKα1 inhibition (Serrán-Aguilera et al., 2015). Compound **10b** showed a reduced ChoKα1 inhibition (IC_{50} = 9.56 μM) attributable to the volume of the 4-(pyrrolidin-1-yl)pyridinium cationic head, causing a decrease in the π-cation interaction (Figure 12C). In this family, compound **10d** showed very poor ChoKα1 inhibition (IC_{50} = 37.54 μM). This result may be due to the presence of the quinuclidine and the consequently low lipophilicity (clogP = -1.01) cationic head that probably prevented the interactions with Tyr333, Tyr354, Trp420, and Tyr440 (Figure 12D). However, although compound **10e** had a 3-hydroxyquinuclidine cationic head and low lipophilicity (clogP = -2.42), it showed better ChoKα1 inhibition (IC_{50} = 9.51 μM) than what could be explained by the establishment of two additional H-bonds with the enzyme (Figure 12E).

In summary, when compounds bind to choline site, such as compound **2** (compound **10a-b**, **d-e**), low lipophilicity values are sufficient to achieve good inhibition of the enzyme, the pydidinic ring being the most appropriate moiety, and the quinuclidine ring decreases the activity unless the lack of aromatic ring is offset by the formation of a H bond provided by the hydroxyl group.

The second group interacted with the choline binding site as compound **4**. Compounds **10c** and **10j-l** showed a good ChoKα1 inhibition (IC_{50} = 1.63, 1.66, 2.02 and 0.92 μM respectively), while compounds **10f-i** showed a slightly reduced ChoKα1 inhibition (IC_{50} = 6.85, 3.27, 2.79 and 16.22 μM, respectively). All these compounds had a 4-substituted and 7-substituted quinolinium cationic head, **10f-l**, except **10c**, which had the rest of the N-methylanilino at the 4 position of the pyridinium cationic head. The structure of the 4-substituted fragment conditions the inhibitory activity of these molecules. In fact, compounds **10j-l** had a 4-cycloalkylamino fragment, while compounds **10c** and **10f-i** had a 4-N-methylanilino substituent. The resulting IC_{50} values indicated that the 4-cycloalkylamino favored the ChoKα1 inhibition, probably promoting a more effective insertion into the additional binding site. In this group the chloro atom increased the volume of molecule and the lipophilicity. Thus, the compound **10l** offered the right balance between volume and lipophilicity. The perhydroazepine group (**10i**) provided the volume to be inserted into the choline binding site properly and the addition of a choro atom slightly depressed the activity (**10j**).

Conversely, the compounds with an N-methylanilino system at the 4 position of the pyridinium or quinolinium cationic heads showed lower IC_{50} than did those in the alkylamine system. In these compounds, the chloro atom in para position of 4-(methyl(phenyl)amino)quinolinium or pyridinium fragment (**10c**, **10g** and **10i**) or in position 7 of the quinolinium ring (**10h** and **10i**) seemed to play an essential role in the enzyme inhibition. In fact, the presence of the chloro atom allowed the cationic head to be accommodated at the choline-binding site, likely by an increase in the lipophilicity provided by the halogen atom, regardless of where the halogen was located (**10c**, **10g**, and **10h** IC_{50} = 1.63, 3.27, and 2.79 μM, respectively). A direct correlation between volume-lipophilic activity was found in these compounds (**10c**, **10f-i**), so that the less bulky and lipophilic compounds offered the best values (**10c**, IC_{50} = 1.66μM, clogP= 1.8) while adding a second aromatic ring slightly diminished the activity of **10f-h**. On the other hand, the two chloro atoms present in compound **10i** made the molecule too bulky to bind to the choline site, lowering its inhibition activity (IC_{50} = 16.22 μM), and raising its lipophilicity (clogP = 4.23). However, the absence of chloro atom in **10f** also considerably decreased ChoKα1 inhibition (IC_{50} = 6.85 μM), highlighting the important role of the chloro atom.

Regardless the binding mode to the enzyme, the best inhibitory activities were found when a fragment of alkylamine or cycloalkylamine was present at the 4 position in pyridinium or quinolinium cationic heads, such as **10a**, **10j**, **10k**, and **10l** (IC_{50} = 1.0, 1.66, 2.02, and 0.92 μM, respectively), These results reveal that the volume of the cationic head probably fits properly into the choline binding site. The only exception was **10b** (IC_{50} = 9.56 μM), and this was a consequence of the higher volume of the 4-(pyrrolidin-1-yl)pyridinium cationic head that diminished the π-cation interaction (Figure 12C) mentioned above.

The crystal structure of the complex ChoKα1/10a shows that the compound binds to the choline binding site

Although the docking studies clearly suggested that the compounds bind to the choline binding site (Figure 12-13) we carried out further crystallization experiments with the most active ChoKα1 inhibitors, **10a** and **10l**, in order to compile more consistent data concerning their binding mode. Despite the large number of trials, we managed to solve only the crystal structure of ChoKα1 in complex with compound **10a** at 1.45Å (PDB ID: 5FTG). The other compound (**10l**) was too hydrophobic (clogP = 2.36) and therefore insoluble in the mother liquor.

For ChoKα1/**10a** complex, successive iterative model building and refinement cycles were carried out to produce a final model with good refinement statistics (R = 0.197, R_{free} = 0.218). The structure is a monomer formed by a small N-terminal and a large C-terminal domain. Whereas the ATP binding site is located in a cleft formed by N- and C-terminal domains, the choline binding site is found in a deep hydrophobic pocket. One molecule of compound **10a** was visualized at the choline binding site with good electron density. One 1-benzyl-4-(dimethylamino)pyridinium fragment was deeply positioned within the pocket and established π-cation interactions with Trp423 and Trp420, whereas it set π-π interactions with Tyr333, Tyr354, Phe435, and Tyr440. The second 1-benzyl-4-(dimethylamino)pyridinium moiety was directed towards the outside part of the choline binding site, where it established π-π and hydrophobic interactions with residues Phe361 and Ile433, respectively (Figure 14A).

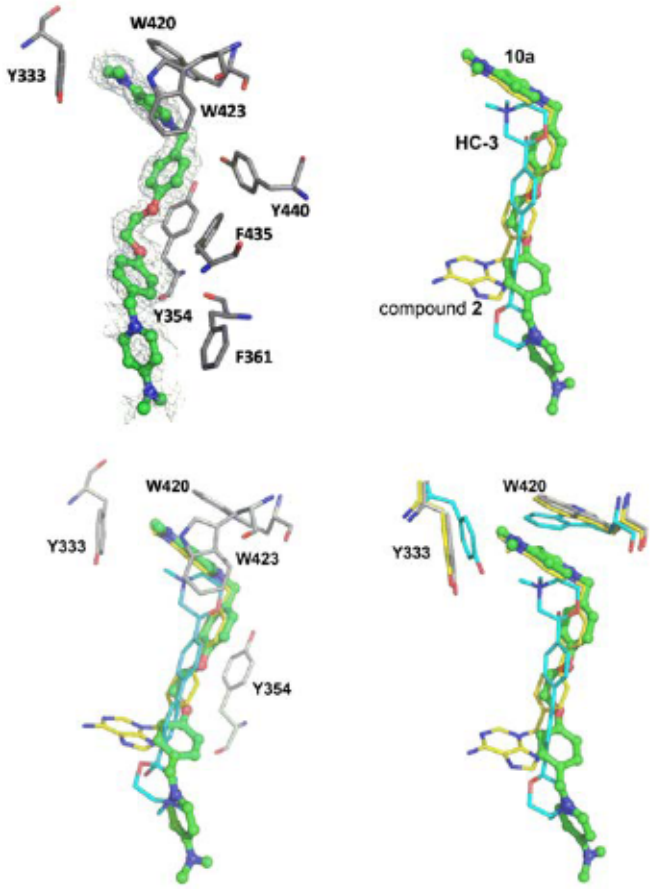

Figure 14: Active site of ChoKα1 in complex with ChoKα inhibitors

(**A**) Active site of ChoKα1 in complex with compound **10a** (PDB ID: 5FTG) (carbon atoms in green color). Unbiased difference electron density maps are shown at 2.2 σ. (**B**) Superimposition of **10a** with **HC-3** (PDB ID: 3G15) (carbon atoms in cyan color) and compound **2** (PDB ID: 3ZM9) (carbon atoms in yellow color). (**C**) Residues that stabilize the positive charge of the cationic head in the three superimposed ligands (carbon atoms in grey color). (**D**) Residues that undergo the most notable conformational changes when compounds **2** or **10a** bind to the choline binding site.

When the crystal pose was compared with the docked one, few differences were found between the two, especially regarding the conformation that the first 1-benzyl-4-(dimethylamino)pyridinium fragment adopted (Figure 15). This moiety was completely superimposed in the two poses, indicating the accuracy of the theoretical predictions. Nevertheless, the second 4-(dimethylamino)pyridinium moiety was flipped almost 90° towards the residue Phe361 but not towards the residue Ile433, as the docking had predicted. The reason for this difference is that the pyridinium ring set π-π interactions with Phe361 in the crystal pose, increasing the stability of the ligand-protein complex.

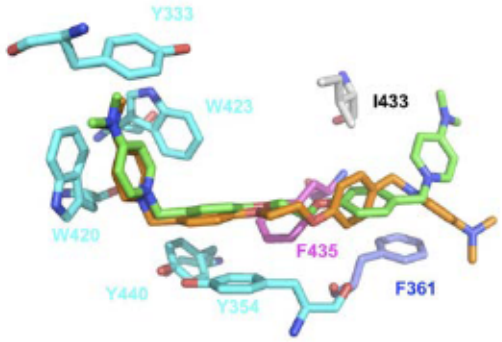

Figure 15: Comparison between crystal and docking poses of 10a

Superposition of the docking pose of compound **10a** (carbon atoms in green color) with the effective crystal pose (carbon atoms in orange color) inserted into Cho binding site.

Remarkably, the positive charge of the quaternary ammonium of the first 1-benzyl-4-(dimethylamino)pyridinium fragment was positioned at the choline binding site in the same place as one of the previously reported ChoKα1 inhibitors, such as compound **2** (PDB ID:4BR3) and **HC-3** (PDB ID: 3G15) (Figure 14B). This indicates that common residues should participate in the positive-charge stabilization regardless of the chemical nature of the spacer groups. As reflected in Figure 14C, these residues are Tyr333, Tyr354, Trp420, and Trp423, which set parallel π-cation and π-π interactions with the quaternary ammonium and the aromatic rings of the 1-benzyl-4-(dimethylamino)pyridinium fragment. Nevertheless, depending on the spacer and the cationic head of the compounds, some conformational changes in some of these residues were observed. For instance, residues Trp420 and Tyr333 underwent a noticeable retraction to open the hydrophobic cavity when compound **10a** or compound **2** bound the protein in order to accommodate the positive charge of the cationic head (Figure 14D).

Comp.	clogP Ann 2005	[a]IC50 (μM) ChoKα1 purified	Antiproliferative activity [b]GI50 (μM)								
			HeLa	HT−29	Jurkat	HL-60	RS4,11	MCF-7	PC-3	A549	MDA-MB-231
10a	−0.36	1.00 ± 0.01	0.079 ± 0.024	0.11 ± 0.01	0.12 ± 0.08	0.10 ± 0.04	0.045 ± 0.005	0.092 ± 0.019	0.051 ± 0.01	0.027 ± 0.010	0.10 ± 0.05
10b	0.36	9.56 ± 1.45	0.082 ± 0.041	4.3 ± 0.42	0.068 ± 0.016	0.042 ± 0.005	1.12 ± 0.22	0.17 ± 0.032	4.5 ± 1.1	2.3 ± 1.1	0.09 ± 0.02
10c	1.8	1.63 ± 0.14	5.6 ± 0.25	4.3 ± 1.1	7.3 ± 0.50	2.1 ± 0.6	2.7 ± 0.13	3.5 ± 0.72	3.1 ± 0.7	4.9 ± 0.7	2.2 ± 0.27
10d	−1.01	37.54 ± 4.45	16.9 ± 2.5	> 100	> 100	84.1 ± 7.4	37.5 ± 4.2	91.4 ± 7.6	94.3 ± 12.4	61.3 ± 16.7	74.3 ± 2.6
10e	−2.42	9.51 ± 1.14	> 100	94.0 ± 4.2	> 100	> 100	66.0 ± 6.6	50.9 ± 11.7	48.0 ± 1.1	> 100	63.2 ± 3.9
10f	3.02	6.85 ± 0.81	0.15 ± 0.031	0.12 ± 0.017	0.060 ± 0.002	0.063 ± 0.013	0.24 ± 0.05	0.17 ± 0.065	0.47 ± 0.12	0.21 ± 0.06	0.001 ± 0.001
10g	3.56	3.27 ± 0.66	0.25 ± 0.06	0.75 ± 0.12	0.098 ± 0.031	0.71 ± 0.24	0.15 ± 0.04	0.46 ± 0.063	0.26 ± 0.01	0.11 ± 0.018	0.19 ± 0.009
10h	3.82	2.79 ± 0.17	0.32 ± 0.062	0.35 ± 0.07	0.31 ± 0.07	0.92 ± 0.06	0.026 ± 0.006	0.32 ± 0.04	0.85 ± 0.32	0.18 ± 0.08	0.23 ± 0.04
10i	4.23	16.22 ± 0.44	1.5 ± 0.73	1.0 ± 0.15	0.76 ± 0.26	0.87 ± 0.28	0.50 ± 0.09	0.66 ± 0.07	0.72 ± 0.09	0.29 ± 0.10	0.15 ± 0.05
10j	2.27	1.66 ± 0.09	0.17 ± 0.084	0.15 ± 0.08	0.11 ± 0.026	0.42 ± 0.22	0.16 ± 0.012	0.11 ± 0.047	0.09 ± 0.04	0.30 ± 0.068	0.01 ± 0.005
10k	2.76	2.02 ± 0.08	0.26 ± 0.074	0.27 ± 0.05	0.072 ± 0.013	0.18 ± 0.06	0.036 ± 0.008	0.28 ± 0.09	0.11 ± 0.028	0.52 ± 0.02	0.061 ± 0.003
10l	2.36	0.92 ± 0.01	0.37 ± 0.18	0.56 ± 0.21	0.007 ± 0.003	0.16 ± 0.07	0.42 ± 0.14	0.022 ± 0.007	0.8 ± 0.2	0.14 ± 0.06	0.05 ± 0.02
MN58b	0.01	0.78 ± 0,03	1.9 ± 0.1	1.9 ± 0.4	0.35 ± 0.1	0.32 ± 0.03	1.0 ± 0.3	1.8 ± 0.06	n.d.	0.54 ± 0.2	0.31 ± 0.12
RSM932A	2.92	1.92 ± 0,06	0.83 ± 0.1	0.4 ± 0.2	0.41 ± 0.1	0.93 ± 0.1	0.17 ± 0.04	0.18 ± 0.10	n.d.	0.45 ± 0.09	0.17 ± 0.05

Table 3. *In vitro* inhibitory effects of compounds 10a-l.

The table summarizes the clogP calculated by Pallas (3.8.1.1. PrologP), the inhibitory effect on purified human ChoKα1 activity, and the antiproliferative activity in different cancer cell lines. [a]IC_{50} = Compound concentration required to inhibit ChoKα1 enzyme by 50%. [b]GI_{50} = Compound concentration required to inhibit tumor-cell proliferation by 50%. n.d. not determined. Values are the mean ± SEM for three independent experiments.

Cancer-cell growth inhibition

All compounds were evaluated for their antiproliferative activity against a panel of nine different human tumor-cell lines (Table 3). All were given GI_{50} values generally lower than 1 μM, some of them even at nanomolar concentrations. Only two compounds, i.e. **10d** and **10e**, registered GI_{50} values higher than 10 μM against all tested lines. Compounds **10a**, **10b**, **10f**, and **10l** offered the best antiproliferative activities against all cell lines. In particular, **10a** gave GI_{50} values ranging from 0.027 to 0.12 μM, although the best value was by **10f** in MDA-MB-231 cell line (GI_{50} = 0.001 μM). Compared to quinolinium derivatives, in general the pyridinium moiety provided better results in all tested cell lines.

In the pyridinium family, the best results were found when the substitution was an alkyl or cycloalkylamine (**10a-b**). The switching of dimethylamine to pyrrolidine caused a curious decline in activity for the majority of cell lines (**10b**, GI_{50} = 0.042 μM to 4.5 μM). The replacement of this tertiary amine by a conjugate aromatic system (4- (4-chloro-N-methylanilino)pyridinium, **10c**) resulted in lower activity (GI_{50} = 2.1 μM to 7.3 μM). It bears noting that despite of their low lipophilicity (**10a**, clogP = -0.36 and **10b** clogP = 0.36), the compounds **10a-b** provided better results than did compound **10c** (clogP = 1.8). This finding can be explained by the different mode to bind to enzymes of these compounds, as mentioned above.

Replacing the pyridinium system with quinuclidine as cationic head, such as compounds **10d** and **10e**, led to a total loss of activity in all cell lines. This result may be due to the very low lipophilicity of **10d-e** (clogP = -1.01 and -2.42 respectively) and to the low IC_{50} value.

Regarding the quinolinium family (**10f-l**), all compounds had GI_{50} in the range of submicromolar values, **10l** being the best compound (GI_{50} = 0.007 μM for Jurkat cells). No differences in the activity were detected between the different substituents in the 4 position upon the quinolinium system, since **10f** and **10l** (with N-methylanilino and 4- pyrrolidine in the 4 position, respectively) offer the best antiproliferative activity over nearly all the cell lines. However, the presence or not of a chloro atom over the quinolinium system, seems to play a crucial role in inhibiting cell growth. The chloro atom provided not only a higher lipophilicity to these compounds, improving the passage through the plasma membrane, but also a larger volume that impaired the insertion in the choline binding site. In fact, compound **10f**, which has an N- methylanilino group at the 4 position without any

chloro atom, exhibited better antiproliferative activity than did compound **10h** or **10g**, which have a chloro atom in the quinolinium. However, **10f** registered a lower value of ChoKα1 inhibition (IC_{50} = 6.86 μM) than **10g** and **10h** (IC_{50} = 3.27 and 2.79 μM, respectively) with chloro in para position of the N-methylanilino system (**10g**) or in 7 position of quinolinium fragment (**10h**). The chloro atom provided lipophilicity and good results of enzyme inhibition but this lipophilicity can allow binding to other targets in the cancer cells. On the other hand, the presence of two chloro atoms make compound **10i** too bulky to inhibit the enzyme (IC_{50} = 16.22 μM), strongly reducing the antiproliferative activity, and it is also more lipophilic (clogP = 4.23), and thus does not bind to other targets. In conclusion, among the quinolinium family, the compounds with an N-methylanilino system upon the 4 position (**10f-i**), **10f** offers the best antiproliferative values but lower inhibition of the enzyme (6.85 μM). This could be due to a greater affinity of **10f** by the enzyme in a whole cancer cell while the higher lipophicility of **10g-h** could help them to be more suitable for binding to other targets. This highlights the need for a balance between lipophilicity, inhibitory activity of the enzyme isolated (affinity and selectivity), and antiproliferative activity for achieving successful results. The insertion of chloro in position 7 as in compound **10k** improves the activity. This suggests that although the enzymatic inhibitory activity is almost the same for these compounds (IC_{50} from 0.92 to 2.02 μM), the chloro leads to an appreciable increase in the antiproliferative activity (**10j** vs. **10k**) in nearly all the cell lines.

Finally, **10a** and **10l** were the compounds with the best GI_{50} values in almost all the cell lines. The two belong to different subfamilies. The first one, **10a**, has a residue of dimethylaminopyridinium as a cationic head which could offer the best volume to fit in a choline binding site, while the compound **10l** has a residue of 7-Chloro-4-pyrrolidinequinolinium which provides more lipophilicity to the quinolinium moiety, allowing the compound to cross the plasma membrane more easily.

Trypan blue exclusion assay

The cell viability in the presence of **10a** was also evaluated by the trypan blue exclusion assay. The results depicted in Figure 4 reflect that **10a** significantly inhibited cell growth in three cell lines (Figure 16, panel A = Jurkat, Panel B = HeLa; panel C = MDA-MB-231) tested in a concentration-dependent manner, roughly confirming the results found with the MTT test (see Table 3). Notably, we observed that the inhibition of cell proliferation was

not dependent on the presence of the molecule in the incubation medium. In fact, experiments in which the cells treated with **10a** were harvested, washed, and incubated with fresh medium without **10a** proliferation continued to be inhibited, suggesting that the catalytic activity of the enzyme may have been irreversibly inhibited (Figure 17).

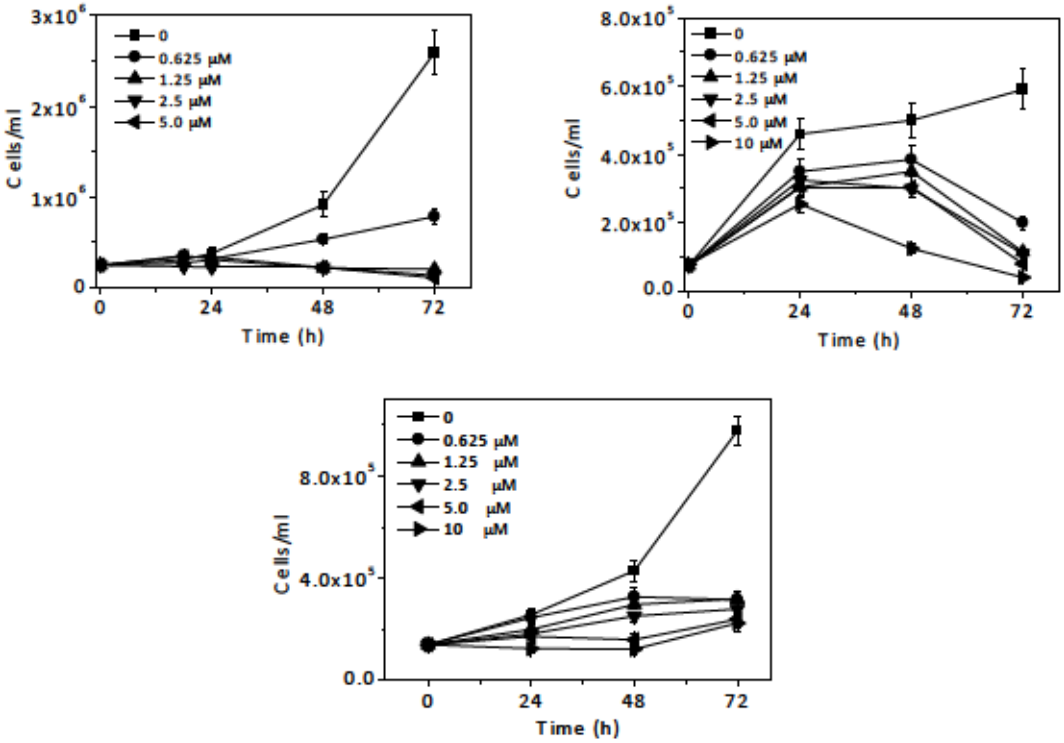

Figure 16: 10a inhibits cell viability/proliferation

Cell viability evaluated by trypan blue negative cell count in Jurkat cells (**A**) HeLa cells (**B**) and MDA-MB-231 (**C**) after incubation with the indicated concentrations of compound **10a**. Data are presented as mean±SEM of three independent experiments.

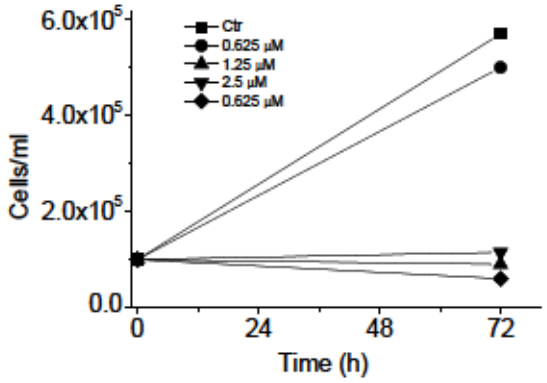

Figure 17: 10a inhibits cell proliferation after comcompound removal

Jurkat cells were treated with the indicated concentration of **10a** for 72h and then cells were harvested, washed, counted, and incubated in a drug-free medium. After further 72h of incubation, cell viability was analyzed by trypan blue exclusion assay as described in the experimental section.

Effect of 10a in non-tumoral cells

We investigated the effect of the most active compound (**10a**) in non-tumoral cells, e.g. human lymphocytes and human umbilical-vein endothelial cells (HUVEC) from healthy donors. As shown in Table 4, in general, in resting lymphocytes, fibroblasts, and HUVEC, compound **10a** had lower toxicity compared to tumor cells. Instead, in lymphocytes stimulated with a mitogen (e.g. phytohematoagglutinin, PHA), the compound had cytotoxicity comparable to that seen in tumor cells, indicating a certain preference only towards proliferating cells. In this context, it bears noting that other choline kinase inhibitors such as **MN58b** or **RSM932A** presented low or reduced cytotoxicity in oncogene-transformed cells and in tumor cells, in agreement with previously published data (Báñez-Coronel, 2004; Cabezon et al., 2000; Cantrill et al., 2000; Gruber et al., 2012; Xiao et al., 2007).

Antiproliferative activity[a] GI_{50} (μM)				
Comp	**PBL(resting)**	**PBL(+Pha)[b]**	**Human fibroblasts**	**HUVEC**
10a	1.5 ± 0.64	0.034 ± 0.007	5.8 ± 1.3	5.1 ± 0.43
10b	34.8 ± 15.6	1.88 ± 0.71	30.5 ± 9.6	n.d.
10f	1.4 ± 0.6	0.10 ± 0.03	9.8 ± 2.5	n.d.
10g	0.98 ± 0.25	0.55 ± 0.11	7.4 ± 2.4	10.4 ± 3.5
10h	1.0 ± 0.42	0.32 ± 0.03	3.7 ± 0.43	16.0 ± 6.6
10j	2.0 ± 0.24	0.095 ± 0.021	14.3 ± 1.2	n.d.
10k	2.1 ± 0.80	0.034 ± 0.007	3.2 ± 0.86	n.d.
10l	3.8 ± 0.55	0.49 ± 0.15	9.6 ± 1.3	11.4 ± 5.9
RSM932A	1.1 ± 0.09	0.23 ± 0.05	n.d	0.46 ± 0.047
MN58b	2.0 ± 0.4	0.15 ± 0.05	n.d.	2.1 ± 0.58

Table 4: *In vitro* inhibitory effects of selected compounds in non-tumoral cells.

[a]GI_{50}= Compound concentration required to inhibit tumor-cell proliferation by 50% Values represent the mean ± SEM for three independent experiments. n.d. not determined. [b]Pha, Phytohematoagglutinin.

10a induces G1 phase cell-cycle arrest

Compound **10a** induced a G1 arrest of the cell cycle, which occurred in a concentration-dependent manner in the three cell lines tested (Jurkat, MCF-7 and MDA-MB-231). Together with the G1 increase, a concomitant reduction was found in the S phase (Figure 18). Notably, cells with hypodiploid DNA content, suggestive of activation of apoptotic signaling, were not detected (data not shown). Similar results were also found with the two lead compounds **RSM932A** and **MN58b**, suggesting a common mechanism of action. Our

results agree with the data of Granata et al. (Granata et al., 2014) which showed that ChoKα downregulation in ovary-cancer cells inhibits cell proliferation without affecting survival signaling pathways whereas, a reduction in the S-phase, proportional to growth inhibition, was observed in cells knocked down for ChoKα1. The cell cycle also showed a slight G1 cell-cycle arrest in silenced cells compared with controls. On the contrary, Sanchez-Lopez et al. (Hernández-Alcoceba et al., 1999) showed that **RSM932A** and **MN58b** induce a significant decrease of the G1 phase in breast- and colon-cancer cells without any alteration of the other phases of the cell cycle. It should be noted that these data correspond to a concentration (15 μM) higher than that used in the present study.

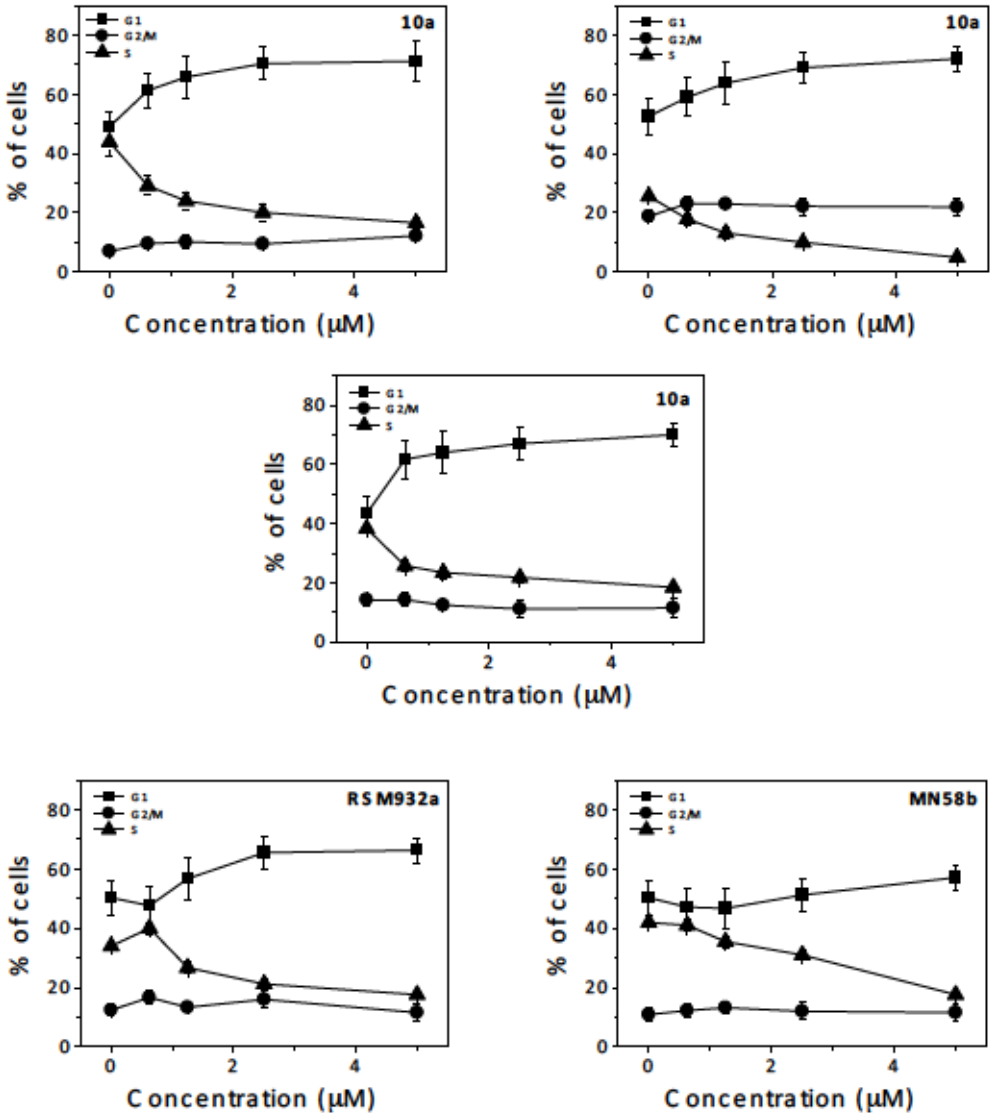

Figure 18: 10a induced a G1 arrest of the cell cycle

Percentage of cells in each phase of the cell cycle in Jurkat (Panels A), MCF-7 (Panel B) and MDA-MB231 cells (Panels C-E) treated with the indicated compounds at the indicated concentrations for 24 h. Data are presented as mean ± SEM of three independent experiments.

10a induces low levels of apoptosis

To evaluate whether **10a** causes cell death, we conducted a biparametric cytofluorimetric analysis using propidium iodide (PI), which stains DNA and enters only dead cells, together with fluorescent immunolabeling of the protein annexin-V (AV), which binds to phosphatidylserine in a highly selective manner. Dual staining for AV and with PI enables the discrimination between live cells (AV-/PI-), early apoptotic cells (AV+/PI-), late apoptotic cells (AV+/PI+), and necrotic cells (AV-/PI+). For a positive control, we used two well-known anticancer drugs such as Cis-Pt and Etoposide that in all cell lines tested induce significant apoptosis (data not shown). As depicted in Figure 19, **10a** after 72h of incubation induced a modest increment in apoptotic cells only in Jurkat cells while both in MCF-7 and MDA-MB-231 the increase appeared not to be significantly different from that of the untreated cells.

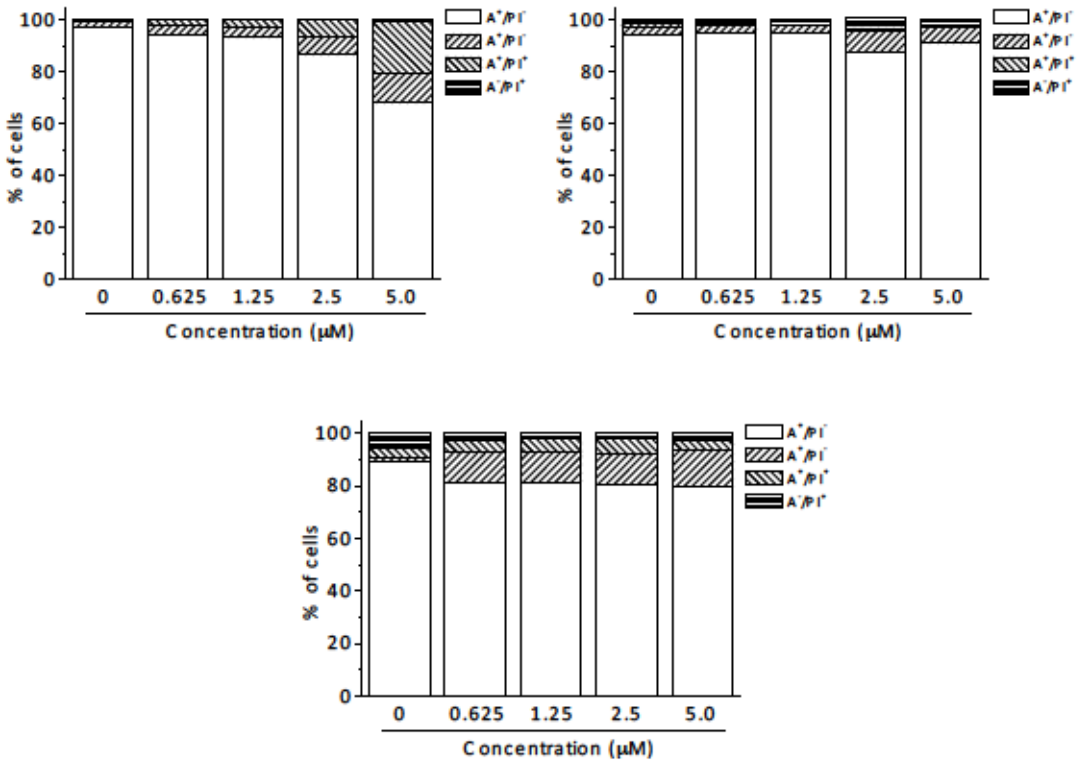

Figure 19: 10a induces only a moderate apoptotic effect

Flow cytometric analysis of apoptotic cells after treatment of Jurkat (panel A), MCF-7 (panel B) and MDA-MB-231 (panel C) cells with **10a** at the indicated concentrations after incubation for 72 h. The cells were harvested and labeled with annexin-V-FITC and PI and analyzed by flow cytometry. Data are represented as mean ± SEM of three independent experiments.

3.1.4 DISCUSSION

The synthesis of a novel family of 1,1'-(((ethane-1,2-diylbis(oxy))bis(4,1-phenylene)) bis(methylene))-bispyridinium or –bisquinolinium bromide (**10a-l**) and their evaluation as inhibitors of choline kinase against a panel of cancer-cell lines are described in this work. These compounds were efficiently synthesized in three steps, starting from the building block **6**. The chemistry used was appropriate to obtain the designed target compounds, and both the yield and the time of reaction were improved considerably with microwave irradiation.

Preliminary docking studies performed on both crystal structures, ChoKα1/**2** (PDB ID: 4BR3) and ChoKα1/**4** (PDB ID: 4CG8), and the analysis of the resulting poses, indicated that these compounds (**10a-l**) could adopt similar behaviour to that of compound **2** or to compound **4** thanks to the synclinal conformation of the linker that allowed the insertion of these molecules inside the Cho binding site and consequently enhanced the antiproliferative effect. The first experimental validation of the docking studies is shown with the results of tryptophan assays for these compounds, which offer very good Kd values. Among all the compounds, those belonging to the families of pyridinium and quinolinium offered similar or better IC_{50} ChoKα1 than did the lead compounds **MN58b** and **RSM932A**. In fact, the best inhibitors were **10a** and **10l**, and the crystal structure of ChoKα1/**10a** showed that the compound binds to the choline binding site, indicating the accuracy of the theoretical predictions, wherein the first one-benzyl-4-(dimethylamino) pyridinium represents the appropriate fragment to inhibit the enzyme.

Also, we have shown these compounds to have an excellent antiproliferative profile, better than that of the two lead compounds **RSM932A** and **MN58b** in a panel of human tumor-cell lines. More importantly, our compounds presented lower or reduced toxicity in some non-tumor-cell lines in comparison to transformed cells. Indeed our results agree with previous observations indicating increased ChoKα1 activity in cell cultures treated with growth factors or insulin (Rodríguez-González et al., 2003; Uchida and Yamashita, 1990; Warden and Friedkin, 1985). In this context it is important to note that our results indeed confirm these previous findings, and compound **10a** in fact presented higher activity only in rapidly proliferating cells such as mitogen-stimulated lymphocytes in comparison to quiescent cells.

Another important finding is that **10a** significantly arrested the cell cycle in G1 together

with a sharp reduction of the S phase, confirming their ability to inhibit cell growth. Curiously, despite their ability to block cell proliferation, **10a** induced a low proportion of cell death, as reflected by a low level of Annexin-V positive cells. Notably, this occurred also for the two reference compounds **RSM932A** and **MN58b**, which even at the maximum concentration used showed a negligible percentage of apoptotic cells, according to the analysis of the cell cycle. It is important to note that, although some reports (Hernández-Alcoceba et al., 1999) indicate these two compounds may induce apoptosis, this takes place at concentrations much higher than the IC_{50} (15 μM), which can have an off-target effect. This intriguing aspect is under active investigation by our group. Nevertheless, our data demonstrate that **10a** is a highly promising new ChoKα1 inhibitor and is worthy of further preclinical evaluation as a potential anticancer drug.

3.2 The novel choline kinase alpha inhibitor EB-3D induces cellular senescence in triple-negative breast cancer and reduces tumor growth and metastatic dissemination.

Elena Mariotto, Roberta Bortolozzi, Roberto Ronca, Davide Carta, Valentina Serafin, Giuseppe Basso, Luisa Carlota López-Cara, Giampietro Viola.

3.2.1 ABSTRACT

Identification of novel strategies for kinase inhibition is one of the most challenging goal in cancer pharmacology. Choline kinase (ChoK) is the first enzyme of the Kennedy's pathway leading to the biosynthesis of phosphatidylcholine (PtdCho), the most abundant phospholipid in eukaryotic cell membranes. Compound **EB-3D** is a novel ChoKα1 inhibitor with a potent antiproliferative activity against a panel of several cancer cell lines. ChoKα1 is particularly overexpressed and hyperactivated in aggressive breast cancer. Here we report that **EB-3D** strongly impairs triple-negative MDA-MB-231 proliferation, migration and invasion and the effect is irreversible. Reverse-phase protein array (RPPA) data revealed the activation of the AMP-activated protein kinase (AMPK) metabolic sensor causing the dephosphorylation of the mammalian target of rapamycin complex 1 (mTORC1) downstream targets such as p70 ribosomal protein S6 kinase (p70S6K) and S6K and the eukaryotic translation initiation factor 4E-binding protein 1 (4E-BP1), suggesting that **EB-3D** may affect protein synthesis. Moreover we demonstrate that **EB-3D** strongly synergizes with drugs used for triple-negative breast cancer treatment, in particular with cisplatin. The absence of cell death previously reported in MDA-MB-231 following **EB-3D** treatment is essentially due to the induction of cellular senescence. Moreover **EB-3D**-induced senescence significantly sensitizes MDA-MB-231 cells to the apoptotic effect of cisplatin. The antitumorigenic potential of **EB-3D** was evaluated also *in vivo* in syngeneic orthotopic EO771-C57BL/6 mouse model of breast cancer. The compound induces a significant reduction of the tumor mass at low doses. In addition, we also tested the possible anti-metastatic effect of **EB-3D** in both syngeneic EO771-C57BL/6 and xenogeneic NOD/SCID model engrafted with MDA-MB-231. In both models we observed a significant reduction of lung metastasis. Altogether, our results indicate that the novel ChoKα1 inhibitor **EB-3D** could be a promising new anticancer agent to improve aggressive triple negative breast cancer treatment protocols.

3.2.2 INTRODUCTION

Metabolic reprogramming has been recognized as one of the ten hallmarks of cancer (Hanahan and Weinberg, 2011). Malignant cells need to change their cellular energy metabolism in order to support exacerbate cell growth and proliferation and to adapt to new microenvironment conditions and to different challenges. Lipid metabolism is no exception: a sustained biosynthesis of membrane phospholipids is required to meet the demand of rapidly proliferating cells. In fact, alteration in choline (Cho) metabolism has been observed in many cancers (Asim et al., 2016; Iorio et al., 2010; Nakagami et al., 1999; Ramírez de Molina et al., 2002d; Ramírez de Molina et al., 2007) and it has been related to deregulated cell proliferation, invasion and metastasis. The so-called "cholinic phenotype" consists in increased level of phosphocholine (PCho) and in general of total choline-containing metabolites (tCho) mainly due to the overexpression and/or hyperactivation of the α1 isoform of choline kinase (ChoKα1). ChoKα1 catalyzes the phosphorylation of choline to phosphocholine is the first step of the Kennedy's pathway ultimately leading to the synthesis of phosphatidylcholine (PtdCho), the most abundant phospholipid of eukaryotic cell membrane. Increased expression of ChoKα1 has been extensively described in breast cancer, where it correlates with histological tumor grade and poor clinical outcome (Ramírez de Molina et al., 2002a). For all these reasons, ChoKα1 has been proposed as a new appealing target for cancer therapy and during the past decades extensive efforts have been made to synthesize and improve ChoKα1 inhibitors.

EB-3D (previously known as compound **10a**) is a novel symmetrical biscationic ChoKα1 inhibitor that was recently shown to impair cell proliferation in a panel of different cancer cell lines (Schiaffino-Ortega et al., 2016). Here we provide evidence that **EB-3D** targets ChoKα *in vitro,* reducing phosphocholine levels measured by magnetic resonance spectroscopy (^{1}H-MRS) in cells treated with the compound. The purpose of this study was to deeply investigate the effect of **EB-3D**-mediated ChoKα inhibition both *in vitro* and *in vivo* in triple-negative breast cancer (TNBC) models. To accomplish this goal we used MDA-MB-231 breast cancer cell line, where the overexpression of ChoKα and its consequences are well documented. We examined the effects of **EB-3D** *in vitro* on cell viability, cell proliferation, signaling pathways modulation, cell migration and invasion. In addition, the ability of **EB-3D** to enhance the anti-tumorigenic potential of drugs commonly used in breast cancer treatment protocols was also tested. We previously

reported that **EB-3D** has a more potent *in vitro* cytostatic effect on compared to **MN58b** and **RSM932A**, chosen as reference compounds for symmetrical ChoKα1 inhibitors, causing a strong reduction of cell proliferation and G0/G1 phase cell cycle arrest. In this work, we show that **EB-3D** is less toxic in resting non-tumoral mammary cells compared to the stimulated tumor-like counterpart, in agreement to previously reported compounds (Rodriguez-Gonzalez et al., 2004; Trousil et al., 2016).

Cellular senescence is the permanent growth arrest that occurs in normal cells to prevent unlimited cell proliferation. Neoplastic transformation requires the inhibition of senescence machinery, however it has now become clear that tumor cells can be induced to undergo senescence by chemotherapy treatments and treatment-induced senescence was shown to be involved in tumor response to therapies (Achuthan et al., 2011). Indeed, senescent cells are able to secrete proteins implied both in tumor suppression and survival (Pérez-Mancera et al., 2014). Here we give proof that **EB-3D** is able to induce cellular senescence that sensitizes resistant cancer cells to chemotherapy.

3.2.3 RESULTS

Inhibition of ChoKα by EB-3D reduces soluble choline metabolites in MDA-MB-231

To evaluate if **EB-3D**-mediated ChoKα inhibition effectively reduces choline metabolites, ^{1}H-NMR spectra were analyzed after treatment of MDA-MB-231 with the ChoKα1 inhibitor. The variation of choline metabolites during time is summarized in Figure 20.

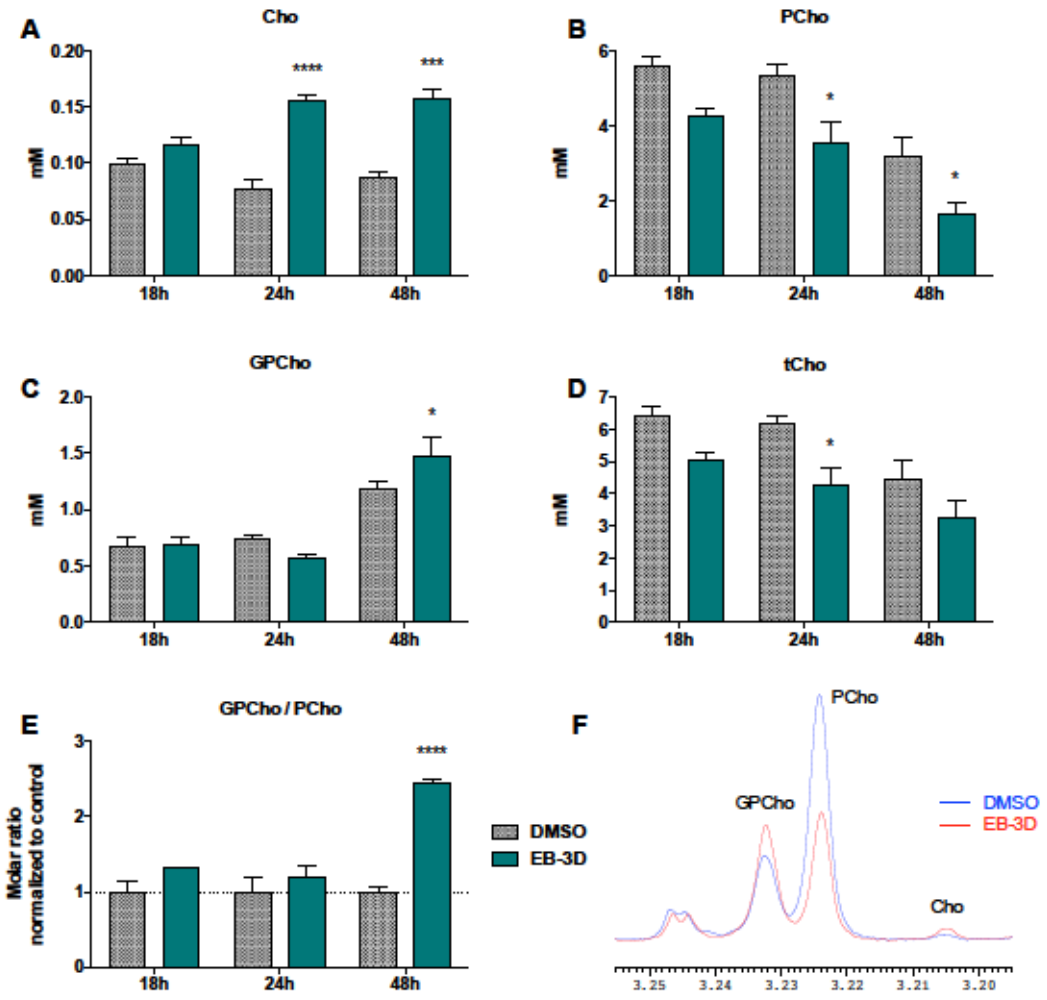

Figure 20: Choline-containing metabolites variations

Millimolar levels of Cho (**A**), PCho (**B**), GPCho (**C**) and tCho (**D**) quantified from ^{1}H-NMR spectra of MDA-MB-231 cells treated with 1μM of **EB-3D** or DMSO for the indicated time points. (**E**) GPCho/PCho molar ratio normalized to each time-point control. Values represent the mean ± SEM of two independent experiments. Differences between each time-point treatement and its control were analyzed using two-way ANOVA. (**F**) Representative ^{1}H-MR spectra from the 3.20–3.25 ppm region of water-soluble extracts from MDA-MB-231 cells after 48h of treatment with DMSO (blue line) and 1μM of **EB-3D** (red line).

After 24 h of treatment with 1μM of **EB-3D**, the pool of free Cho is about two-fold compared to control (0.156 ± 0.003 vs. 0.077 ± 0.005 mM) and this gap is mainteined at 48 h (Figure 20 A). On the contrary, **EB-3D** treatment reduces the amount of the ChoKα reaction product over time, halving PCho intracelluar level in 48 h (1.62 ± 0.25 mM in treated cells vs. 3.17 ± 0.38 mM in control) (Figure 20 B). GPCho levels significantly increses only at 48 h (1.47 ± 0.12 vs. 1.18 ± 0.06 mM) (Figure 20 C) while a general decrease in tCho levels was observed during time (Figure 20 D). Lastly, the GPCho/PCho ratio is slighly increased after ChoKα inhibition at all time points but it becomes strongly significant only after 48 h of treatment (Figure 20 E). Figure 20 F shows representative spectra superimposition of water-soluble extracts of cells treated with 1μM of **EB-3D** for 48 h and its control.

EB-3D irrevesible cytostatic effect

Our previous data showed that **EB-3D** is a potent cytostatic agent that causes a G0/G1 cell cycle arrest in two different breast cancer cell lines without affecting cell viability (Schiaffino-Ortega et al., 2016). It is worth to add that there is a relevant shift between the **EB-3D** dose-response curves obtained for non-tumoral MCF-10A breast cell line cultured in resting condition (minimal medium) and stimulated with mitogenic factors (Figure 21). In fact mitogen-stimulated MCF-10A respond to **EB-3D** with two orders of magnitude lower GI_{50}.

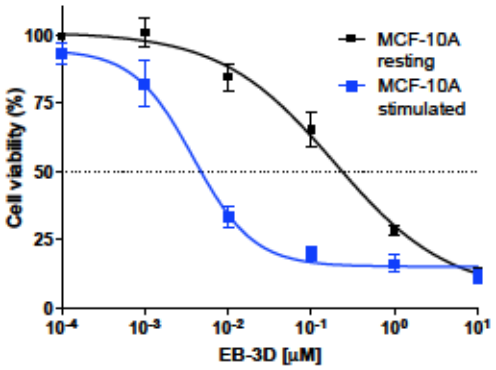

Figure 21: EB-3D cytotoxicity in non tumoral MCF-10A breast cell line

MTT cell proliferation assay of non tumoral MCF-10A breast cell line treated with **EB-3D** in resting (black line) and stimulated condition (blue line). Cell viability percentages are normalized to untreated cells. Symbols and bars represent respectively the mean ± SEM of three replicates.

In addition, we report also a significant dose-dependent reduction of the relative colony formation rate in MDA-MB-231 cells (Figure 22). To investigate deeply the effects of **EB-**

3D over time, we treated MDA-MB-231 cells with 0.5 µM of **EB-3D** up to 6 days and we observed a persistent arrest in cell proliferation (Figure 23 A), with no significant increase in cell death (Figure 23 B).

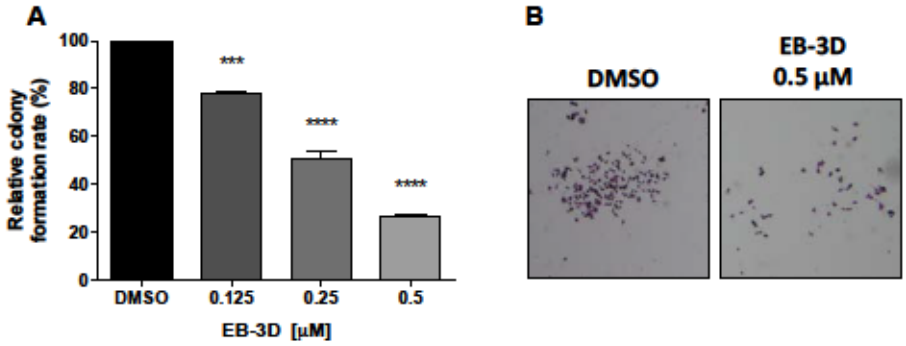

Figure 22: ChoKα inhibition reduces MDA-MB-231 clonogeneicity

(A) Relative colony formation rate of MDA-MB-231 treated with the indicated concentration of **EB-3D**. Data are depicted as mean ± SEM of three independent experiments. **Differences between control and treatements were analyzed using one-way ANOVA with Newman-Keuls correction.** (B) Representative pictures of one well-defined colony (>50 cells) with DMSO and undefined colony in **EB-3D-treated cells.**

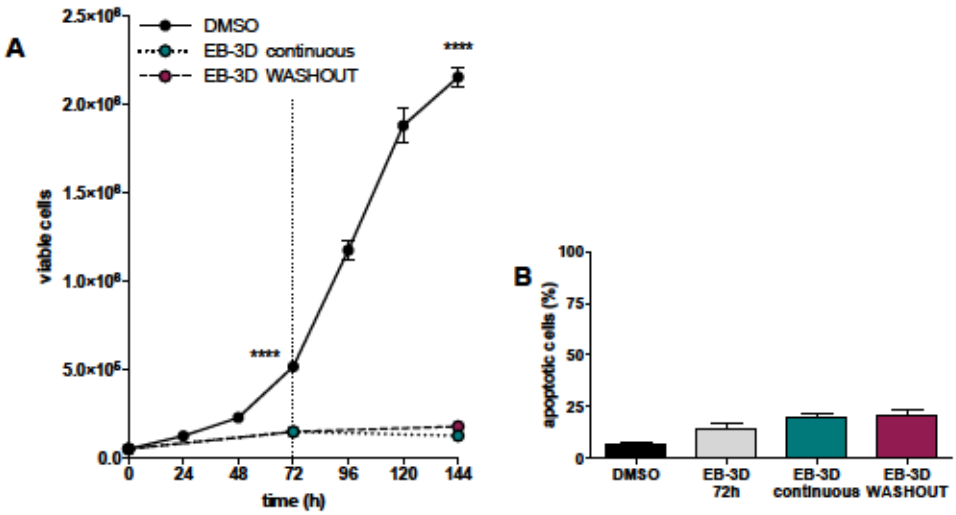

Figure 23: EB-3D irreversible cytostatic effect

(A) Trypan blue exclusion assay and **(B) flow cytometry analysis of cell death.** MDA-MB-231 cells were treated with 0.5 µM of **EB-3D** for 72 h and then medium were replaced with fresh medium with (**EB-3D** continuous) or without (**EB-3D** WASHOUT) the ChoKα inhibitor for further 72 h. Data are represented as mean ± SEM of three independent experiments. **Differences between control and both treatment schedules were analyzed using two-way ANOVA with Newman-Keuls correction. There is no significant difference in cell proliferation or cell death between EB-3D-continuous exposure (green) and EB-3D-washout (purple) at the final time point (144 h).**

More interestingly, the removal of **EB-3D** from media culture after 72 h of exposition suggests that the effects of ChoKα1 inhibition led to a irreversible cell growth. In fact we

do not observe a proliferation restart or any differences in cell number between continuous exposure of the drug and its withdrawn (Figure 23 A). This suggest that **EB-3D** induces MDA-MB-231 cell line to enter into an irreversible quiescent, rather than an apoptotic state.

EB-3D induces cellular senescence

The prolonged and irreversible effect of **EB-3D** treatment could be explained by the induction of cellular senescence. Indeed, we observed a strong increase in senescence-associated beta-galactosidase (SA-βgal) activity, a biomarker of senescent cells, through the conversion of its substrate C_{12}FDG after 72 h of **EB-3D** treatment (Figure 24 A). The analysis of mean fluorescence intensity (MFI) indicates that the effect is dose-dependent and, as expected, is irreversible even after **EB-3D** wash-out (Figure 24 B). The onset of senescence is confirmed also by the observation of typical morphological changes: cell size and granularity appear increased in MDA-MB-231 treated with **EB-3D** compared to control, confirmed also by the increase in forward scatter (FSC) and side scatter (SSC) observed by flow cytometry (Figure 25).

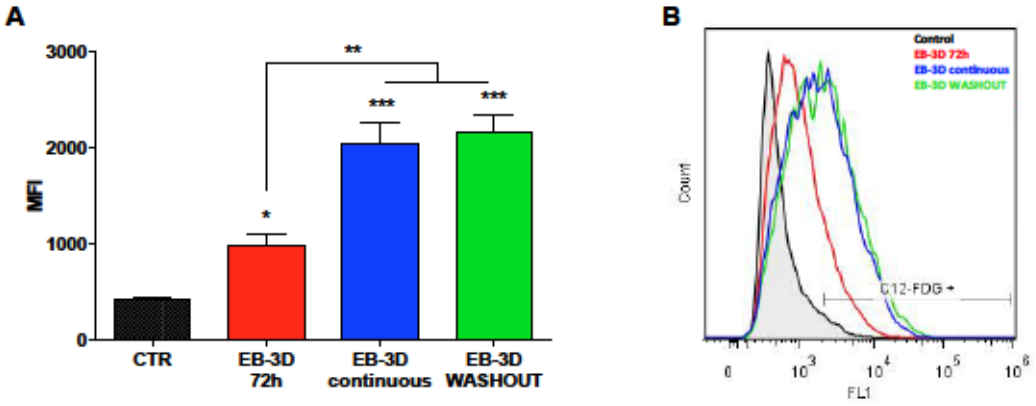

Figure 25: EB-3D induces cellular senescence

(A) Flow cytometry analysis of cellular senescence using C_{12}FDG probe and (**B**) representative histogram plot. MDA-MB-231 cells were treated with 0.5 μM of **EB-3D** for 72h (red color) and then medium were replaced with fresh medium with (**EB-3D** continuous, blue color) or without (**EB-3D** WASHOUT, green color) the ChoKα inhibitor for further 72h. Data are represented as mean ± SEM of three independent experiments. Differences between control and 72 h time point were analyzed using one-way ANOVA with Newman-Keuls correction.

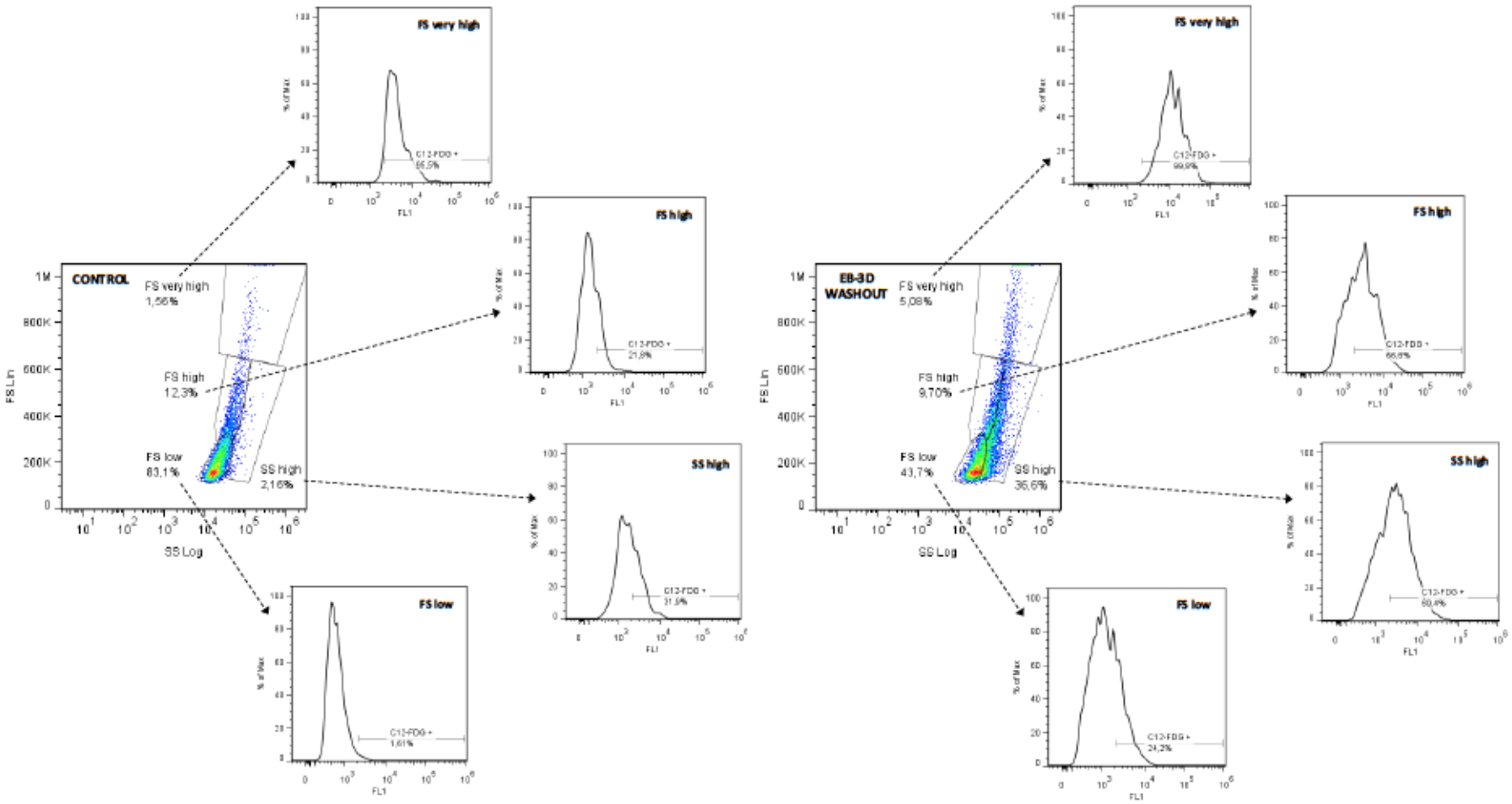

Figure 25: MDA-MB-231 morphological changes correlates with cellular senescence caused by EB-3D

Representative cytofluorimetric analysis of cellular senescence in MDA-MB-231 untreated (CONTROL, left panes) or treated for 72h with **EB-3D** 0.5µM and the following drug removal for other 72h (**EB-3D** WASHOUT, right panels). Biparametric density plots of forward scatter (FS) vs. side scatter (SS) showing the entire population (10000 events recorded). Cellular senescence was evaluated using C_{12}FDG probe (FL1) as described in the experimental section (A1-4 and B1-4). Untreated cells were divided in four gates according to their physical parameters: FS low, FS high, FS very high, SS high. After **EB-3D** treatment, MDA-MB-231 cells increase both in size (FS) and granulosity (SS), which corresponds to the increase in the percentage of senescent cells.

EB-3D sensitizes triple-negative breast cancer to common chemotherapeutic drugs.

Since **EB-3D** induced a strong decrease in cancer cell proliferation, we evaluated whether this drug had promise when used in combination with commonly used chemotherapeutics in TNBC treatment. To this end, MDA-MB-231 cells were treated for 48 h with **EB-3D** in combination with selected chemotherapeutic agents, i.e. doxorubicin (Doxo), 5-fluorouracil (5-FU) and cisplatin (Cis-Pt). **EB-3D** was combined with drugs at fixed molar ratio, and cell viability was analyzed by MTT assay. As previously described (Schiaffino-Ortega et al., 2016), **EB-3D** alone remarkably reduce MDA-MB-231 cell viability when used as a single agent, but when used in combination with chemotherapeutic drugs, we observed a synergistic increase in cytotoxicity with 5-FU (Figure 26 A), Doxo (Figure 26 B) and Cis-Pt (Figure 26 C). The synergistic effect is also confirmed by combination index (CI) values (Figure 26 D) obtained by the analytic method of Chou (Chou, 2006). For all tested combinations, we obtained CI < 0.3 that indicate a strong drug synergism.

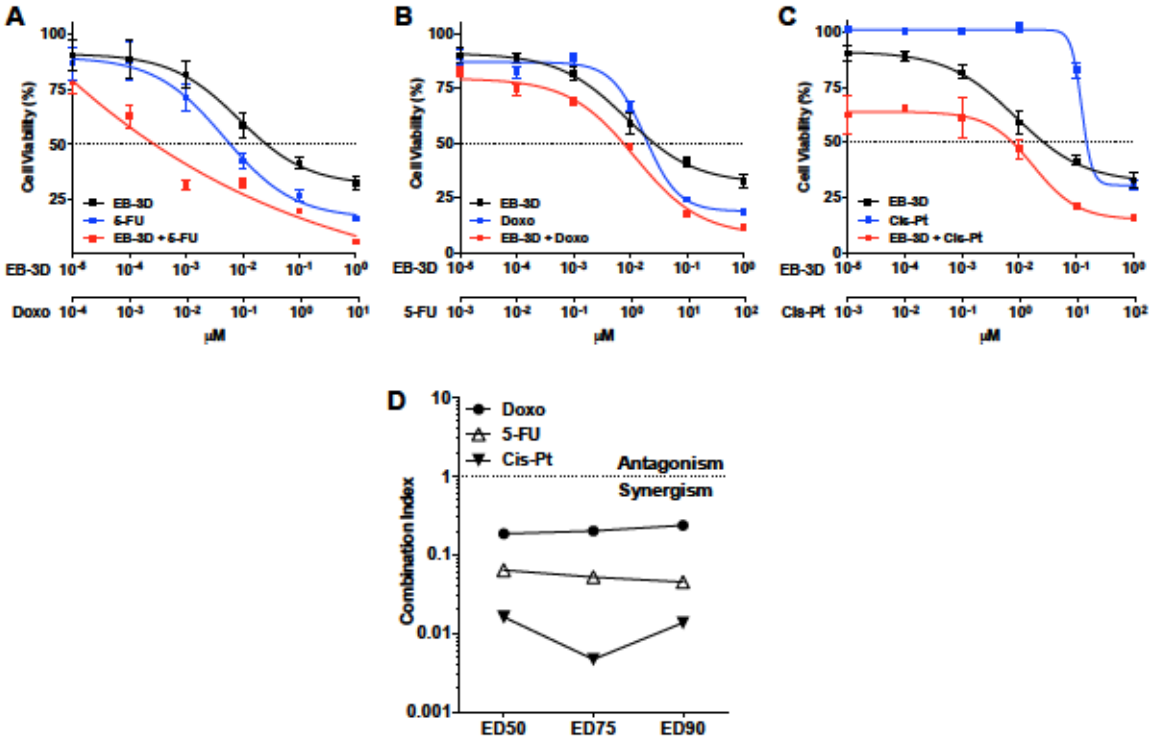

Figure 26: Drug synergism

Cell viability was evaluated by MTT analysis, performed after **EB-3D** (black lines), Doxo (**A**), 5-FU (**B**) and Cis-Pt (**C**) single drug treatments (blue lines) and their combination at fixed molar ratios (red lines). Points represent the mean ± SEM of three independent experiments. (**D**) Combination index (CI) values calculated at ED50, ED75 and ED90 for each drug combination described above.

Given the highly synergistic effect obatained with **EB-3D**/Cis-Pt, we then further characterized this combination. The simultaneous addition of **EB-3D** (1μM) and Cis-Pt (20μM) significantly increases the percentage of apoptotic cells compared to the single Cis-Pt treatment (12.8 ± 0.8 vs. 4.8 ± 0.6). Moreover, the pre-treatment with 1μM of **EB-3D** for 72h, which does not induce apoptosis itself, was able to drastically boost the apoptotic response to Cis-Pt in MDA-MB-231 cells (41.8 ± 1.7) (Figure 27).

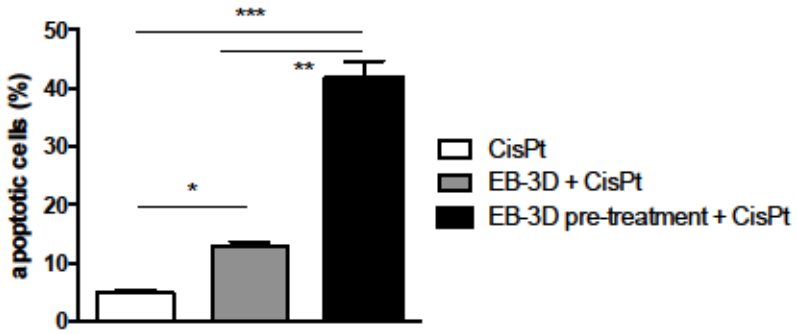

Figure 27: EB-3D pre-treatment sensitizes MDA-MB-231 cells to cisplatin

The apoptotic effect of **EB-3D** and cisplatin (CisPt) drug combination was evaluated by flow cytometry using Annexin-V-FITC (AV) and propidium iodide (PI) dual staining. MDA-MB-231 cells were treated for 72h with CisPt (20μM) alone, the simultaneous addition of **EB-3D** and CisPt or pre-treated with **EB-3D** and then treated with CisPt for further 72h. Were considered as apoptotic/dead cells all cells being alternatively stained for AV, PI or both. Bars represent the represent the mean ± SEM of three independent experiments. Differences between single CisPt treatment and the two combination schedules or within the two combinations, were analyzed using two-way ANOVA with Newman-Keuls correction.

ChoKα1 inhibition affects AMPK-mTOR signaling pathway

Reverse-phase protein array (RPPA) enables the measure of protein phosphorylation levels with high sensitivity and specificity, using antibodies specifically validated for RPPA. As depicted in Figure 28, MDA-MB-231 cells show a significant modulation in AMPK-mTOR signaling pathway following **EB-3D** treatment. RPPA data show that the treatment with 1 μM **EB-3D** triggers the activation of the metabolic stress sensor AMPK by the increase in phosphorylation of residue T172 of catalytic subunit α. AMPKα represses mTORC1 pathway as shown by mTOR S2448 dephosphorylation. The inhibition of mTOR in turn reduces p70S6K S371, 4E-BP1 S65 and S6K ribosomal protein S235/236 phosphorylations. Phosphorylation of 4E-BP1 and S6K required for the initiation and progression of mRNA translation process respectively.

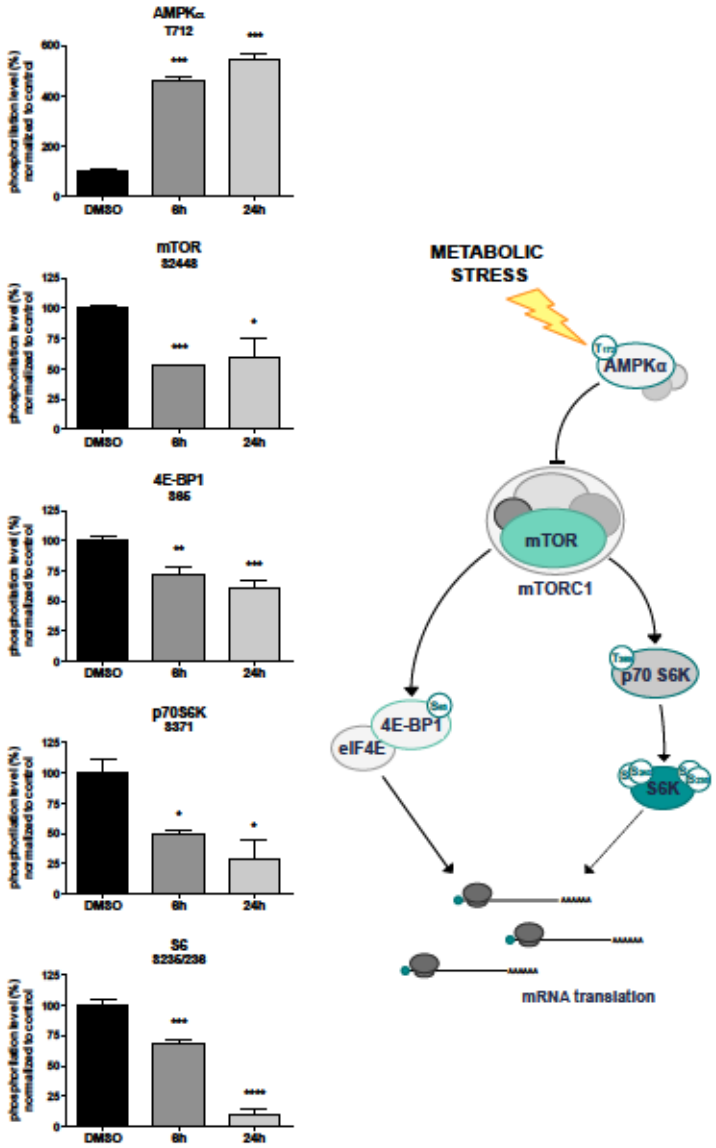

Figure 28: EB-3D affects AMPK-mTOR signaling pathway

MDA-MB-231 cells were treated with 1µM of **EB-3D** or vehicle for the indicated time points. Cells were then lysed and whole cell proteome was subjected to RPPA analysis using validated antibody against AMPKα-T712, mTOR-S2448, 4EBP1-S65, p70S6K-S371 and S6-S235/236 phosphorylations. Bars represent mean ± SEM of three independent experiments. Differences between control and treated samples were analyzed using ANOVA test for repeated measures with Newman-Keuls correction.

In vivo tumor growth inhibition

To examine the antitumorigenic potential of **EB-3D** *in vivo*, we opted in favour of a immunocompetent syngeneic EO771-C57BL/6 mouse model. The fact that there is more than 88% of sequence homology between human and mouse ChoKα1 and that all the aminoacids shown to be important for interaction with **EB-3D** or its stabilization (Schiaffino-Ortega et al., 2016) are perfectly conserved (Supplementary Table 1), suggests

that our compound should inhibits also the mouse homolog. EO771, a mammary adenocarcinoma cell line derived from a C57BL/6 mouse, are immunohistochemically classified as basal-like tumour, a subtype associates with poor prognosis in humans. EO771 are immunosuppressive and highly aggressive, giving rise to lung metastasis that closely mirror those of the human breast tumor (Johnstone et al., 2015). Preliminarly, the cytostatic effect of **EB-3D** was confirmed also in murine cells. **EB-3D** reduces EO771 cell viability with GI_{50} = 0.31 μM and is more efficient than **MN58b** (GI_{50} = 1.65 μM) and **RSM932A** (GI_{50} = 2.86 μM) (Fig. 29 A) without relevant cytotoxic effects (Fig. 29 B), confirming the *in vitro* data obtained in human MDA-MB-231 cell line.

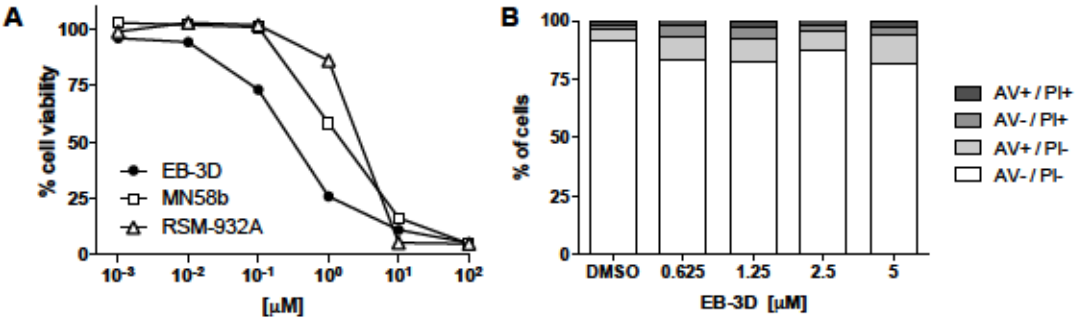

Figure 29: *In vitro* cytostatic effect of EB-3D in mouse EO771 breast cancer cell line

(**A**) EO771 cell viability was evaluated by MTT assay after 72h of treatment with **EB-3D**, **MN58b** and **RSM-932A**. (**B**) Analysis of apoptosis induced by **EB-3D** at the indicated concentrations for 72h in EO771 cells. Apoptosis was evaluated by flow cytometry by staining cells with Annexin-V-FITC (AV) and propidium iodide (PI).

C57BL/6 mice treated with **EB-3D** displayed a significant reduction in tumor growth at the low dose of 1 mg/kg (Figure 30) Interestingly, a significant decrease of the tumor volume appears just after the second injection and remain till the completion of the experiment. At this point we observed a reduction of about 210% of the tumor volume. Healthy C57BL/6 mice were treated with 2.5 mg/kg of **EB-3D** for toxicity and no significant weight loss, behavioral changes and fur appearance were observed in treated mice compared to controls (data not shown).

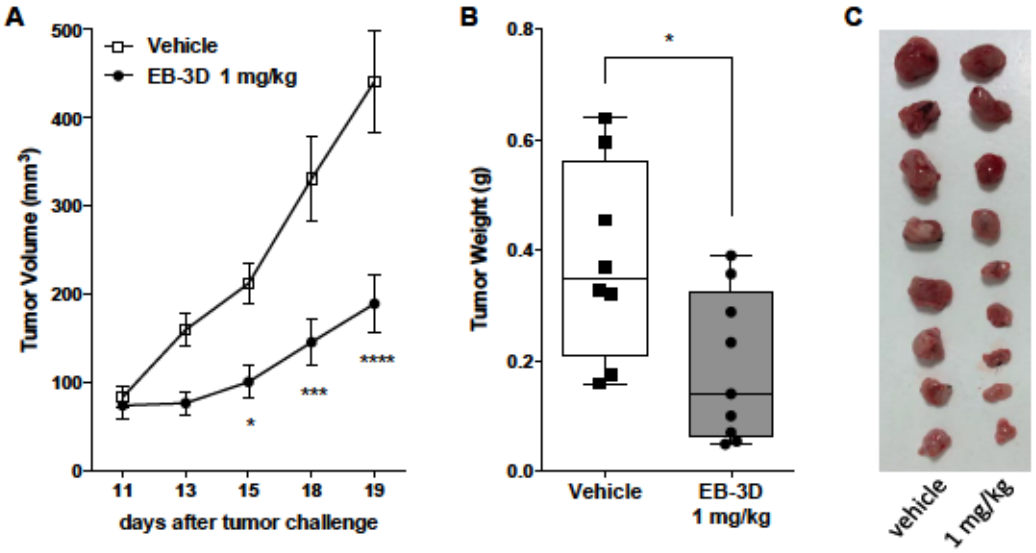

Figure 30: ChoKα inhibition impairs mammary tumor growth in vivo.

Average mammary EO771 tumor volume of mice injected with either vehicle (DMSO) or 1 mg/kg of **EB-3D** (n = 8/treatment) (**A**); Average weight (**B**) and macroscopic images (**C**) of resected tumors at the conclusion of the experiment. Values are depicted as mean ± SEM. Tumors were measured in two dimensions and tumor volume V (mm^3) was calculated according to the formula V=(D x d2)/2, where D and d are the major and minor perpendicular tumor diameters, respectively. Differences between control and treated mice were analyzed using Student t test using Bonferroni correction.

EB-3D suppresses *in vitro* cell migration and invasion

Since ChoKα is involved in phosphatidylcholine biosynthesis and the alteration of cell membrane structure can reduce motility and invasiveness of tumor cells, we evaluated if **EB-3D** is able to suppress MDA-MB-231 migration and invasion upon treatment. Figure 31 A shows the representative images of wound-healing assay in MDA-MB-231 cells treated with different concentration of **EB-3D**. The inhibition of ChoKα mediated by **EB-3D** resulted in a dramatic impairment of migration of MDA-MB-231 cells that are no longer able to close the scratch in a concentration dependent manner (Fig 31 B). In addition, a cell matrix invasion assay has been performed in MDA-MB-231 cells pre-treated with **EB-3D** for 24 h. ChoKα inhibition significantly impairs the ability of the highly invasive MDA-MB-231 to pass through a basal membrane extract (BME)-coated transwell within 24 h (Figure 31 C).

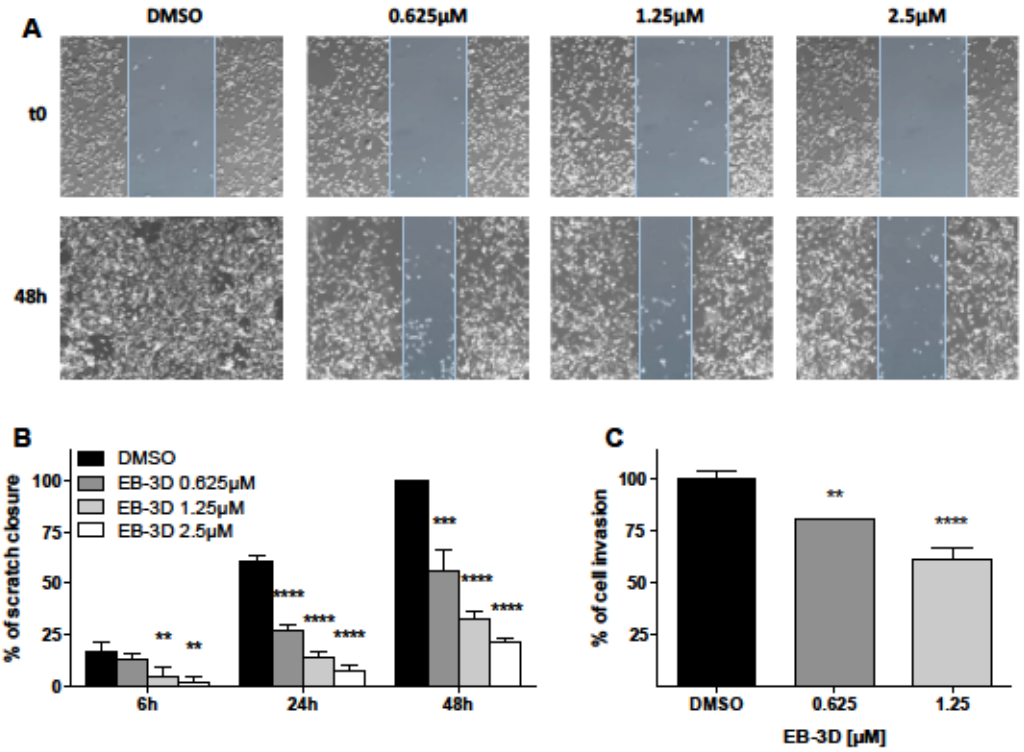

Figure 31: EB-3D impairs MDA-MB-231 motility and invasiveness

Confluent MDA-MB-231 monolayer was scratched and treated with **EB-3D** at the indicated concentrations and monitored at 6, 24 and 48 h. (**A**) Representative images of wound closure after treatment with **EB-3D**, 10X magnification. The distance between the two edges of the scratch is marked in blue. (**B**) Bar graphs showing relative quantification of the distance between scratch edges at the indicated time points. (**C**) Relative quantification of BME-based invasion assays performed with MDA-MB-231 pre-treated with **EB-3D** at the indicated doses. Difference between DMSO and treated cells were analyzed using one-way ANOVA using Newman Keuls correction.

Metastasis formation is reduced by EB-3D treatment

Since we observed that ChoKα inhibition mediated by **EB-3D** is involved in cell migration and invasion, two common features of metastatic cells, we decided to test if **EB-3D** is able to reduce metastasis formation *in vivo*. The treatment of EO771-C57BL/6 mice after primary tumor removal shows only a trend in reduction of the number of spontaneous lung macro- and micro-metastasis (Figure 32 A-B). It must be pointed out that the complexity of the experimental procedure implies high variability in the number of metastasis within controls. However, the observed trend is corroborated by the statistically significant reduction of experimentally-induced lung macro- and micro-metastasis (Figure 32 C-D) in **EB-3D** treated mice compared to untreated ones.

Lastly, **EB-3D** administration also inhibits the number of experimental lung macro-metastasis (Figure 32 E) and resected lung weight (Figure 32 F-G) after intravenous

injection of MDA-MB-231 cells in xenograft NOD/SCID mice. Representative photomicrographs of lung tissue sections from control and treated xenograft MDA-MB-231-NOD/SCID mice are shown in Figure 32 H, where the reduction of metastatic lesion size between control and **EB-3D** treated becomes evident.

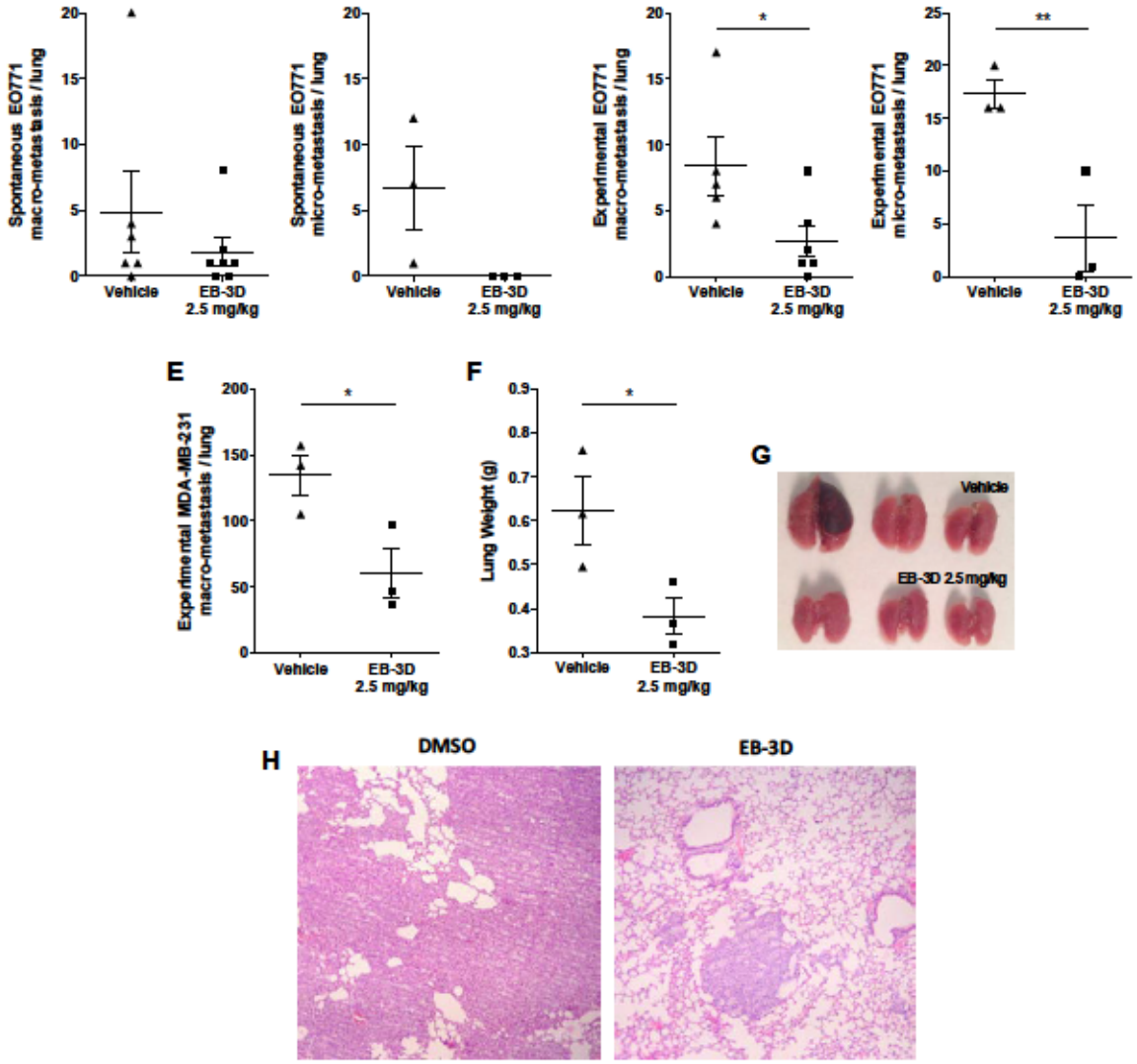

Figure 32: ChoKα inhibition reduces lung metastasis formation

(**A**) Number of spontaneous lung macro-metastasis and (**B**) micro-metastasis after primary EO771 tumor removal. Mice were treated i.p. for 4 weeks every other day with either vehicle (DMSO, n=5) or 2.5 mg/kg of **EB-3D** (n=7); (**C**) Number of experimentally-induced lung macro-metastasis and (**D**) micro-metastasis after i.v. injection of EO771 cells and 3 weeks treatement with either vehicle (DMSO, n=5) or 2.5 mg/kg of **EB-3D** (n=6); (**E**) Number of experimentally-induced lung macro-metastasis after i.v. injection of human MDA-MB-231 cells in NOD/SCID mice and 7 weeks treatement with either vehicle (DMSO, n=3) or 2.5 mg/kg of **EB-3D** (n=3) and (**F**) average lung weight and (**G**) macroscopic images of resected lungs at the conclusion of the experiment. Values are depicted as mean ± SEM. Differences between control and treated mice were analyzed using Student t test using Bonferroni correction. (**H**) Representative H&E staining performed on lung tissue sections from control and treated xenograft MDA-MB-231-NOD/SCID mice. Original magnification 10X.

3.2.4 DISCUSSION

In this study we proved that the new choline kinase inhibitor **EB-3D**, belonging to the class of symmetrical biscationic ChoKα inhibitors, is a promising agent for triple-negative breast cancer treatment. We observed impaired cell proliferation and clonogenicity as well as the increase in drug sensitivity upon **EB-3D** treatment in MDA-MB-231 cells.

Here we demonstrated that the small molecule **EB-3D** specifically targets ChoKα enzyme as pointed out by the decrease of PCho and the matched decrease of tCho levels in water-phase extracts of treated cells. We also observed a two-fold increase in Cho levels after treatment that can be explained as the accumulation of ChoKα substrate, supporting the enzymatic inhibition. The absence of Cho decrease is reassuring but we cannot rule out the possibility of choline transport inhibition, as this event was not examined here. The increase in PCho level is required for G1-S transition (Rodriguez-Gonzalez et al., 2004) and its reduction is consistent with the previously reported cycle arrest in G0/G1 phase due to **EB-3D** (Schiaffino-Ortega et al., 2016). Blockade of cell proliferation is maintained even after compound removal suggesting that ChoKα inhibition is irreversible or at least that the damages caused by **EB-3D** are permanent. Indeed, to our knowledge we proved for the first time that cellular senescence can be induced by targeting choline metabolism in TNBC. The pharmacological inhibition of ChoKα with **EB-3D** significantly increases the activity of the senescent marker SA-βgal in MDA-MB-231 breast cancer cells and **EB-3D** removal does not lead to growth recovery, conversely to what has been reported for the novel non-symmetrical ChoKα inhibitor **V-11-0711** (Falcon et al., 2013). In addition, the two-fold increase of GPCho/PCho ratio observed has also been described as a feature of senescent cells, independently from the type of senescence (Gey and Seeger, 2013). The induction of cellular senescence in triple-negative MDA-MB-231 is also in perfect agreement with the absence of cytotoxicity observed in this cell line compared to other tumor cells treated with **EB-3D**, such as Jurkat and HeLa (Schiaffino-Ortega et al., 2016). The absence of apoptosis is in contrast to published data for **MN58b** (Rodriguez-Gonzalez et al., 2005; Rodriguez-Gonzalez et al., 2004) and **RSM-932A** (Lacal and Campos, 2014), whereas similar behavior has been reported for **V-11-0711** (Falcon et al., 2013; Mori et al., 2015). It has been described that in MDA-MB-231 cells the gain-of-function mutant p53 is stabilized by phospholipase D preventing cell death during starvation (Hui et al., 2006) and excessive/uncontrolled p53 activation has been associated to aging (Rufini et al., 2013). Thus, the overexpression and stabilization of p53 protein could explain the peculiar non-

lethal response to **EB-3D** observed in MDA-MB-231 compared to p53 wild-type cell lines (e.g. HeLa) or p53-null cell lines (e.g. Jurkat).

Whilst cellular senescence is known to be a permanent and irreversible process, the senescence-associated secretory phenotype (SASP) has been pointed out as a potential strategy to promote tumor progression (Pérez-Mancera et al., 2014) and drug resistance (Canino et al., 2011). Thus, the induction of cellular senescence could be a double-edged sword in cancer. On the contrary, we demonstrated that **EB-3D**-induced senescence sensitizes MDA-MB-231 cells to the apoptotic effect of cisplatin. This result reveals that the onset of cellular senescence in tumoral cells might be advantageous in this case. **EB-3D** also enhances the chemotherapeutic effects of 5-FU and doxorubicin significantly lowering their GI_{50} values. All together, these data suggest that ChoKα inhibition could be a potential neoadjuvant and could augment the effects of conventional chemotherapy for TNBC, pointing towards its potential clinical utility although if further studies are needed to better understand the molecular mechanism(s) involved in the synergistic effect.

To investigate the mechanisms underlying cell cycle arrest and cellular senescence induced by **EB-3D**, we adopted a phosphoproteomic approach using reverse-phase protein array (RPPA). RPPA data highlighted a modulation of the AMPK-mTOR metabolic pathway. Indeed, Trousil *et al.* recently described that the ChoKα inhibitor **ICL-CCIC-0019** reduces mitochondria respiration and ATP production, leading to AMPK activation, without increasing ROS species production (Trousil et al., 2016) revealing a non-canonical mitochondrial damage response (Houweling et al., 2002). We report the activation of AMPK stress sensor, that causes the reduction of mTOR phosphorylation and its downstream targets 4E-BP1, p70S6K and S6K. The dephosphorylated form of 4E-BP1, which sequester the eukaryotic translation initiation factor 4E (eIF4E), together with the absence of the active hyperphosphorylated form of S6K, prevent that initiation and progression of mRNA translation process. Collectively, these data suggests that ChoKα inhibition by **EB-3D** is sensed like a metabolic insult in MDA-MB-231 cells causing the of mTORC1 final effectors required for protein synthesis. These observations corroborate the observed reduction in cell proliferation and G0/G1 cell cycle arrest following **EB-3D** treatment. In this context it is interesting to note that increased AMP-ATP ratio and AMPK activity were observed during cellular senescence in fibroblasts (Wang et al., 2003). Consistently, sustained AMPK activation was observed during radiation-induced senescence (Liao et al., 2014) although other research groups report that activation of

AMPK prevents H_2O_2-induced senescence (Han et al., 2016; Ido et al., 2012) triggering autophagy (Guo et al., 2012). Therefore, the induction of AMPK activation by **EB-3D** could be involved in cellular senescence in MDA-MB-231 cells. Thus it will be important to demonstrate through future experiments the possible relationship and the link between the inhibition of choline kinase α and the activation of metabolic stress, consequently leading to cellular senescence.

In this work we have also demonstrate the efficacy of **EB-3D** as potent antitumor agent *in vivo* in a syngeneic mouse model. It is worth to note that the effect of the drug is evident already after the second administration at low dose (1 mg/Kg i.p.), indicating a potent antitumor effect and a favourable pharmacokinetics. Importantly we did not observe any sign of apparent toxicity.

Since ChoKα is the first enzyme involved in phosphatidylcholine biosynthesis, the most abundant membrane lipid, is reasonable to assume that ChoKα plays an important role in cell membrane stability and therefore in migration and invasion processes. Indeed it has been recently reported that ChoKα inhibition suppresses epithelial-to-mesenchimal (EMT) transition in glioblastoma (Koch et al., 2016). **EB-3D**-mediated ChoKα inhibition drastically reduces tumor cell motility and invasiveness *in vitro* in the highly aggressive MDA-MB-231.

The high mortality rate associated with TNBC is due primarily to the onset of metastases, mainly targeting lung, liver, bones and brain. Hence, research efforts should focus also on the development of new therapies for secondary metastatic lesions prevention. For this reason, the anti-metastatic effect of **EB-3D** was tested also *in vivo* using both allogeneic and xenogeneic models. Indeed, an essential component for new pharmacological agents testing is the assessment of their efficacy in preclinical settings. However, very few preclinical models that incorporate the relevant features of human metastatic disease are available. We were able to provide preliminary evidence of reduction of spontaneous lung metastatic nodules in mice treated with **EB-3D** after primary tumor resection, but the effect become more evident when tumor cells were injected intravenously.

To conclude, the new ChoKα a inhibitor **EB-3D** provided excellent antiproliferative effects *in vitro* and resulted to be an effective antitumoral agent in preclinical TNCB model. For these reasons, we claim that **EB-3D** is worthy of further studies in breast cancer as well as in other tumors.

3.3 Choline kinase alpha inhibition as a new potential therapeutic strategy in pediatric T acute lymphoblastic leukemia (T-ALL)

Elena Mariotto, Ilaria Volpin, Roberta Bortolozzi, Davide Carta, Valentina Serafin, Benedetta Accordi, Giuseppe Basso, Luisa Carlota López-Cara, Giampietro Viola

3.3.1 ABSTRACT

Aberrant choline metabolic profile and concomitant ChoKα overexpression have been described in most human tumors, including lung, breast, and prostate cancer. Very little is known about the role of ChoKα and choline metabolism in hematological malignancies. With this purpose we investigated the effect of a novel and selective ChoKα inhibitor namely **EB-3D** in T acute-lymphoblastic leukemia (T-ALL). We first demonstrate that, as occurs in other tumors, ChoKα is upregulated also in T-ALL cell lines in comparison to healthy lymphocytes, suggesting a potential role of this enzyme in tumor growth and proliferation. The drug exhibits a potent antiproliferative activity in a panel of T-leukemia cell line with a GI_{50} ranging from 0.9 to 479 nM and it also displays a significant activity in primary cultures derived from pediatric T-ALL patients. The antiproliferative activity is likely due to a remarkable decrease of phosphocholine levels observed upon treatment of CCRF-CEM cells with **EB-3D** indicating that ChoKα may be essential in T-ALL cell survival and proliferation. Moreover, the drug strongly induces apoptosis as evidenced by the appearance of Annexin-V positive cell upon treatment and, more importantly, it enhances T-leukemia cell sensitivity to chemotherapeutic and biotherapeutic agents, such as dexamethasone and L-asparaginase. In addition we also evaluated in detail, by means of Reverse Phase Phosphoproteomic Analysis (RPPA), the initial alterations of protein phosphorylation levels in T-ALL cells upon treatment with the purpose to investigate the mechanism of action. The results show that the compound is able to induce an early activation of AMP-activated protein kinase (AMPK), the main regulator of cellular energy homeostasis, by its phosphorylation at residue T712 of catalytic subunit α. This in turn represses the mammalian target of rapamycin complex 1 (mTORC1) pathway as shown by mTOR S2448 dephosphorylation. The inhibition of mTOR affects the activity of several known downstream targets, such as 4E-BP1, p70S6K, S6K and GSK3, ultimately leading to a reduction of protein synthesis and cell cycle arrest. Interestingly, **EB-3D** induces only a modest activation over time of AMPK-mTOR in healthy lymphocytes that does not impact on downstream effector inactivation, suggesting other pathways intervention. Taken together, our findings suggest that targeting ChoKα may be an interesting option for treating T-ALL and that **EB-3D**, could represent a valuable therapeutic tool, although further experiments are needed.

3.3.2 INTRODUCTION

T cell acute lymphoblastic leukemia (T-ALL) is an aggressive hematologic disorder resulting from the malignant transformation of T cell progenitors. T cell transformation is a multi-step process in which different genetic alterations cooperate to alter the normal mechanisms that control thymocytes development. T-ALL accounts for about 15% of pediatric ALL cases. The overall 5-year survival rate for children with T-ALL is now more than 75% (Schrappe et al., 2011), however the outcome of T-ALL patients with primary resistant or relapsed leukemia remains poor (Locatelli et al., 2012). For this reason, there is still an intense effort in finding new therapeutic strategies to improve protocols for high-risk leukemic patients.

Dysregulation of specific tyrosine kinases in sustaining T-ALL pathogenesis has been described (Kruse et al., 2010; Roberts et al., 2012). However, although a low percentage of patients are successfully treated with kinase inhibitors, most of them do not take advantage from this form of therapy. Starting from the evidence that signal transduction proteins regulate nearly all aspects of cell life and death by the phosphorylation of proteins which is catalyzed by protein kinases and that their deregulation plays a critical role in hematologic disorders, kinases are the first choice druggable targets as they are enzymes, whose biological activity can be therefore turned off by drugs that block their catalytic site.

Choline kinase α1 (ChoKα1) has recently become an interesting therapeutic target since its overexpression has been associated to tumorigenesis in many cancers (Granata et al., 2014; Hernández-Alcoceba et al., 1999; Ramírez de Molina et al., 2002d). In particular ChoKα expression has been extensively described in breast cancer, where it correlates with tumor grade and poor clinical outcome (Ramírez de Molina et al., 2002a). ChoK catalyzes the phosphorylation of choline (Cho) to phosphocholine (PCho) in the first step of the CDP-choline branch of Kennedy's pathway for phosphatidylcholine (PtdCho) synthesis. In humans, three isoforms of ChoK have been described (Aoyama et al., 1998a; Aoyama et al., 1998b): ChoKα1 (457 amino acids) and ChoKα2 (439 amino acids) are alternative splicing forms generated from a single gene *CHKA*, and ChoKβ (395 amino acids) encoded by *CHKB* gene. ChoK isoforms are ubiquitously expressed in tissues (Aoyama et al., 2002) and isoforms associates to form homo- or hetero-dimers that constitute the active enzymatic form (Ishidate, 1997). Despite high gene and protein sequences similarity, only ChoKα1 isoform has been proposed as oncogenic promoting factor. Indeed, specific *CHKA* silencing induces apostosis in tumor cells, while *CHKB* silencing has no effect (Gruber et

al., 2012). Besides the overexpression of ChoKα is sufficient to drive cell proliferation of quiescent human mammary epithelial cells promoting DNA synthesis and cell cycle progression (Ramírez de Molina et al., 2004a). Thus, the overexpression and overactivation of ChoKα lead to abnormal choline metabolism, resulting in higher levels of phosphocholine and total choline-containing compounds (tCho) in general. This phenomenon has recently been called "cholinic phenotype" and it has been associated with oncogenesis and tumor progression (Glunde et al., 2011)

As much as the cholinic phenotype has been described for various solid tumors, far too little is known about it in lymphoblastic disorders. Recently, a serum metabolomic study performed in T-cell lymphoma patients has highlighted the dysregulation of choline metabolism (Xiong et al., 2015). The purpose of this study is to give insight into choline metabolism in T acute lymphoblastic leukemia and to accomplish this goal we inhibited choline kinase with the recently described ChoKα1 inhibitor **EB-3D**.

EB-3D (also referred as **10a**) is a symmetrical biscationic ChoKα1 inhibitor reported to strongly impair cell proliferation in a variety of different cancer cell lines (Schiaffino-Ortega et al., 2016). In triple-negative breast cancer, **EB-3D** induced the irreversible arrest of cell proliferation prompting cells to cellular senescence, inhibited both cell migration and invasion and modulated the AMPK-mTOR signaling pathway ultimately leading to protein synthesis blockade (Mariotto et al., unpublished data). In addition, **EB-3D** showed good antitumoral and antimetastatic activity *in vivo*.

The effects of **EB-3D** *in vitro* on cell viability, cell proliferation and cell death were evaluated in this work. In addition, we performed a phosphoproteomic analysis by Reverse-Phase Protein Array (RPPA) which pointed out a relevant difference in pathway modulation between tumoral cell lines and normal lymphocytes. Lastly, the ability of **EB-3D** to enhance the anti-tumorigenic potential of drugs commonly used in pediatric T-ALL protocols was also tested.

3.3.3 RESULTS

ChoKα is overexpressed in T-ALL cell lines

Since ChoKα is overexpressed in many tumors but very little is known about its expression in haematological malignancies, ChoKα expression levels were evaluated in a panel of T leukemic cell lines. Figure 33 shows the collective overexpression of ChoK isoforms in T-ALL cell lines compared to peripheral blood lymphocytes (PBL) collected from healthy donor, PBL stimulated with phytohemagglutinin (PHA) or CD3-positive (CD3+) T lymphocytes (Figure 3). ChoKα isoforms are strongly overexpressed in T-ALL cell lines while their expression is almost undetectable in controls. In particular, it is worth to note that the oncogenic isoform ChoKα1 (457 aa) is expressed at higher levels than ChoKα2 (439 aa) in all T-ALL cell lines. The predominant isoform of choline kinase in normal lymphocytes appears to be the ChoKβ isoform, wherease the ChoKα/ChoKβ ratio is weighted in favour ChoKα in T-ALL.

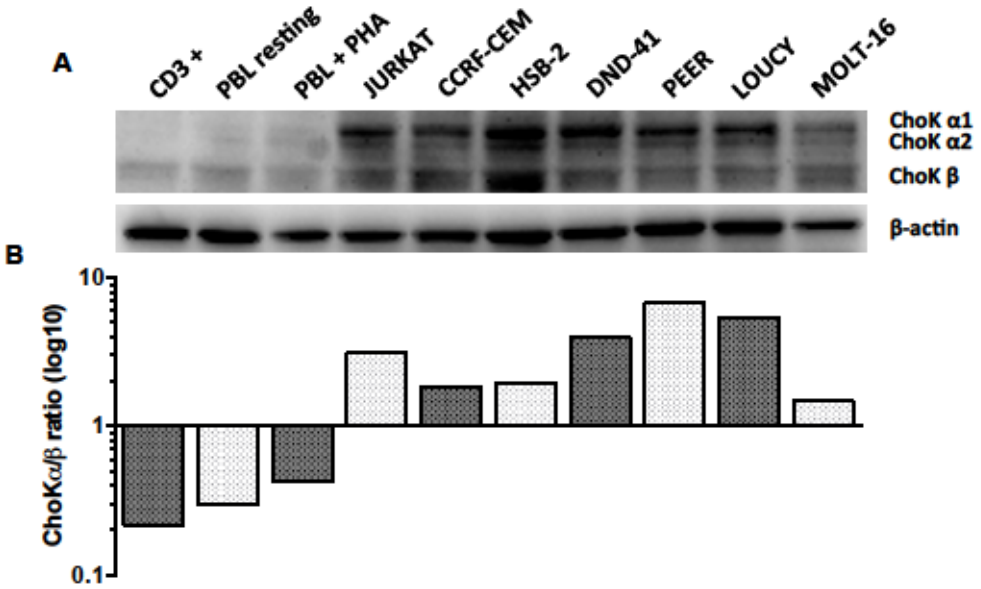

Figure 33: ChoKα is overexpressed in T-ALL cell lines

(**A**) Immunoblot analysis of ChoK isoforms in different T-ALL cell lines and healthy controls and (**B**) densitometry analysis of ChoKα/β ratio. PBL, peripheral blood lymphocytes. PHA, phytohemagglutinin. CD3+, T lymphocytes

EB-3D antiproliferative activity in T-ALL cell lines and primary cells

As shown in Table 5, **EB-3D** displays excellent antiproliferative activity against a wide cohort of T leukemic cell lines, with GI_{50} values in the nanomolar range and resulting more

cytotoxic compared to the reference compounds **RSM932A** and **MN58b**. The most sensitive cell line is MOLT-16 with GI_{50} of 0.9 ± 0.6 nM whereas CCRF-CEM was the less sensitive with GI_{50} of 479 ± 152 nM. However there is no correlation between GI_{50} and ChoKα expression level nor ChoKα/β ratio. In addition the novel ChoKα inhibitor **EB-3D** shows lower cytotoxicity in PBLs (GI_{50} 1500 ± 640 nM) compared to leukemic T cell lines (Table 6). On the other hand, the treatment results more toxic when PBLs are stimulated with PHA (GI_{50} 34 ± 10 nM), indicating a certain preference toward cells in active phase of proliferation (Figure 34 A).

ChoKα1 Inhibitor	Antiproliferative activity GI_{50} (nM)							
	JURKAT	CCRF-CEM	HSB-2	MOLT-16	DND-41	LOUCY	PEER	ALL-SIL
EB-3D	**136.2 ± 36.2**	**478.8 ± 152.5**	**17.7 ± 1.8**	**0.9 ± 0.6**	**60.6 ± 28.6**	**200.0 ± 51.6**	**265.0 ± 31.9**	**132 ± 101**
MN-58b	634.8 ± 226.4	214.6 ± 89.1	138.0 ± 24.8	19.7 ± 3.7	443.4 ± 112.4	236.8 ± 118.4	496.7 ± 46.3	336 ± 102
RSM-932A	563.6 ± 163.9	608.9 ± 146.4	173.3 ± 20.3	171.1 ± 82.2	152.7 ± 70.5	1016.7 ± 370.5	386.7 ± 37.6	295 ± 125

Table 5: EB-3D antiproliferative activity in T-ALL cell lines

In vitro antiproliferative effect of **EB-3D**, **RSM932A** and **MN58b** in T leukemia cell lines. [b] GI_{50} = Compound concentration required to inhibit tumour cell proliferation by 50%. Values are the mean ± SEM for three independent experiments.

ChoKα1 Inhibitor	Antiproliferative activity GI_{50} (nM)	
	PBL resting	PBL + PHA
EB-3D	**1500 ± 640**	**34 ± 10**
MN-58b	2000 ± 420	150 ± 30
RSM-932A	900 ± 210	230 ± 50

Table 6: EB-3D antiproliferative activity in primary normal lymphocytes

In vitro antiproliferative effect of **EB-3D**, **RSM932A** and **MN58b** in healthy peripheral blood lymphocytes (PBL) in resting condition and stimulated with phytohemagglutinin (PHA). [b] GI_{50} = Compound concentration required to inhibit tumour cell proliferation by 50%. Values are the mean ± SEM for three different donors.

The antiproliferative effect of **EB-3D** was confirmed also in primary T-ALL collected from pediatric patients at diagnosis. As depicted in Figure 34 B, there is a certain variability of response to the treatment between different patients that could be due to the

different sub-classes of T-ALL. In particular, two patients who were diagnosed as Early T cell Precursor (ETP) leukemia, characterized by poor response to standard intensive chemotherapy and very high risk of relapse, appear quite resistant to **EB-3D** compared to later phenotype stage T-ALLs (T-III).

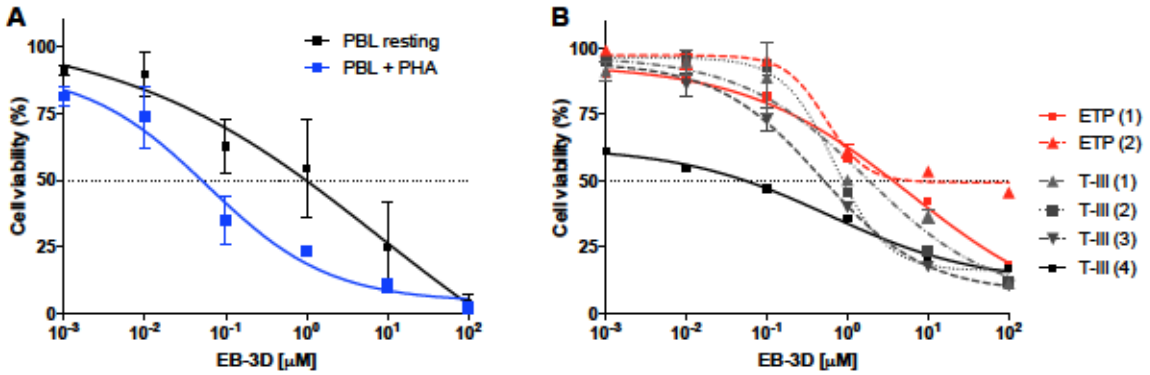

Figure 34: EB-3D cytotoxicity in healthy PBLs and primary T-ALL pediatric samples

(**A**) MTT cell proliferation assay carried out after 72 h in peripheral blood lymphocytes (PBL) collected from healthy donors treated with **EB-3D**, with or without phytohemagglutinin (PHA) stimulation. (**B**) MTT cell proliferation assay in primary T-ALL treated with **EB-3D** and carried out after 48 h of treatment. Cell viability percentages are normalized to untreated cells. Symbols and bars represent respectively the mean ± SEM of three different donors (A) or experimental triplicate of the same T-ALL patient (B). ETP, Early T cell Precursor. T-III, cortical T-ALL.

The cytotoxic effect caused by EB-3D is irreversible

We previously reported that **EB-3D** treatment significantly inhibits cell growth in different tumoral cell lines, including Jurkat cells, in a concentration dependent manner, due to a strong G0/G1 arrest of the cell cycle (Schiaffino-Ortega et al., 2016). Contrary to what we observed in breast cancer (Mariotto et al., unpublished data), **EB-3D** induces a dose-dependent increase in apoptotic cells in T-ALL cell lines after 72 h of treatment (Figure 35 A). Moreover, the mechanisms activated by ChoKα inhibition that trigger apoptosis are rapid and irreversible since wash-out experiments demonstrate that 24 h of exposure to **EB-3D** (that causes only a slight increase of apoptosis) are sufficient to induce a strong apoptotic response 72 h after compound withdrawal (Figure 35 B).

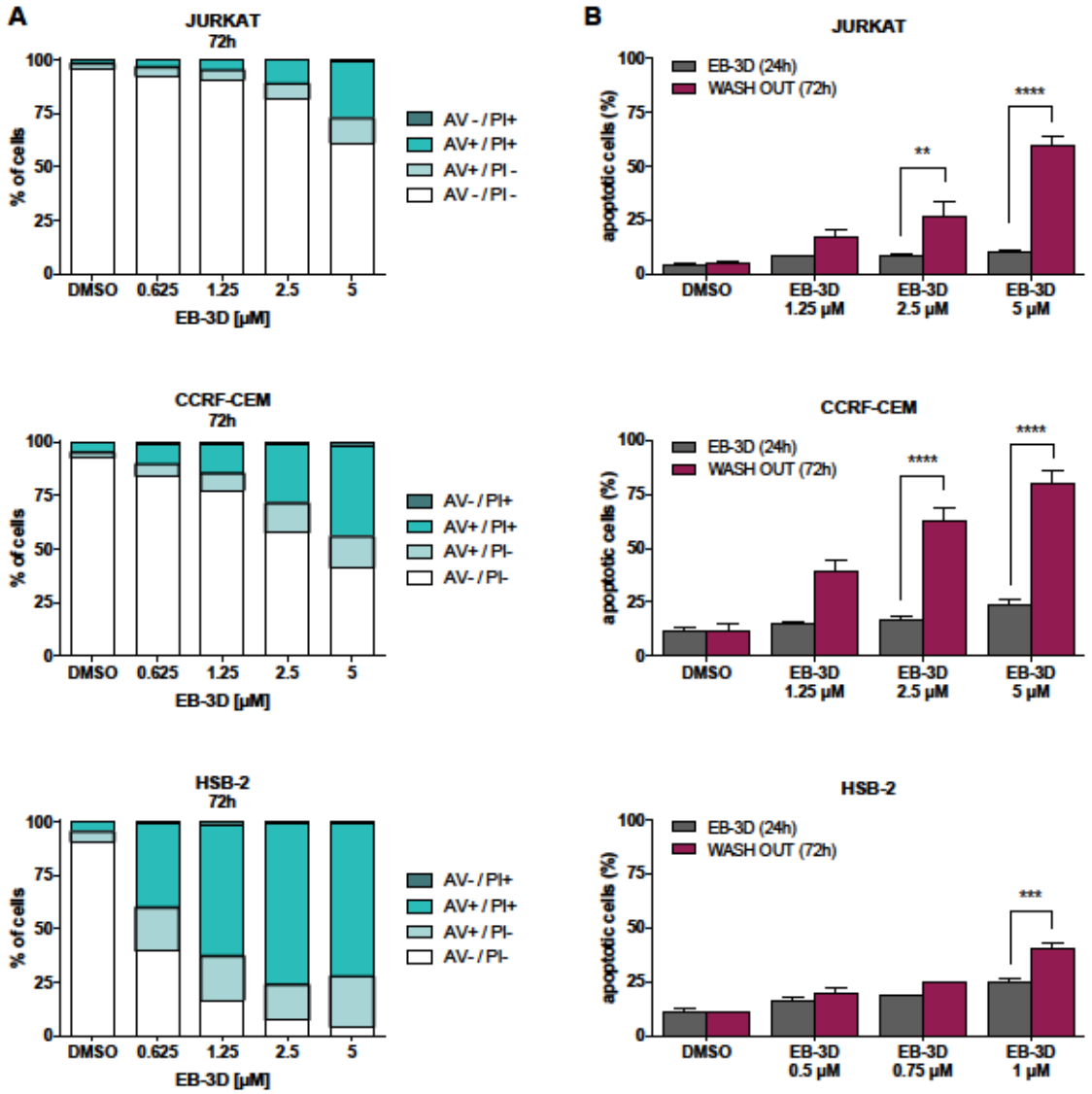

Figure 35: EB-3D-induced apotosis increases after drug removal

Flow cytometric analysis of apoptotic cells after treatment of Jurkat, CCRF-CEM and HSB-2 cells with compound **EB-3D** at the indicated concentrations after 72 h of incubation (**A**) or after 24h of **EB-3D** treatment and then after 72h from **EB-3D** wash-out (**B**). The cells were harvested and labeled with annexin-V-FITC (AV) and propidium iodide (PI) and analyzed by flow cytometry. Data are represented as mean ± SEM of three independent experiments. Differences between WASH OUT and pre-treatements were analyzed using one-way ANOVA with Newman-Keuls correction.

EB-3D targets ChoKα in leukemia cell line

To assess the effective ChoKα inhibition in the leukemic model, we measured choline metabolites by high-resolution nuclear magnetic resonance (^{1}H-NMR) spectroscopy. The pediatric T leukemia cell line CCRF-CEM treated with two doses of **EB-3D** for 48 h showed a significant dose-dependent reduction of PCho and the subsequent reduction of total choline-containing compounds (tCho), indicating that **EB-3D** is able to enter inside

cells and inhibit the specific target (Figure 36). We observed no relevant changes in Cho and GPCho levels.

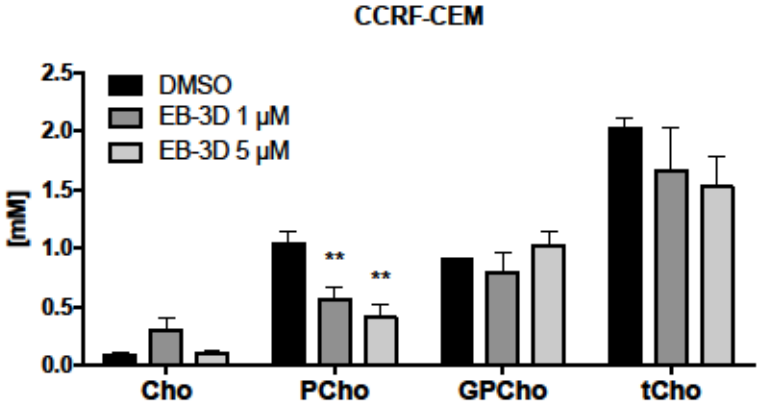

Figure 36: EB-3D targets ChoKα in T-ALL cells

Millimolar levels of Cho, PCho, GPCho and tCho quantified from ^{1}H-NMR spectra of water-soluble extracts from CCRF-CEM cells treated with DMSO and two different doses of **EB-3D**. Differences between control and treatements were analyzed using two-way ANOVA with Newman-Keuls correction.

ChoKα inhibition affects AMPK-mTOR signaling pathway

Reverse-phase protein array (RPPA) is a high-throughput technology enabling the measure of protein expression and phosphorylation levels on a multitude of samples simultaneously. Protein lysates are arrayed as microspots on nitrocellulized coated glass slides and probed with highly specific antibodies that have been validated for RPPA. Each microspot contains the whole proteome repertoire of the cell.

RPPA analysis was performed on lysates of Jurkat, CCRF-CEM, HSB-2 and PEER leukemic cell lines treated with about two-fold the GI_{50} dose (0.3 µM, 1 µM, 50 nM and 0.5 µM respectively) for 1 h and 6 h to be able to observe the starting changes in phosphorylation levels while avoiding the cytotoxic effect of **EB-3D**. As depicted in Figure 37, ChoKα inhibition causes the activation of AMPK metabolic stress sensor by the phosphorylation at residue T712 of its catalytic subunit α, as previously described for triple-negative breast cancer (Mariotto et al., unpublished data). AMPK activation represses mTORC1 pathway as shown by mTOR S2448 dephosphorylation. The inhibition of mTOR in turn affects the activity of several known downstream target, such as 4E-BP1, p70S6K, S6K and GSK3. 4E-BP1 results dephosphorylated at S65, expecially in CCRF-CEM. The p70S6K S371 dephosphorylation is even stronger and significant in all tumoral cell lines and increases over time. The phosphorylation at S235/236 residues of S6K is

notably reduced at all time points, expecially in CCRF-CEM cells, while HSB-2 seems to be more refractory compared to other cell lines.

The dephosphorylated form of 4E-BP1 sequesters the eukaryotic translation initiation factor 4E (eIF4E) which is required to start mRNA translation together with the active (phosphorylated) form of S6K that is necessary to progress through the translation process. Collectively the RPPA data suggests that Chokα inhibition by **EB-3D** is sensed like a metabolic insult in leukemic cells, causing the activation of AMPK, which in turn represses the downstream effectors of mTORC1 required for protein synthesis. These observations are in agreement with the observed reduction in cell proliferation. In fact the phosphorylation of both 4E-BP1 and S6K becomes almost undetectable at 48h, despite the variations of mTOR activity during time (Figure 39).
The glycogen synthase kinase-3 (GSK-3) has been described as a target of both mTOR and p70S6K. The activity of GSK-3 is silenced by phosphorylation at S21 in the α subunit, and by phosphorylation at S9 in the β subunit. Following **EB-3D** treatment, we observed a strong reduction of GSK-3α/β S21/S9 phosphorylations, in particular in CCRF-CEM and HSB-2 where the reduction of these phosphorylations is more than 50% (Figure 37).

The inhibition of mTOR pathway is attenuated in normal lymphocytes

For comparative purposes, the same RPPA analysis has been performed also in quiescent PBL and PHA-activated collected from healthy donor. PBL were treated with the higher dose of **EB-3D** used for T-ALL cell lines, corresponding to 1 μM used for CCRF-CEM. It is worth to note that while this dose is very close to GI_{50} value of PBL resting, it is 30-fold higher than GI_{50} value of PHA-stimulated PBL. PBL were also treated with 0.1 μM of **EB-3D** (data not shown) and no significant differences were observed comparing the two doses.

EB-3D induces a modest activation over time of AMPK in resting PBL and its activation leads to a temporary inhibition of mTOR that is then hyperphosphorylated at 6 h. On the other hand, AMPK activation strongly occurs at 1 h in proliferating lymphocytes and then returns to basal level, while mTOR phosphorylation is significantly reduced at later time compared to the resting counterpart (Figure 37). Surprisingly, the inhibition of mTOR has no impact on the downstream effectors 4E-BP1, p70S6K and S6K. In fact we observed the hyperphosphorylation of p70S6K S371 and S6K S235/236 in stimulated PBL, and the temporary increase of both S6K and 4E-BP1 phosphorylations in resting PBL (Figure 37).

On the contrary GSK3α/β still results strongly dephosphorylated in lymphocytes, only temporary in PBL resting while augmenting over time in proliferating PBL. These data suggest that other mechanisms contribute to healthy lymphocytes response to ChoKα inhibition. Indeed we observed the activation of AKT by the increase of T308 and S473 phosphorylations, which are both required for its activation, occuring only in normal lymphocytes. Moreover, also the activation of MAPK signaling occurs only in PBL while in T-ALL cell lines remains unchanged or its even downregulated. **EB-3D** treatment causes the significant phosphorylation of MEK1/2 S271/S221 and ERK1/2 T202/Y204 that increase 2-fold and 10-fold respectively in PBL resting after 6 h of treatment (Figure 38). It must be said that augmented AKT S473 and ERK1/2 T202/Y204 phosphorylations has been observed also in Jurkat cells treated with **EB-3D** but only at later time (Figure 39).

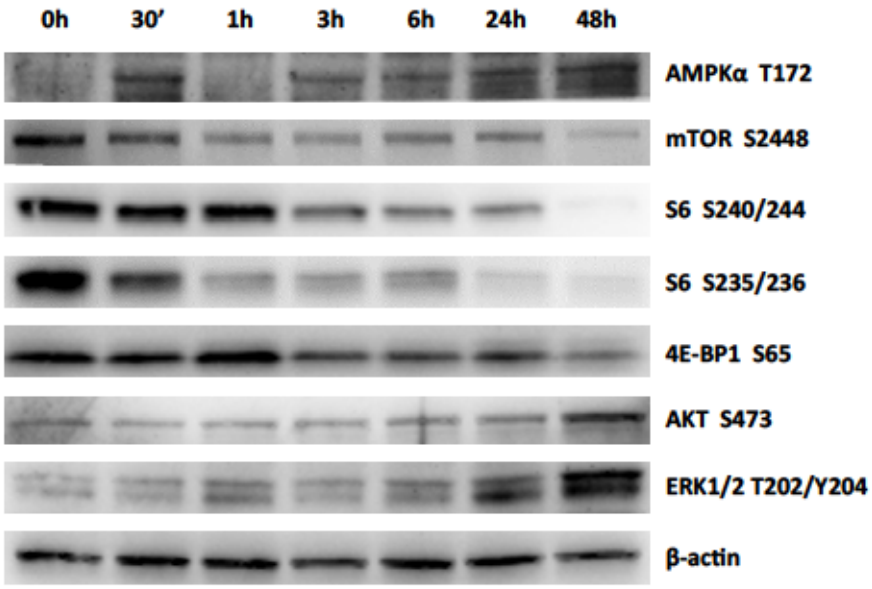

Figure 39: EB-3D induces complete dephosphorylation of m TOR downstream targets

Time-course immunoblot analysis of Jurkat cells treated with a sub-lethal dose of **EB-3D** (0.3 μM).

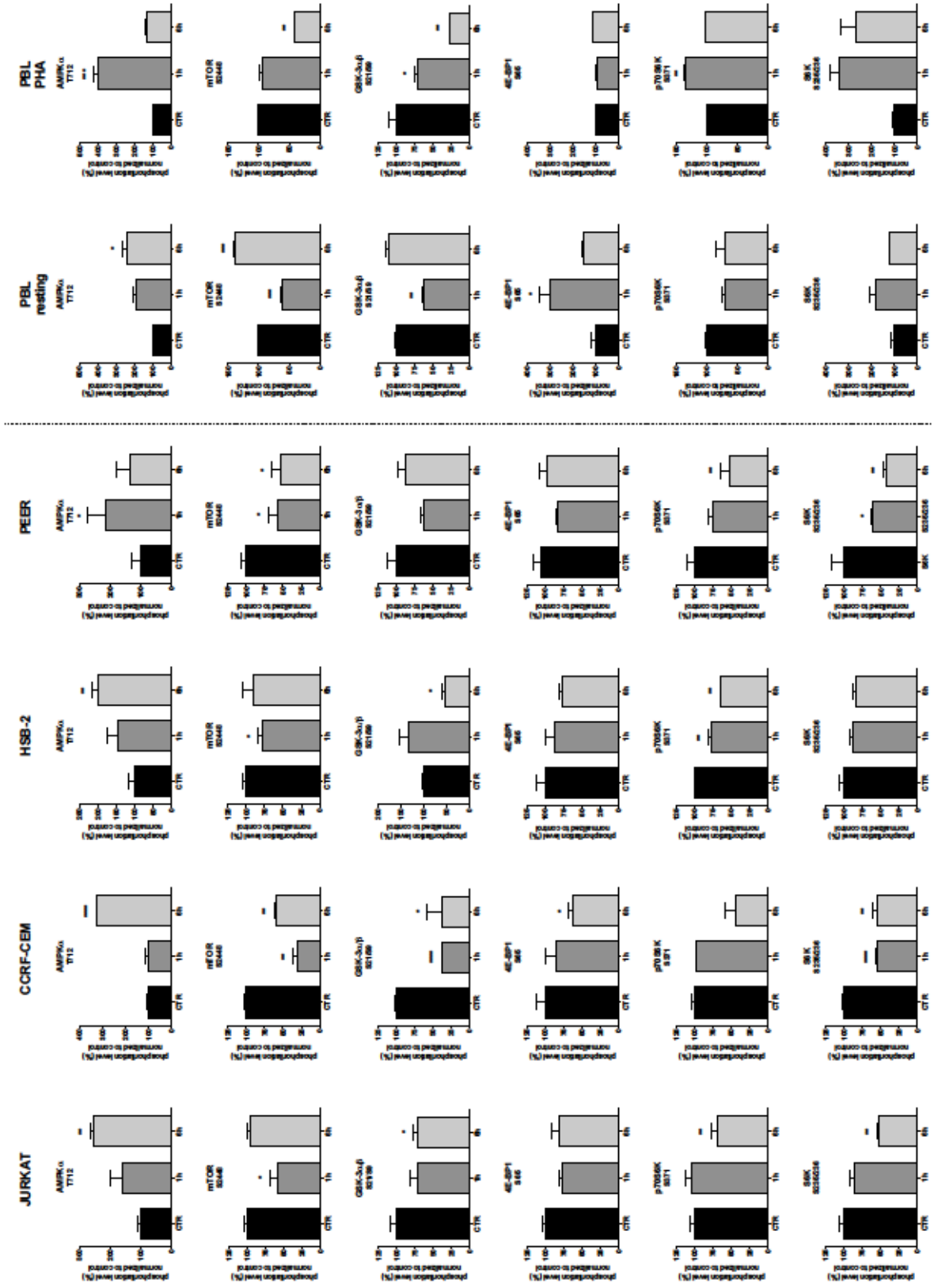

Figure 37: ChoKα inhibition affects AMPK-mTORC1 signaling pathways

RPPA analysis of T-ALL cell lines (left panel) treated with **EB-3D** (Jurkat 0.3 μM, CCRF-CEM 1 μM and HSB-2 50 nM, PEER 0.5 μM) or vehicle (CTR) for the indicated time points. PBL collected from healthy donor (right panel) were treated with 1 μM of **EB-3D**. Data are represented as mean ± SEM of three independent experiments. Differences between control and treatment were analyzed using ANOVA test for repeated measures.

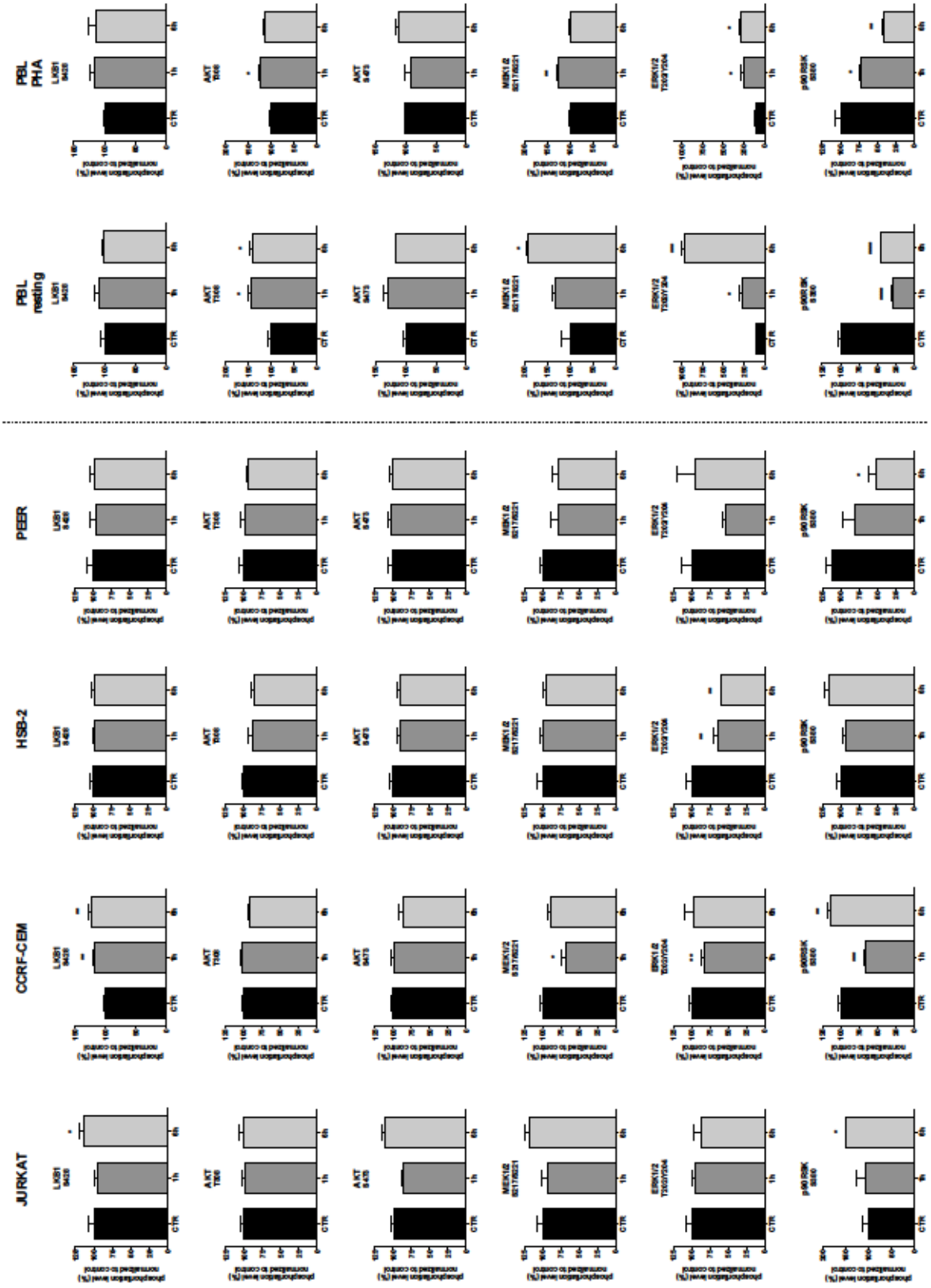

Figure 38: ChoKα inhibition affects MAPK signaling pathways in normal lymphocytes

RPPA analysis of T-ALL cell lines (left panel) treated with **EB-3D** (Jurkat 0.3 μM, CCRF-CEM 1 μM and HSB-2 50 nM, PEER 0.5 μM) or vehicle (CTR) for the indicated time points. PBL collected from healthy donor (right panel) were treated with 1 μM of **EB-3D**. Data are represented as mean ± SEM of three independent experiments. Differences between control and treatment were analyzed using ANOVA test for repeated measures.

EB-3D strongly synergizes with L-asparaginase

We also tested **EB-3D** in combination with two chemotherapeutic drugs used routinely for leukemia treatment, dexamethasone (DEX) and L-asparaginase (L-ASP), to test if ChoKα targeting could increase sensitivity to standard treatments. Indeed, cell viability assay of 1:1 fixed-molar ratio combination drugs indicates that **EB-3D** significantly lowers the GI_{50} of both single DEX and L-ASP treatments. These data pointed out that **EB-3D** synergizes with DEX, except for Jurkat that are glucocorticoid-resistant, and even strongly with L-ASP, as confirmed by combination index (CI) much lower than 1 (Figure 40), where CI<1 indicates drug synergism according with the model proposed by Chou (Chou, 2006). Thus, the combination of the ChoKα inhibitor **EB-3D** and standard chemotherapies could be beneficial in the management of leukemia cell burden.

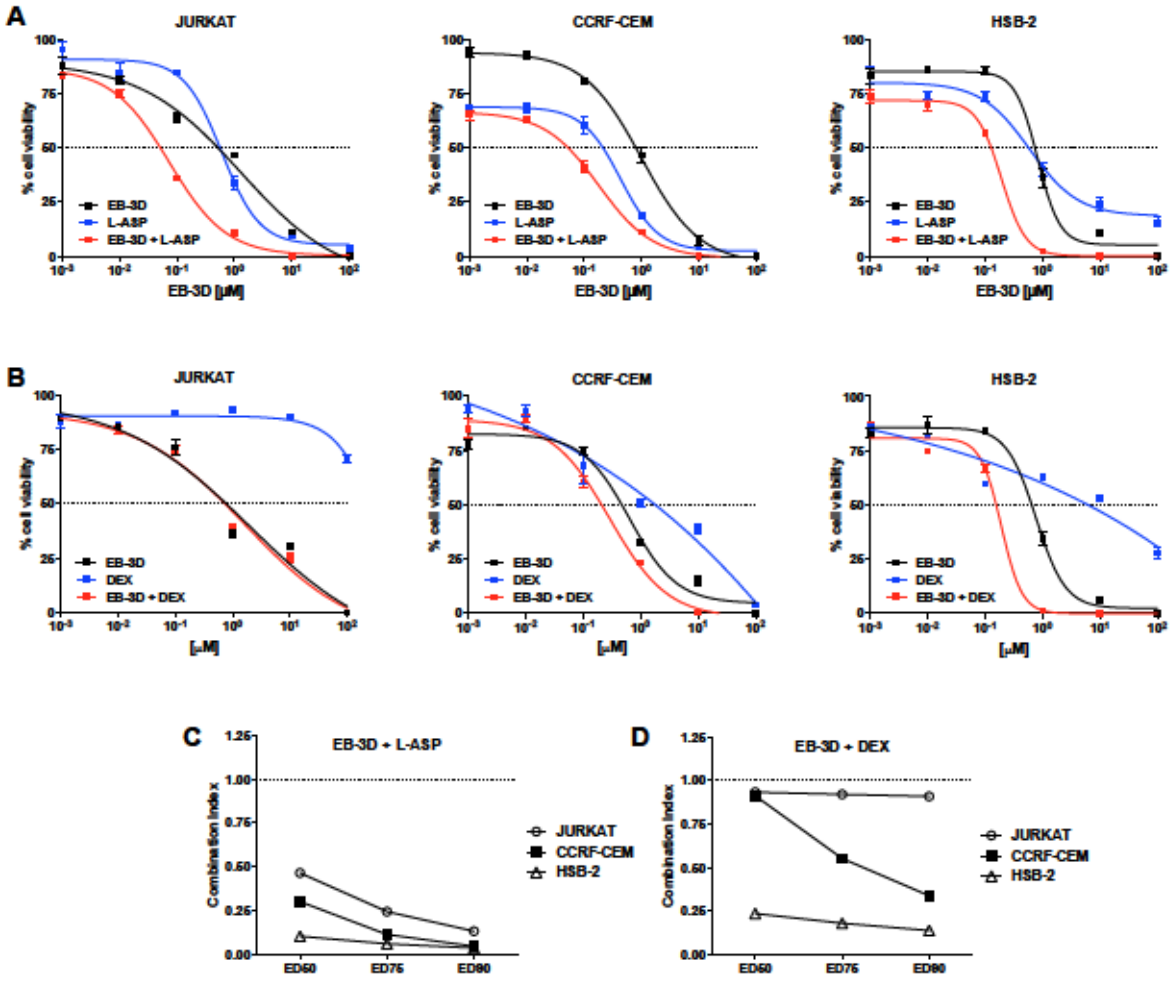

Figure 40: EB-3D synergizes with common leukemia treatments

MTT cell proliferation assay in T-ALL cell lines treated with **EB-3D** in combination with L-asparaginase (L-ASP) (**A**) or dexamethasone (DEX) (**B**) and Combination Index (CI) calculated at the respective ED50, ED75 and ED90 for L-ASP (**C**) and DEX (**D**) combination. Cell viability percentages are normalized to untreated cells. Symbols and bars represent the mean ± SEM of triplicates.

We then further characterized the synergistic effect of the **EB-3D**/L-ASP combination. The simultaneous addition of **EB-3D** and L-ASP increases the percentage of apoptotic cells compared to the single treatments (Figure 41).

Since L-ASP also interferes on leukemia cell metabolism by asparagine aminoacid deprivation, we hypothesized that the synergic effect of the **EB-3D**/L-ASP combination relies on targeting the same signaling pathway. Indeed the combination of **EB-3D** and L-ASP caused a stronger dephosphorylation of S6K compared to the single treatments that is completely abolished after 24 h of co-treatment (Figure 42).

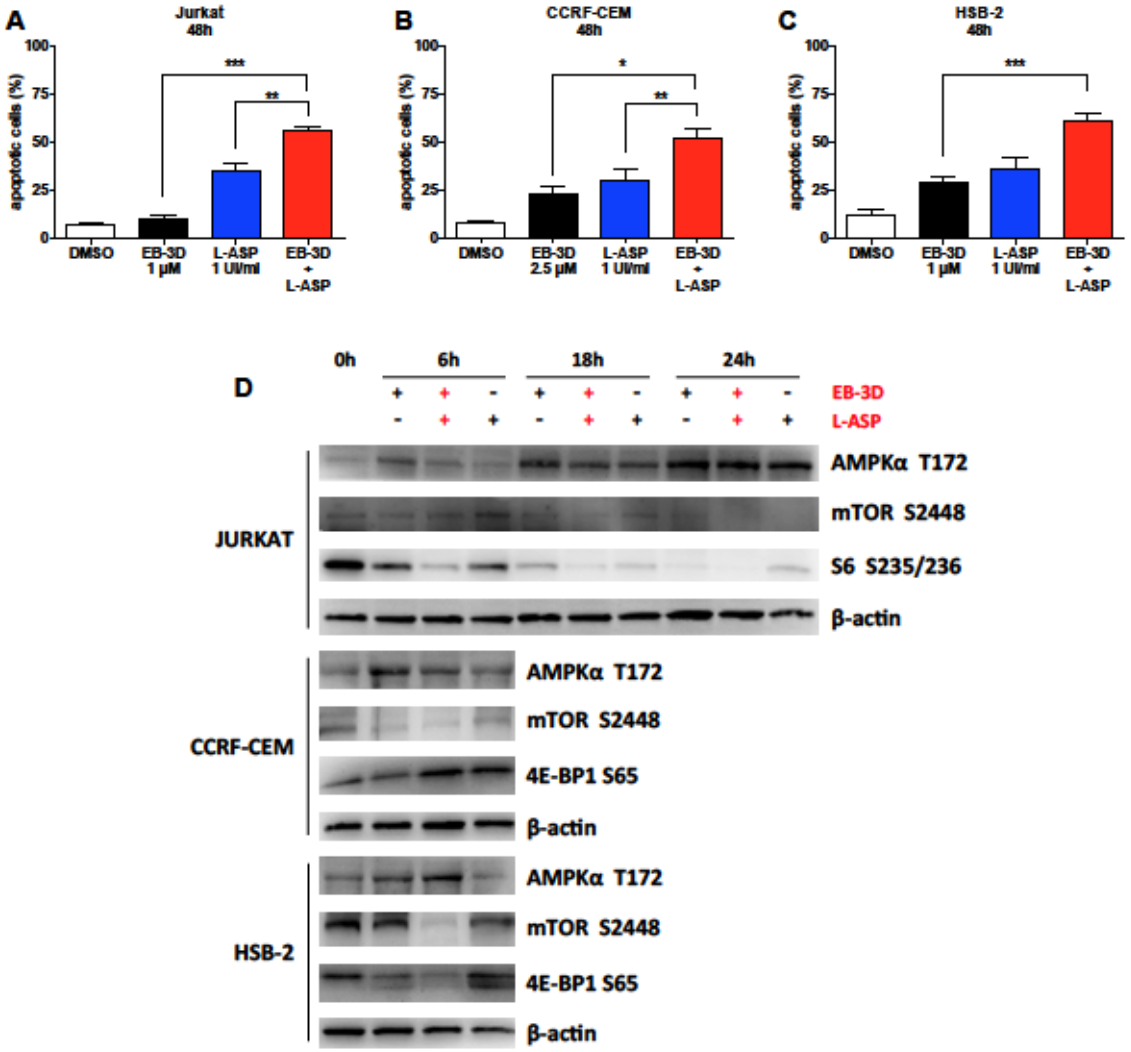

Figure 41: EB-3D boosts the apoptotic effect of L-ASP acting on the same signaling pathway

Flow cytometric analysis of apoptotic cells after treatment of Jurkat (**A**), CCRF-CEM (**B**) and HSB-2 (**C**) cells with **EB-3D**, L-ASP or the combination of the two drugs at the indicated concentrations for 48 h. The cells were harvested and labeled with annexin-V-FITC and PI and analyzed by flow cytometry. Data are represented as mean ± SEM of three independent experiments. Differences between **EB-3D**/L-ASP combination and single treatments were analyzed using one-way ANOVA test with Newman Keuls correction. (**D**) Immunoblot analysis of **EB-3D**, L-ASP and **EB-3D**/L-ASP combination treatment for the indicated time points in Jurkat (1:1), CCRF-CEM (2.5:1) and HSB-2 (1:1).

3.3.4 DISCUSSION

Despite significant improvements have been achieved for a more reliable stratification and treatment of childhood T-ALL however, relapse still remains a frequent feature (Nguyen et al., 2008; Schrappe et al., 2011) and most children die after relapse (Locatelli et al., 2012; Schrappe et al., 2011). Moreover, the increasing evidence that relapses may arise from selection of pre-existing drug resistant clones (Kunz et al., 2015) or from acquired reduced sensitivity to chemotherapeutic agents (Pui, 2015), suggests the urgent need of new strategies for T-ALL treatment. Since many years, abnormal choline metabolism has become an important hallmark of tumor metabolism that characterized different kind of tumors and, in many cases, it has been associated to oncogenesis and tumor progression. In this context we wanted to assess the *in vitro* effects of a new and selective inhibitor of choline kinase namely **EB-3D** in T-ALL cells.

To investigate a possible implication of ChoKα in T-ALL pathogenesis, we measured ChoKα protein levels in a panel of T-ALL cell lines with respect to their correspondent non-tumorigenic primary lymphocytes. As in many other tumors, ChoKα was found upregulated respect normal lymphocytes suggesting that Chokα may have a role also in T cell leukemia development. Interestingly the expression levels of the enzyme are similar within T-ALL cell lines irrespective of their genetic characteristics.

We also evaluated the ratio between ChoKα and ChoKβ isozymes and we observed that the ratio is shifted toward ChoKα in T-ALL cells in contrast to normal lymphocytes where the predominant isoform is the non tumorigenic ChoKβ. These findings supported the concept that higher level of ChoKα and especially high ChoKα/ChoKβ ratio, are required for the proliferation of leukemia cells. Indeed Gruber *et al.* reported that silencing, by specific siRNA, of ChoKα alone induced cell cycle arrest ultimately leading to apoptosis, while the double knockdown of both ChoKα and ChoKβ isoforms rescued cells from undergoing apoptosis (Gruber et al., 2012). Therefore, these observations point out that choline kinase inhibition as an anticancer strategy, must focus on the specific inhibition of ChoKα, without affecting the activity of ChoKβ, in order to induce maximum apoptosis only in target cancer cells. Indeed we previously demonstrated a high selectivity of **EB-3D** toward ChoKα suggesting that this small molecule could be a valuable pharmacological tool (Schiaffino-Ortega et al., 2016).

As expected, the drug exhibits a remarkable potency in inhibiting T-ALL cell lines growth with GI_{50} in the nanomolar range and lower respect the two reference drugs **RSM932A** and

MN58b. Moreover **EB-3D** also demonstrates a good efficacy in inhibiting cell growth in primary cell cultures derived from pediatric T-ALL patients. Importantly, the drug is endowed with lower toxicity in healthy lymphocytes and showed an antiproliferative activity only in cells in active phase of proliferation. We also observed that the compound induces a block of the cell cycle in G0/G1 with a concomitant decrease of the S phase that ultimately leads to apoptotic cell death.

We also investigated the effects of the simultaneous treatment of T leukemia cells with dexamethasone and L-asparaginase, two drugs commonly used in the T-ALL therapeutic protocols. Our results show that **EB-3D** enhanced the chemotherapeutic effects of these drugs, significantly lowering their GI_{50}. In particular the most prominent effect was observed with L-asparaginase. Indeed we give evidence that both L-asparaginase and **EB-3D** impact on the same metabolic pathway thus explaining the synergistic effect. On the light that a consistent percentage of T-ALL patients relapse, with leukemic cells becoming resistant to treatments, our results suggest that ChoKα inhibition could augment the effects of conventional chemotherapy for T-ALL and pointed towards the potential clinical utility of choline kinase inhibitors, although further studies are needed to better understand the molecular mechanism(s) involved in the synergistic effect.

In this context we evaluated by mean of RPPA analysis the signaling pathways that could be activated by **EB-3D** in T-ALL cell lines. Interestingly we observed the rapid activating phosphorylation of AMPK followed by a deregulation of the mTOR pathway. AMPK is the main regulator of energy homeostasis in eukaryotic cells and under metabolic stress conditions it becomes activated by a double mechanism. Under conditions that lowered intracellular ATP levels, such as during nutrient deprivation or hypoxia, AMP or ADP can directly bind to the γ regulatory subunit, leading to a conformational change that favours the phosphorylation of T172 in the activation loop of AMPKα, strictly required for its activation. The liver kinase B1 (LKB1) is the major kinase phosphorylating T172 of AMPKα activation loop under conditions of energy stress. We observed a slight phosphorylation of LKB1 in Jurkat and CCRF-CEM cell lines that, in our opinion, is not sufficient to explain the remarkable activation of AMPK. Indeed, in all the four leukemic cell lines investigated (Jurkat, CCRF-CEM, HSB-2 and PEER), the AMPK T172 phosphorylation occurs just after one hour of treatment suggesting a rapid effect of the drug. If this effect is directly linked to the inhibition of ChoKα remain to be evaluated and will be the object of future studies. It would be interesting to investigate alteration in the AMP/ATP ratio to better characterize the link between **EB-3D** and AMPK activation.

The activation of AMPK resulted in down regulation of mTOR S2448 and its target p70S6K T371. The mammalian target of rapamycin (mTOR) kinase is a master regulator of many cellular processes, including cell proliferation and survival. mTOR is downstream of the PI3K/AKT pathway and this axis is often deregulated in many cancers, making mTOR as an attractive target for cancer therapy. AKT can activate mTOR indirectly promoting the dissociation of the tuberous sclerosis complex 2 (TSC2), which sequesters mTOR. AKT is partially activated through an initial phosphorylation at T308 by PDK-1 and then fully activated by the subsequent phosphorylation at S473 by several kinases. Since we do not observe any relevant changes in both AKT T308 and S473 phosphorylation sites, we can assert that AKT is not involved in the initial mTOR inhibition observed after **EB-3D**, which is mainly controlled by AMPK activation. On the other hand, only at later time we observed the increase in AKT S473 suggesting that other mechanisms intervene to the modulation of ChoKα inhibition effects. The involvement of PI3K/AKT/mTOR pathway in choline metabolism has already been reported although more studies are needed to understand the mechanisms more deeply since it is involved at many levels. Indeed the uptake of choline into cancer cells is positively regulated by the PI3K/AKT/mTOR pathway (Wang et al., 2007) while ChoKα hyperactivation has been associated with overactive RAS signaling, mediated through both the PI3K/AKT/MTOR and MAPK pathways (Ramírez de Molina et al., 2002b). Contrary to what we observed in Jurkat cell line after 48 h of **EB-3D** treatment, phosphorylation of AKT S473, but not T308, can be reduced by inhibition of ChoKα *via* siRNA or small molecule inhibitors, in PI3K-independent way (Chua et al., 2009).

We would like to point out that that the AMPK/mTORC1 axis represents a recently identified promising therapeutic target in different tumors (Shaw, 2009; Sujobert and Tamburini, 2015) as its activity is frequently deregulated in cancer cells including T-ALL. In fact constitutive activation of mTORC1 is a common event in T-ALL, which emphasizes the potential of using mTORC1-targeting drugs as therapeutic agents in this disorder. Among these drugs rapamycin, an mTORC1 inhibitor has showed a modest efficacy in preclinical models of T-ALL while more encouraging results come from studies in which an activator of AMPK, such as metformin, was tested (Shi et al., 2012). At the present stage, how **EB-3D** targets AMPK-mTOR pathway remains to be explored although a recent work showed, through a metabolomic approach, that the ChoKα inhibitor **ICL-CCIC-0019** leads to a metabolically stressed phenotype and AMPK activation (Trousil et

al., 2016). Thus, in well agreement with our findings, the pharmacological inhibition choline pathway seems to critically affect cell metabolic function beyond the reduction os phospholipids synthesis.

In parallel manner we studied in both normal quiescent lymphocytes and PHA-activated the effect of treatment on the AMPK-mTOR pathways. Contrary to what was observed in T-ALL cell lines **EB-3D** induces a modest activation over time of AMPK in quiescent lymphocytes and its activation leads to a temporary inhibition of mTOR that is then hyperphosphorylated at later times. A similar behavior was observed also in proliferating lymphocytes. Surprisingly, the inhibition of mTOR does not affect the downstream effectors 4E-BP1, p70S6K and S6K. These data suggest that other mechanisms contribute to the response of healthy lymphocytes to ChoKα inhibition. A recent study in fact pointed out that different metabolic features exist between normal and T-ALL cells (Kishton et al., 2016). Thus it is possible that normal lymphocytes utilize a distinct metabolic program in comparison to T-ALL in response to ChoKα inhibition that may be due, as described above, to the remarkable difference of ChoKα enzyme level between normal and transformed lymphocytes.

Another interesting observation is that activation of MAPK signaling occurs only in normal lymphocytes while in T-ALL cells remains unchanged or its even downregulated. In particular MEK1/2 S271/S221 and ERK1/2 T202/Y204 were found phosphorylated after **EB-3D** treatment in quiescent lymphocytes. Indeed, the accumulation of PCho has shown to be essential for the constitutive activation of MAPK and PI3K/AKT/mTOR signaling pathways since siRNA-mediated and pharmacological inhibition of ChoKα attenuate both survival pathways (Clem et al., 2011; Yalcin et al., 2010), demonstrating the existence of a reciprocal relationship between oncogenic signal transduction and choline metabolism. Several studies have demonstrated that AMPK activators can modulate the MAPK pathway. Huai *et al*. reported that metformin activates ERK in the human leukemia cell line NB-4 (Huai et al., 2012) and an independent group found that the AMPK activator AICAR stimulates MAPK pathway in a different leukemia cell lines (Lalic et al., 2014). It is therefore possible that the difference in the metabolic response to treatment exhisting between healthy and leukemic cells will also be reflected on MAPK pathway activation. However, further experiments are needed to clarify this point.

In conclusion, in this study we clearly showed that choline kinase inhibition could be a valuable therapeutic strategy in T-ALL treatment and **EB-3D** can be considered a an interesting new molecule worthy of further evaluation as a potential chemotherapeutic agent.

4. CONCLUSIONS

In this thesis, novel ChoKα inhibitors were tested *in vitro* for their antiproliferative activity. The most promising compound **EB-3D** was chosen as lead compound for further *in vitro* and *in vivo* studies and used to characterise choline metabolism in hematological tumor.

The compound exhibited high antiproliferative activity against a panel of solid and hematological cancer cell lines, while normal quiescent cells were less sensitive to treatment compared to their proliferating counterpart. ChoKα inhibition decreased PCho and subsequently tCho levels and caused the accumulation of Cho substrate. In both triple-negative breast cancer and T acute lymphoblastic leukemia, **EB-3D** triggered AMPK activation leadind to downregulation of pro-survival mTOR pathway. The inactivation of mTOR downstream targets 4E-BP1, p70S6K and S6K is known to cause the arrest of mRNA translation processes. Thus, the inhibition of protein synthesis could explain the striking reduction of cell proliferation induced by **EB-3D**. In contrast, normal lymphocytes were less affected by **EB-3D** treatment, showing reduced dephosphorylation of mTOR effectors, presumably via the activation of MAPK alternative pathway.

The final macroscopic effect, in both tumor contexts, was a strong reduction of cell proliferation and G0/G1 cell cycle arrest. Surprisingly, while **EB-3D** caused cell death in all tested T-ALL cell lines, it was unable to induce cell death in MDA-MD-231 triple-negative breast cancer cells. The explanation for this different behavior is the onset of early and irreversible of cellular senescence in MDA-MB-231 that prevents cell death but still sensitizes cell to subsequent exposure to chemotherapy. Collectively, the results obtained *in vitro* highlighted potential opportunities for targeted combination therapies.

Last, pre-clinical *in vivo* experiments indicated a strong antitumoral effect of **EB-3D** in aggressive breast cancer model, with strong reduction of tumor growth at low dose. The ChoKα inhibitor also reduced cell migration and invasion of the higly invasive MDA-MB-231 cells. The antimetastatic power of **EB-3D** was confirmed *in vivo* by reduction of lung metastatic foci and metastasis size. Taken together, these data indicates a potent antitumor and antimetastatic effect of **EB-3D** and a favourable pharmacokinetics. Importantly we did not observe any sign of apparent toxicity.

To conclude, this work has given a proof that ChoKα is a novel attractive therapeutic target in T-ALL and justify the further development of **EB-3D** ChoKα inhibitor.

MATHERIALS AND METHODS

Chemistry

General procedure C for the synthesis of the final compounds 10a-l

A solution of 1eq 1,2-bis(4-bromomethylphenoy)ethane (**8**) in dry CH_3CN was added drop to drop to a solution of **9a-l** (2 eq) in dry CH_3CN under argon conditions. The mixture was heated under reflux for a further 3 days and, after cooling down to room temperature, washed with diethyl ether and hexane, filtered and dry to vacuum to afford **10a-l** as a solid product. Characterization data for final products are described below.

1,1'-(((ethane-1,2-diylbis(oxy))bis(4,1-phenylene))bis(methylene))bis(4-(dimethylamino)pyridinium) bromide (10a). Following general procedure C furnished **10a** as a yellow solid, yield 42%, mp: 62-63°C. ^{1}H NMR (300 MHz, CD_3OD) δ: 8.20 (d, J = 7.86 Hz, 4H), 7.35 (d, J = 8.73 Hz, 4H), 7.02 (d, J = 8.73 Hz, 4H), 6.99 (d, J = 7.86 Hz, 4H), 5.30 (s, 4H), 4.33 (s, 4H), 3.24 (s, 12H). ^{13}C RMN (75 MHz, CD_3OD) δ: 161.80 x 2, 158.87 x 2, 143.76 x 4, 131.98 x 4, 129.20 x 2, 117.30 x 4, 109.93 x 4, 68.86 x 2, 62.22 x 2, 41.20 x 4. HRMS (m/z): $[M]^{2+}$ calcd for $C_{30}H_{36}N_4O_2$: 242.1419, found: 242.1409.

1,1'-(((ethane-1,2-diylbis(oxy))bis(4,1-phenylene))bis(methylene))bis(4-(pyrrolidin-1-yl)pyridinium) bromide (10b). Following general procedure C furnished **10b** as a brown solid, yield 48%, mp: 129-130°C. ^{1}H NMR (300 MHz, CD_3OD) δ: 8.17 (d, J = 7.77 Hz, 4H), 7.34 (d, J = 8.73 Hz, 4H), 7.01 (d, J = 8.73 Hz, 4H), 6.84 (d, J = 7.77 Hz, 4H), 5.28 (s, 4H), 4.32 (s, 4H), 3.54 (t, J = 6.84 Hz, 8H), 2.11 (t, J = 6.86 Hz, 8H), ^{13}C NMR (75 MHz, CD_3OD) δ: 161.79 x 2, 156.05 x 2, 143.68 x 4, 131.92 x 4, 129.31 x 2, 117.29 x 4, 110.51 x 4, 68.86 x 2, 62.26 x 2, 50.28 x 4, 26.98 x 4. HRMS (m/z): $[M]^{2+}$ calcd for $C_{34}H_{40}N_4O_2$: 2681576, found: 268.1568.

1,1'-(((ethane-1,2-diylbis(oxy))bis(4,1-phenylene))bis(methylene))bis(4-((4-chlorophenyl)(methyl)amino)pyridinium) bromide (10c). Following general procedure C furnished **10c** as a white solid, yield 30%, mp: >300°C. ^{1}H NMR (600 MHz, CD_3OD) δ: 8.28 (d, J = 8.5 Hz, 4H), 7.58 (d, J = 8.5 Hz, 4H), 7.37 (m, 8H), 7.02 (d, J = 8.4 Hz, 4H), 6.92 (m, 4H), 5.35 (s, 4H), 4.33 (s, 4H), 3.53 (s, 6H). ^{13}C NMR (75 MHz, CD_3OD) δ: 160.85 x 2, 158. 31 x.2 143.52 x 4, 135.52 x 2, 131.94 x 4, 131.13 x 4, 129.28 x 4, 127.95

x 2, 116.27 x 8, 110.27 x 2, 67.81 x 2, 61.64 x 2, 30.55 x 2. **HRMS** (m/z): $[M]^{2+}$ Calcd for $C_{20}H_{19}N_2OCl$: 338.1186, found: 338.1194.

1,1'-(((ethane-1,2-diylbis(oxy))bis(4,1-phenylene))bis(methylene))bis(quinuclidinium) bromide (10d). Following general procedure C furnished **10d** as a white solid, yield 56%, mp: > 300°C. ^{1}H NMR (300 MHz, CD_3OD) δ: 7.47 (d, J = 8.78 Hz, 4H), 7.13 (d, J = 8.78 Hz, 4H), 4.43 (s, 4H), 4.35 (s, 4H), 3.48 (m, 12H), 2.18 (dt, J = 6.44, 3.23 Hz, 2H), 2.01 (dt, J = 8.23, 3.23 Hz, 12H). ^{13}C NMR (75 MHz, CD_3OD) δ: 162.80 x 2, 136.48 x 4, 121.54 x 2, 117.14 x 4, 69.52 x 2, 68.87 x 2, 56.39 x 6, 25.81 x 6, 22.33 x 2. HRMS (m/z) $[M]^{2+}$ calcd for $C_{30}H_{42}N_2O_2$: 231.1623, found: 231.1628.

1,1'-(((ethane-1,2-diylbis(oxy))bis(4,1-phenylene))bis(methylene))bis(3-hydroxyquinuclidinium) bromide (10e). Following general procedure C furnished **10e** as a white solid, yield 63%, mp: 268-270°C. ^{1}H NMR (300 MHz, DMSO-d^6) δ: 7.48 (d, J = 8.66 Hz, 8H), 7.13 (d, J = 8.66 Hz, 8H), 4.43 (s, 8H), 4.41 (s, 8H), 4.08, 3.64, 3.35, 3.04, 2.27, 2.10 (6m, 52H), ^{13}C NMR (75 MHz, DMSO-d^6) δ: 159.52 x 4. 134.43 x 8, 119.63 x 4, 114.77 x 8, 65.61 x 4, 62.26 66.37, 63.27, 53.46, 52.52, 26.83, 20.87, 17.29 x 4. HRMS (m/z) $[M]^{2+}$ calcd for $C_{30}H_{42}N_2O_4$: 247.1572, found: 247.1565.

1,1'-(((ethane-1,2-diylbis(oxy))bis(4,1-phenylene))bis(methylene))bis(4-(methyl(phenyl)amino)quinolinium) bromide (10f). Following general procedure C furnished **10f** as a yellow solid, yield 64%, mp: 169-170°C. ^{1}H NMR (300 MHz, CD_3OD) δ: 8.86 (d, J = 7.44 Hz, 2H), 8.13 (d, J = 8.37 Hz). 7.81 (dt, J = 5.57, 1.43 Hz, 2H), 7.62 (dd, J = 8.8, 1.3 Hz, 2H), 7.53 (m, 4H), 7.46 (t, J = 7.36 Hz, 2H), 7.40-7.29 (m, 12H), 7.03 (d, J = 8.76 Hz, 4H), 5.89 (s, 4H), 4.33 (s, 4H), 3.84 (s, 6H). ^{13}C NMR (75 MHz, CD_3OD) δ: 161.47 x 2, 160.80 x 2, 150.14 x 2, 148.54 x 2, 141.68 x 2, 135.51 x 2, 132.75 x 4, 130.63 x 4, 130.28 x 2, 130.15 x 2, 128.64 x 2, 127.85 x 2, 127.73 x 4, 122.29 x 2, 120.97 x 2, 117.30 x 4, 107.73 x 2, 68.85 x 2, 59.94 x 2, 46.75 x 2. HRMS (m/z) $[M]^{2+}$ calcd for $C_{48}H_{44}N_4O_2$: 354.1732, found: 354.1736.

1,1'-(((ethane-1,2-diylbis(oxy))bis(4,1-phenylene))bis(methylene))bis(4-((4-chlorophenyl)(methyl)amino)quinolinium) bromide (10g). Following general procedure C furnished **10g** as a yellow solid, yield 70%, mp: 178-180°C. ^{1}H NMR (400 MHz, CD_3OD) δ: 8.90 (d, J = 7.40 Hz, 2H), 8.16 (dd, J = 8.9, 0.6 Hz, 2H), 7.84 (dt, J = 5.64,

1.36 Hz, 2H), 7.67 (dd, J = 8.8, 1.2 Hz, 2H), 7.52 (d, J = 8.91 Hz, 4H), 7.41-7.37 (m, 8H), 7.33 (d, J = 8.77 Hz, 4H), 7.03 (d, J = 8.77 Hz, 4H), 5.91 (s, 4H), 4.33 (s, 4H). 3.82 (s, 6H), ^{13}C NMR (75 MHz, CD_3OD) δ: 161.48 x 2, 160.92 x 2, 148.81 x 2, 148.77 x 2, 141.68 x 2, 135.68 x 2, 135.58 x 2, 132.72 x 4, 130.69 x 4, 130.00 x 2, 129.28 x 4, 128.52 x 2, 128.20 x 2, 122.41 x 2, 121.13 x 2, 117.30 x 4, 108.36 x 2, 68.84 x 2, 60.09 x 2, 46.53 x 2. HRMS (m/z) $[M]^{2+}$ calcd for $C_{48}H_{42}N_4O_2Cl_2$: 388.1342, found: 388.1338.

1,1'-(((ethane-1,2-diylbis(oxy))bis(4,1-phenylene))bis(methylene))bis(7-chloro-4-(methyl(phenyl)amino)quinolinium) bromide (10h). Following general procedure C furnished the crude residue which was purified by flash chromatography using CH_2Cl_2: MeOH (9:1 v/v) as eluent to obtain **10h** as a yellow-green solid, yield 61%, mp: 181-183°C. ^{1}H NMR (300 MHz, CD_3OD) δ: 8.82 (d, J = 7.50 Hz, 2H), 8.15 (d, J = 1.89 Hz, 2H), 7.56-7.53 (m, 6H), 7.47 (t, J = 7.4 Hz, 2H), 7.41-7.40 (d, J = 7.48 Hz, 4H), 7.34-7.31 (m, 6H), 7.29 (dd, J = 9.3, 1.9 Hz, 2H), 7.06-7.03 (d, J = 8.70 Hz, 4H), 5.85 (s, 4H), 4.34 (s, 4H), 3.82 (s, 6H, CH_3). ^{13}C NMR (75 MHz, CD_3OD) δ: 161.58 x 2, 160.51 x 2, 149.76 x 2, 148.95 x 2, 142.51 x 2, 141.90 x 2, 132.92 x 4, 131.80 x 2, 130.77 x 4, 130.59 x 2, 128.35 x 2, 128.24 x 2, 127.72 x 4, 128.24 x 2, 120.68 x 2, 120.45 x 2, 117.41 x 4, 107.93 x 2, 68.86 x 2, 59.91 x 2, 46.87 x 2. HRMS (m/z): $[M]^{2+}$ calculado for $C_{48}H_{42}N_4O_2Cl_2$: 388.1342, found: 388.1331.

1,1'-(((ethane-1,2-diylbis(oxy))bis(4,1-phenylene))bis(methylene))bis(7-chloro-4-((4-chlorophenyl)(methyl)amino)quinolinium) bromide (10i). Following general procedure C furnished the crude residue which was purified by flash chromatography using CH_2Cl_2: MeOH (9:1 v/v) as eluent to obtain **10i** as a yellow solid, yield 39%, mp: 185-186°C, ^{1}H NMR (300 MHz, CD_3OD) δ: 8.87 (d, J = 7.46 Hz, 2H), 8.20 (d, J = 1.93 Hz, 2H), 7.63 (d, J = 9.31 Hz, 2H), 7.55 (d, J = 8.78 Hz, 4H), 7.42 (d, J = 8.78 Hz, 4H), 7.40 (d, J = 1.96 Hz, 2H), 7.38 (d, J = 7.47 Hz, 2H), 7.35 (d, J = 8.73 Hz, 4H), 7.06 (d, J = 8.73 Hz, 4H, H-2), 5.88 (s, 4H), 4.35 (s, 4H), 3.82 (s, 6H, CH_3). ^{13}C NMR (75 MHz, CD_3OD) δ: 161.59 x 2, 160.65 x 2, 149.22 x 2, 148.45 x 2, 142.50 x 2, 142.06 x 2, 135.92 x 2, 132.88 x 4, 131.68 x 2, 130.85 x 4, 129.33 x 4, 128.71 x 2, 128.15 x 2, 120.82 x 2, 120.61 x 2, 117.40 x 4, 108.57 x 2, 68.85 x 2, 60.05 x 2, 46.69 x 2. HRMS (m/z) $[M]^{2+}$ calcd for $C_{48}H_{40}N_4O_2Cl_4$: 422.0953, found: 422.0952.

1,1'-(((ethane-1,2-diylbis(oxy))bis(4,1-phenylene))bis(methylene))bis(4-(azepan-1-yl)quinolinium) bromide (10j). Following general procedure C furnished **10j** as a yellow

solid, yield 67%, mp: 75-77°C. ^{1}H RMN (300 MHz, CD_3OD) δ: 8.54 (d, J = 7.73 Hz, 2H), 8.42 (dd, J = 8.62, 1.28 Hz, 2H), 8.05 (dd, J = 8.83, 1.05 Hz, 2H), 7.90 (dt, J = 5,67, 1,33 Hz, 2H), 7.66 (dt, J = 5.77, 1.15 Hz, 2H), 7.27 (d, J = 8.80 Hz, 4H), 7.10 (d, J = 7.74 Hz), 7.00 (d, J = 8.80 Hz, 4H), 5.74 (s, 4H), 4.30 (s, 4H), 4.09 (m, 8H), 2.09 (m, 8H), 1.75 (dt, J = 5.40, 2.54 Hz, 8H), ^{13}C NMR (75 MHz, CD_3OD) δ : 161.91 x 2, 161.34 x 2, 146.48 x 2, 142.10 x 2, 135.52 x 2, 130.48 x 4, 130.44 x 2, 128.98 x 2, 127.04 x 2, 121.41 x 2, 120.33 x 2, 117.22 x 4, 104.55 x 2, 68.84 x 2, 58.99 x 2, 56.06 x 4, 29.37 x 4, 29.23 x 4. HRMS (m/z) $[M]^{2+}$ calcd for $C_{46}H_{52}N_4O_2$: 346.6700, found 346.2039.

1,1'-(((ethane-1,2-diylbis(oxy))bis(4,1-phenylene))bis(methylene))bis(4-(azepan-1-yl)-7-chloroquinolinium) bromide (10k). Following general procedure C furnished the crude residue which was purified by flash chromatography using CH_2Cl_2: MeOH (8:1 v/v) as eluent to obtain **10k** as a white solid, yield 41%, mp: 87-88°C. ^{1}H RMN (400 MHz, CD_3OD) δ: 8.51 (d, J = 7.75 Hz, 2H), 8.40 (d, J = 9.21 Hz, 2H), 8.07 (d, J = 1.82 Hz, 2H), 7.29 (d, J = 8.64 Hz, 4H), 7.65 (dd, J = 9.2, 1.9 Hz, 2H), 7.11 (d, J = 7.78 Hz, 2H), 7.03 (d, J = 8.64 Hz, 4H), 5.72 (s, 4H), 4.33 (s, 4H), 4.08 (m, 8H), 2.08 (m, 8H), 1.74 (m, 8H). ^{13}C NMR (75 MHz, CD_3OD) δ :161.56 x 2, 161.44 x 2, 146.77 x 2, 142.95 x 2, 141.82 x 2, 132.31 x 2, 130.59 x 4, 128.57 x 2, 127.45 x 2, 119.88 x 2, 119.78 x 2, 117.32 x 4, 105.00 x 2, 68.85 x 2, 59.00 x 2, 56.12 x 4, 29.28 x 4, 29.16 x 4. HRMS (m/z) $[M\text{-}Br]^{+}$ calcd for $C_{46}H_{50}N_4O_2Cl_2Br$: 839.24949, found: 839.2494.

1,1'-(((ethane-1,2-diylbis(oxy))bis(4,1-phenylene))bis(methylene))bis(7-chloro-4-(pyrrolidin-1-yl)quinolinium) bromide (10l). Following general procedure C furnished the crude residue which was purified by flash chromatography using CH_2Cl_2: MeOH (9:1 v/v) as eluent to obtain **10l** as a white solid, yield 48%, mp: 118-120°C. ^{1}H RMN (300 MHz, CD_3OD) δ: 8.63 (d, J = 9.23 Hz, 2H), 8.51 (d, J = 7.69 Hz, 2H), 8.04 (d, J = 2.02 Hz, 2H), 7.66 (dd, J = 9.2, 2.0 Hz, 2H), 7.27 (d, J = 8.75 Hz, 4H), 7.01 (d, J = 8.75 Hz, 4H), 6.90 (d, J = 7.69 Hz, 2H), 5.71 (s, 4H), 4.32 (s, 4H), 4.02 (m, 8H), 2.20 (m, 8H). ^{13}C NMR (75 MHz, CD_3OD) δ: 161.37 x 2, 157.92 x 2, 146.91 x 2, 142.45 x 2, 141.76 x 2, 131.76 x 2, 130.45 x 4, 128.68 x 2, 127.71 x 2, 120.16 x 2, 119.73 x 2, 117.29 x 4, 104.64 x 2, 68.83 x 2, 59.06 x 2, 55.43 x 4, 24.64 x 4. HRMS (m/z) $[M]^{2+}$ calcd for $C_{42}H_{42}N_4O_2Cl_2$: 352.1337, found: 352.1353.

Docking Studies

Molecular-modeling studies were performed by using Sybyl program [51]. Crystal structures of human ChoKα1 in complex with compounds **2** (PDB entry 4BR3) and **4** (PDB entry 4CG8) were used for docking studies. In both cases, using the Structure Preparation Tool module of Sybyl refined protein structure. Missing side chains of those residues situated far away from the binding sites were added and protein N- terminal and C-terminal were fixed with ACE and NME, respectively. Hydrogens and charges were also added and protonation type of Glu, Asp, Gln and Asp was analyzed and fixed. Hydrogen orientations were also checked in order to maintain intramolecular hydrogen bonds within the protein. Finally, the molecules of compounds **2** and **4** inserted into the ATP binding site were carefully checked to assure the correction of these molecules. Structures of compounds **10a-l** were constructed from standard fragments of the Libraries of the Sybyl program, and used as ligands for docking studies. As previously described (Conejo-García et al., 2003a), a new type of atom was necessary to define in order to build the molecules: N.ar4, the quaternary nitrogen of the pyridinium fragments. Additional parameters were also developed from initio calculations to optimize the geometry of these molecules Atomic charges were calculated by means of Gaussian Program [53] and optimizations were undertaken using the BFGS method.

The Surflex-Dock (Jain, 2007), module implemented in the Sybyl program was used for docking studies. Surflex Dock Protomol was prepared using compound **2** or **4** inserted into the ChoK binding site, with a threshold value of 0.5 and a Bloat of 0 A. Surflex- Dock GeomX (SFXC) protocol was used, the search grid was expanded in 5 Å, 50 additional starting conformations were used for each molecule and 30 conformations per fragment. The results were analyzed using the Sybyl program and the most stable pose for each molecule was chosen as the preferred one inside the ChoK enzyme. Figures were built using the PyMOL program.

Determination of human choline kinase α1 (ChoKα1) activity

The inhibitory effect of the different compounds was assayed in human ChoKα1 purified enzyme as previously described (Rubio-Ruiz et al., 2014). In each experiment DMSO-assays were always run in parallel as a control. DMSO in no case exceeded a concentration of 0.1% in order to avoid unspecific ChoKα inhibition. ChoKα1 activity was assayed by

measuring the rate of incorporation of ^{14}C from [methyl-^{14}C]choline into phosphocholine both in the presence or absence of different inhibitor concentrations. Briefly, the final reaction mixture contained 100 mM Tris (pH 8.5), 10 mM $MgCl_2$, and 10 mM ATP, and 20 ng of purified ChoKα1. After the samples were preincubated at 37°C for 5 min, the reaction was initiated with 1 mM [methyl-^{14}C]choline (4500 dpm/nmol) and incubated at 37°C for 10 min, the final volume being 55 µl. The assay was stopped by immersing the reaction tubes in boiling water for 3 min. Aliquots of the reaction mixture were applied to the origin of Silica Gel plates in the presence of phosphocholine (0.1 mg) and choline (0.1 mg) as carriers. The chromatography was developed in methanol/0.6% NaCl/28% NH_4OH in water (50:50:5, v/v/v) as solvent. Phosphocholine was visualized under exposure to iodine vapor and the corresponding spot was scraped and transferred to scintillation vials for measurement of radioactivity by a Beckman 6000-TA (Madrid, Spain) liquid-scintillation counter. At least three experiments were performed in all assays. The 50% inhibitory concentrations (IC_{50} values) were determined from the % activity of the enzymes at different concentrations of synthetic inhibitors by using a sigmoidal dose-response curve (the ED_{50}plus v1.0 software).

Tryptophan fluorescence quenching

All compounds were prepared in 100% DMSO. Their K_ds against human ChoKα1 were measured by monitoring the quenching of tryptophan fluorescence. All experiments were performed in Cary Eclipse spectrofluorometer (Varian) at 25°C with the enzymes at 1 µM, and concentrations of compounds varying from 0.1 to 5 µM for ChoKα1 in 25 mM Tris, 150 mM NaCl, pH 7.5. Fluorescence emission spectra were recorded in the 300-400 nm range with an excitation wavelength of 280 nm, with slit width of 5 nm. Controls were determined by incubating the enzymes with equivalent amounts of DMSO. As indicated previously, data analysis was performed in Prism (GraphPad software) considering a model with a single binding site (Eq.1), where F0 is the intrinsic fluorescence of the enzyme in the absence of quencher (Q), F1 is the observed fluorescence at a given quencher concentration, f_a is the fractional degree of fluorescence, and K_d is the dissociation constant.

Eq 1. $$1 - \frac{F1}{F0} = \frac{fa * [Q]}{Kd * [Q]}$$

Protein crystallography

ChoKα1 at 20 mg/ml in buffer 25 mM Tris/HCl, 150 mM NaCl pH 7.5 was used as the protein solution. The sitting-drop vapor-diffusion method was used to produce apo-crystals by mixing 0.5 µl of the protein solution and an equal volume of mother liquor (crystals appeared in 20% polyethylene glycol [PEG] 3350 and 0.25M potassium isothiocyanate). Tetragonal crystals (space group P43212) grew within in 3-4 days and were soaked in 2 µL of the mother liquor with 0.2 µL of a dilution 500 mM of compounds **10a**, **10g**, **10h**, **10k**, and **10l** in DMSO (DMSO was at 10% final concentration in the mix whereas compounds were at 50 mM) for two days. Only crystals soaked with compound **10a** contained the compound. The crystals used in this study were cryoprotected in mother-liquor solutions containing 20% ethylenglycol and frozen with nitrogen gas stream cooled to 100 K. Diffraction data of the binary complexes were collected at beamline I04-1 (Diamond, Oxford). The data was processed and scaled using the XDS package and CCP4 software.

Structure determination and refinement

The structure of the binary complex was solved by molecular replacement using PDB ID 3G15 as a template. Initial phases were further improved by cycles of manual model building in Coot and refinement with REFMAC5. The final model was validated with PROCHECK. Coordinates and structure factors have been deposited in the Worldwide Protein Data Bank (PDB).

BIOLOGY

Cell lines and culture conditions

Human T-cell leukaemia (Jurkat, CCRF-CEM, MOLT-3, MOLT-16, P12-ICHIKAWA, DND-41, KOPTK-1, HSB-2, TALL-1, ALL-SIL, PEER, LOUCY), human B-cell leukemia (RS4;11) and human promyelocytic leukemia (HL-60) cell lines were grown in RPMI-1640 medium (Gibco) while human cervix carcinoma (HeLa), human alveolar basal epithelial carcinoma (A549) and human breast adenocarcinoma (MCF-7 and MDA-MB-231) cell lines were grown DMEM medium (Gibco). Both media were supplemented with 10% fetal bovine serum (FBS), glutamine (2mM), penicillin (100U/ml) and streptomycin (100µg/ml) (all from Thermo Fisher Scientific, Waltham, MA) and cultured at 37°C, 5%

CO_2 in saturated humidity for no longer than 15 passages.

Non tumoral MCF-10A breast cell line was grown in DMEM/F12 medium (Gibco) with 5% horse serum (Invitrogen), penicillin (100U/ml) and streptomycin (100µg/ml), supplemented with EGF 20ng/ml (R&D System), Hydrocortisone (0.5 mg/ml) (Sigma), Cholera Toxin (100 ng/ml) (Sigma) and Insulin 10µg/ml (Sigma). For cell viability experiment, MCF-10A were also cultured in minimal DMEM/F12 medium, defined as "resting", containing only serum and antibiotics.

Mouse breast cancer EO771 cells were grown in complete DMEM medium supplemented with 20% FBS.

All cell lines were purchased from the American Type Culture Collection (ATCC; Manassas, VI). For all experiments, mid-log phase cultures were seeded in fresh medium 24 h before pharmacological treatment.

Human Umbilical Vein Endothelial cells (HUVEC), were prepared from human umbilical-cord veins, as previously described (Porcù et al., 2013). The adherent cells were maintained in M200 medium added by LSGS (low serum growth supplement), containing FBS, hydrocortisone, hEGF, bFGF, heparin, gentamycin/amphotericin (Life Technologies, Monza, Italy). HUVEC were used in experiments from the first to sixth passages.

Human fibroblasts from foreskin were isolated as previously described (Panula and Pera, 2008) and maintained in DMEM medium with 10% fetal bovine serum added.

Pediatric T acute lymphoblastic leukemia (T-ALL) patients

Bone marrow samples from pediatric T-ALL patients were collected at diagnosis at the Pediatric Oncohematology Laboratory of Padova (Italy) and enrolled in the ALL2009 therapeutic protocols of the Associazione Italiana Ematologia Oncologia Pediatrica (AIEOP). Diagnosis was made according to standard cytomorphology, cytochemistry, and immunophenotypic criteria. For all selected patients, T lymphoblasts percentage was comprised between 70% and 98%.

T-ALL bone marrow samples were hemolyzed, washed extensively and resuspended in α-MEM medium supplemented with 10% FBS, 1% penicillin/streptomycin, 1% Glutamine (all from Thermo Fisher Scientific, Waltham, MA), 10% human heat inactivated AB+ serum (Sigma-Aldrich S.r.l., Milan, Italy), human IL-7 (R&D Systems, Minneapolis, MN),

human SCF, human FLT3-ligand (both from Peprotech, London, UK) and insulin (Sigma-Aldrich S.r.l., Milan, Italy). Cells were immediately seeded at a concentration of 10^5 cells/well in 96-well microtiter plates and exposed to the test compound and, after 48h, cell viability was evaluated by MTT assay.

Isolation of peripheral blood lymphocytes and T cells from healthy donors

Blood samples from healthy donors were collected from the blood bank of the Hospital of Padova (Italy). Peripheral blood lymphocytes (PBL) were isolated from heparinized whole blood using a density gradient centrifugation using Lymphoprep (Fresenius KABI Norge AS) solution at 2000 rpm for 20 min. PBL were then carefully recovered, washed extensively, resuspended (10^6 cells/mL) in RPMI-1640 with 10% FBS and incubated overnight to remove residual adherent cells. For MTT cytotoxicity evaluations of PBL cultures, non-adherent cells were resuspended in growth medium and stimulated with 2.5 µg/mL phytohematoagglutinin (PHA) (Irvine Scientific) or not (defined as "resting" medium).

Healthy T lymphocytes (CD3+) were isolated from PBL by depletion of non T-cells using human Pan T Cell Isolation Kit II with a Miltenyi autoMACS magnetic cell sorter (Miltenyi Biotec, Bergisch Gladbach, Germany). The isolated cells purity was confirmed by flow cytometry.

Cell proliferation assay and drug combination sensitivity assay

The cytotoxic activity of selected drugs was determined using a standard 3-[4,5-dimethylthiazol-2-yl]-2,5-diphenyltetrazodium bromide (MTT)-based colorimetric assay (Sigma-Aldrich S.r.l., Milan, Italy). Briefly, cells were seeded at a density of $5x10^3$ cells/well (for adherent cell lines), $2.5x10^4$ cells/well (for non-adherent cell lines) or $1x10^5$ cells/well (for primary PBL or T-ALL) in 96-well microtiter plates and incubated at 37°C in a humidified 5% CO_2 incubator overnight prior to the experiments to ensure exponential growth. After 24h, medium was replaced by fresh medium containing the specific treatment or drug combination (fixed combination ratios) at serial diluition (1:10) for 72h. MTT was added to each well at a final concentration of 0.5mg/ml, and incubated for 3h, 37°C, 5% CO_2. Viable cells with active metabolism convert MTT into a purple-colored formazan product, which is next solubilized with equal volume of isopropanol-HCl to measure the changes in absorbance at 570 nm using a plate reading spectrophotometer

(Victor, Perkin Elmer). The GI_{50} was defined as the compound concentration required to inhibit cell proliferation by 50%, in comparison with cells treated with the maximum amount of DMSO and considered as 100% viability. Each drug concentration was performed in triplicate. To determine the synergistic, additive, or antagonistic effects of the drug combinations, CalcuSyn software (version 2.0, Biosoft) based on the method of the combination index (CI) described by Chou and Talalay was used (Chou, 2006), where synergism is defined by CI<1.

Trypan Blue exclusion assay

The accurate determination of the cell proliferation rate was determined by trypan blue exclusion assay. Cells in exponential growth were treated with different concentrations of **EB-3D** (time 0) and then collected at the indicated time points. Cells were diluted 1:1 with isotonic solution of trypan blue (Thermo Fisher Scientific) and counted on an hemacytometer. Only trypan blue negative cells were considered viable cells.

Cell cycle distribution analysis

For flow cytometric analysis of DNA content, $5x10^5$ cells in exponential growth were treated with different concentrations of **EB-3D** for 24h. After the incubation period, the cells were collected, centrifuged and fixed with ice-cold ethanol (70%). The cells were then treated with lysis buffer containing RNAse A and 0.1% Triton X-100, and then stained with propidium iodide (PI). Samples were analyzed on a Cytomics FC500 flow cytometer (Beckman Coulter). DNA histograms were analyzed using MultiCycle for Windows (Phoenix Flow Systems).

Annexin-V/PI assay

Surface exposure of phosphatidylserine on apoptotic cells was measured by flow cytometry with Cytomics FC500 (Beckman Coulter) by adding simoultaneously annexin-V (AV) conjugated to fluorescein isothiocyanate (FITC) and propidium iodide (PI) to cells according to the manufacturer's instructions (Annexin-V-Fluos staining kit, Roche Diagnostic).

C_{12}-FDG senescence assay

For flow cytometric analysis of cellular senescence, $5x10^4$ cells in exponential growth were treated with different concentrations of **EB-3D** for 3 days and then the medium was replaced with fresh medium containing **EB-3D** or DMSO for the next 3 days. After the incubation period, culture media were replaced to remove any dead cells and remaining cells were incubated (1h, 37°C, 5% CO_2) with 100 nM of bafilomycin A1 to neutralize the acidic pH of lysosomes. Cells were then incubated (1h, 37°C, 5% CO_2) with 33 μM of C_{12}FDG (Thermo Fisher Scientific) and then collected by trypsinization, washed once and resuspended in PBS. Samples were analyzed on a Cytomics FC500 flow cytometer (Beckman Coulter). Mean Fluorescence Intensity (MFI) and graphs overlay were analyzed using FlowJo software (Tree Star, La Jolla, CA).

Western blot analysis

Total cellular proteins were extracted from cells using T-PER lysis buffer containing phosphatase and protease inhibitors. The protein concentration was determined using the BCA protein assay reagents (Thermo Scientific Pierce, Waltham, MA). Equal amounts of protein (10 μg) were resolved using sodium dodecyl sulphate polyacrylamide gel electrophoresis (SDS-PAGE) and transferred to PVDF Immobilon-P Membrane (Merck Millipore, Darmstadt, Germany). Membranes were saturated with BSA 3% for at least 1 h at room temperature and then probed overnight at 4°C with primary antibodies. Membranes were then washed and incubated with HRP-labeled secondary antibodies (goat anti-rabbit or anti-mouse IgG; Perkin Elmer, Waltham, MA) for 60 min, RT. All membranes were stained using ECL Select (GE Healthcare, Catania, Italy) and visualized with Alliance 9.7 (UVITEC, Cambridge, UK), according to manufacturer's instruction. To ensure equal protein loading, each membrane was reprobed with β-actin antibody (Sigma-Aldrich S.r.l., Milan, Italy).

Reverse-phase protein arrays (RPPA)

Cell lysates were diluted to 1 mg/ml in Tris–Glycine SDS Sample Buffer (Invitrogen) containing 5% of β-mercaptoethanol and boiled for 5 min immediately prior to array printing. Lysates were loaded into a 384-well plate and serially diluted with lysis buffer into four-point dilution curves ranging from undiluted to 1:8. Protein lysates were printed

in duplicate in each array set onto nitrocellulose-coated slides (FAST slides) with the 2470 Arrayer (Aushon BioSystems). Printed slides were stored desiccated at -20°C until use.

For RPPA analysis, one slide was stained with Fast Green FCF dye (Sigma) according to the manufacturer's instruction, in order to estimate the total protein amount of each printed sample. Before antibody staining, the arrays were blocked for 3 h RT in blocking solution (2% I-Block in T-PBS). Arrays were then stained with the primary antibodies on an automated slide stainer (Dako Autostainer Plus) using the CSA kit (Dako). Each antibody was previously subjected to extensive validation for single-band specificity by Western blot. Slides were air-dried and scanned on a Epson Perfection V300 Photo at 600 dpi. The TIF images of antibody- and Fast Green FCF-stained slides were analyzed using Microvigene Software (VigeneTech Inc, Boston, MA, USA) to extract numeric intensity values from the array images.

Scratch-migration assay

Nearly confluent MDA-MB-231 cells were gently wounded through the horizontal and vertical axis using a pipette tip. Cells were washed twice to remove cell debris and then treated with **EB-3D** at the indicated concentration for 48h. Quantification of cell motility was evaluated by measuring the distance between the invading front of cells in four random selected microscopic fields for each condition and time point. Images were captured at 0, 6, 24, and 48 h using an inverted microscope equipped with a CCD camera.

Cultrex BME Cell Invasion Assay

To assess the invasive capacity of MDA-MB-231 cells after tretment, cells were added to 24-well Transwell inserts of the Cultrex BME (Basal Membrane Extract) Cell Invasion Assay (Trevigen, Gaithersburg, MD) according to the manufacturer's manual. Invasion was measured 24h after plating, at 485-520 nm using the VICTOR spectrophotometer (Perkin Elmer, Milan, Italy).

Magnetic resonance spectroscopy (^{1}H-MRS)

MDA-MB-321 breast cancer cells or CCRF-CEM T-ALL cells were seeded and cultured for 24h in complete growth medium and then treated with **EB-3D** or DMSO for 48h. Adherent cells were collected by trypsinization, washed twice and then counted.

$1x10^7$ cells were used for each cell extraction. Water-soluble as well as lipid extracts were obtained using the dual-phase extraction method (Mori et al., 2015). Briefly, the pelleted cells were resuspended with ice-cold methanol and vigorously vortexed. Samples were incubated on ice for 15 min, and then mixed with chloroform (1:1), vortexed vigorously and kept on ice for 10 min. Finally, water were added and shaken well. Samples were stored at 4°C overnight for phase separation and later centrifuged at 15000×g at 4°C for 30 min. The upper water/methanol phase containing water-soluble cellular metabolites (Cho, PCho and GPCho) was treated with 50 mg of chelex beads (Sigma-Aldrich) to remove any divalent cations. Beads were removed by filtration and methanol was evaporated. The remaining water phase was lyophilized. Cell extracts were resuspended in 0.7 mL of deuterated water containing 7.006×10^{-8} mol of 3-(trimethylsilyl)propionic-2,2,3,3-d_4 acid (TSP; Sigma-Aldrich) as an internal standard for MR spectral analysis. Fully relaxed ^{1}H-MR spectra of water-soluble extracts were acquired on a Bruker Avance 14.09 T spectrometer (Bruker BioSpin) with flip angle = 90° preceded by 2.0 s presaturation for water signal suppression), sweep width = 10000 Hz, repetition time = 14.0 s, block size = 128k, and scans =128. Signal integrals of N-$(CH_3)_3$ of Cho at about 3.202 ppm, PCho at about 3.224 ppm and GPCho at about 3.232 ppm in water soluble extracts were determined, normalized to cell number and cell volume and compared with the standards. To determine intracellular metabolite concentrations, peak integration (I_{PCho}) from ^{1}H spectra for PCho were compared to that of the internal standard TSP according to the equation [PCho] = A_{TSP} * I_{PCho}/I_{TSP} * N * V where [PCho] represents the intracellular concentration of PCho expressed as mmol/L (mM). A_{TSP} is the number of moles of TSP in the sample, N is the cell number, and V is cell volume (MDA-MB-231: 2,050 μm^3). Because the number of protons contributing to the signal of PCho at ~3.226ppm and the TSP peak at 0 ppm is the same, correction for differences in the number of protons was not required. To determine the cell volume, cell size was determined by trypsinizing the cells and measuring the diameter (d) of 100 randomly selected cells using an optical microscope and calculated as $[(4\pi/3)x(d/2)^3]$. The resulting PCho concentrations were averaged for three or four independent experiments.

***In vivo* antitumoral assay**

Seven week-old C57BL/6 female mice were orthotopically injected into the mammary fat pad with $4x10^5$ EO771 mammary carcinoma cells. When tumors were palpable mice were

randomized to a control and treated groups. Treatment was performed every other day by intraperitoneal (i.p.) injection of **EB-3D** (0.5 and 1 mg/kg) or vehicle (DMSO) in 100 µl final volume. Tumors were measured in two dimensions and tumor volume V (mg) was calculated according to the formula $V=(D \times d^2)/2$, where D and d are the major and minor perpendicular tumor diameters in mm, respectively. Differences between control and treated mice were analyzed using Student t test and Bonferroni correction. At the end of the experimental procedure tumors were harvested, weighted, photographed and embedded in OCT and frozen for histological processing.

***In vivo* metastasis models**

For spontaneous metastases, $5x10^5$ EO771 cells were injected into the mammary fat pad of C57BL/6 female mice and tumors were resected when reached the 8 x 13 mm size. After one week of recovery mice were treated i.p. every other day for four weeks with vehicle or **EB-3D** (2.5 mg/kg) in 100 µl final volume.

For experimentally induced metastasis, murine EO771 ($2x10^5$) or human MDA-MB-231 ($8x10^5$) breast cancer cells in 100 µl of PBS were injected intravenously into the tail vein of 7 week-old C57BL/6 or NOD/SCID female mice, respectively. Animals were treated every other day by i.p. injection with **EB-3D** (2.5 mg/kg) or vehicle (DMSO) in 100 µl final volume for 3 weeks (for EO771 cells) or 7 weeks (for MDA-MB-231 cells).

At the end of the experimental procedure mice were sacrified, lungs were harvested, weighted, formalin-fixed and the number of macro-metastases were counted under a dissecting microscope. Lungs were then embedded in paraffin for histological processing.

Histological analyses

Paraffin-embedded samples were sectioned at a thickness of 5µm, dewaxed, hydrated and stained with hematoxylin and eosin (H&E) according to protocol and analysed by light microscopy. Images were compiled for figures using Adobe Illustrator (Adobe Systems Inc., San Jose, CA)

Statistical analyses

Graphs and statistical analyses were performed using GraphPad Prism software (GraphPad, La Jolla, CA). All data in graphs represented the mean of at least three independent experiments ± standard error of the mean (SEM). Statistical significance was

determined using the two-tailed Student t test or ANOVA (one- or two-way) depending on the type of data. For multiple test comparison, Bonferroni or Newman-Keuls corrections were applied. Asterisks indicate a significant difference between the treated and the control group, unless otherwise specified. *P<0.05, **P<0.01, ***P<0.001, ****P<0.0001.

SUPPLEMENTARY MATHERIALS

```
CHKA_HUMAN         1 MKTKFCTGGEAEPSPLGLLLSCGSGSAAPAPGVGQQRDAASDLESKQLGG     50
                     |||||||||||||||||||||||| |:|||.||||||||||.:|||||||||
CHKA_MOUSE         1 MKTKFCTGGEAEPSPLGLLLSCG-GNAAPTPGVGQQRDAAGELESKQLGG     49

CHKA_HUMAN        51 QQPPLALPPPPPLPLPLPLPQPPPPQPP-ADEQPEPRTRRRAYLWCKEFL     99
                     :..|||||||||.||||    ||||.|| ||||||||||||||||||||||
CHKA_MOUSE        50 RTQPLALPPPPPPPPLPL----PPPPSPPLADEQPEPRTRRRAYLWCKEFL     95

CHKA_HUMAN       100 PGAWRGLREDEFHISVIRGGLSNMLFQCSLPDTTATLGDEPRKVLLRLYG    149
                     ||||||||||:||||||||||||||||||||:.|::||||||||||||||
CHKA_MOUSE        96 PGAWRGLREDQFHISVIRGGLSNMLFQCSLPDSIASVGDEPRKVLLRLYG    145

CHKA_HUMAN       150 AILQMRSCNKEGSEQAQKENEFQGAEAMVLESVMFAILAERSLGPKLYGI    199
                     |||:||||||||||||||.|||||||||||||||||||||||||||||:||
CHKA_MOUSE       146 AILKMRSCNKEGSEQAQNENEFQGAEAMVLESVMFAILAERSLGPKLFGI    195

CHKA_HUMAN       200 FPQGRLEQFIPSRRLDTEELSLPDISAEIAEKMATFHGMKMPFNKEPKWL    249
                     ||||||||||||||||||||.||||||||||||||||||||||||||||||
CHKA_MOUSE       196 FPQGRLEQFIPSRRLDTEELRLPDISAEIAEKMATFHGMKMPFNKEPKWL    245

CHKA_HUMAN       250 FGTMEKYLKEVLRIKFTEESRIKKLHKLLSYNLPLELENLRSLLESTPSP    299
                     ||||||||.:|||:||:.|:|:::|||:|||||||||||||||:.|.||
CHKA_MOUSE       246 FGTMEKYLNQVLRLKFSREARVQQLHKILSYNLPLELENLRSLLQYTRSP    295

CHKA_HUMAN       300 VVFCHNDCQEGNILLLEGRENSEKQKLMLIDFEYSSYNYRGFDIGNHFCE    349
                     ||||||||||||||||||:||||::||||||||||||||||||||||||||
CHKA_MOUSE       296 VVFCHNDCQEGNILLLEGQENSERRKLMLIDFEYSSYNYRGFDIGNHFCE    345

CHKA_HUMAN       350 WMYDYSYEKYPFFRANIRKYPTKKQQLHFISSYLPAFQNDFENLSTEEKS    399
                     |||||:||||||||||:|||::||||||||||..||||||:||:||:.
CHKA_MOUSE       346 WMYDYTYEKYPFFRANIQKYPSRKQQLHFISSYLTTFQNDFESLSSEEQF    395

CHKA_HUMAN       400 IIKEEMLLEVNRFALASHFLWGLWSIVQAKISSIEFGYMDYAQARFDAYF    449
                     ..||:||||||||||||||||||||||||||||||||:|||||:|||
CHKA_MOUSE       396 ATKEDMLLEVNRFALASHFLWGLWSIVQAKISSIEFGYMEYAQARFEAYF    445

CHKA_HUMAN       450 HQKRKLGV    457
                     .|||||||
CHKA_MOUSE       446 DQKRKLGV    453


Identity: 402/457 (88.0%)
Similarity: 433/457 (94.7%)
Gaps: 6/457 (1.3%)
```

Supplementary Table 1: ChoKα alignment between human and mouse protein sequences

Protein sequences alignment generated by EMBOSS Needle Global alignment tools (http://www.ebi.ac.uk/Tools/psa/emboss_needle/). Residues in bold (Tyr333, Tyr345, Phe361, Trp420, Trp423, Ile433, Phe435, Tyr440) shown to be important for interaction with **EB-3D** or its stabilization, are perfectly conserved. Also Asp306 catalytic base for ATP hydrolysis is conserved. Vertical bar (|) indicates fully conserved residue. Colon (:) indicates conservation between groups of strongly similar properties. Period (.) indicates conservation between groups of weakly similar properties.

ABBREVIATIONS

^{18}F-FDG: ^{18}F-fluorodeoxyglucose
5-FU: 5-fluorouracil
ATP: adenosine tri-phosphate
AV: annexin V
C_{12}-FDG: 5-dodecanoylaminofluorescein-di-β-D-galactopyranoside
CCT: phosphocholine cytidylyltransferase
CD3+: cluster of differentiation 3-positive cells
Cho: choline
ChoK: choline kinase
ChoT: choline transporter
Cis-Pt: cisplatin
CPT: choline phosphotransferase
DAG: diacylglycerol
DEX: dexamethasone
Doxo: doxorubicin
EGF: epidermal growth factor
ER: endoplasmic reticulum
FBS: fetal bovine serum
GDPD: glycerophosphocholine phosphodiesterase
GI_{50} = compound concentration required to inhibit cell growth by 50%
GPC: glycerophosphocholine
HUVEC: human umbilical vein endothelial cell
IC_{50} = compound concentration required to inhibit enzyme by 50%
L-ASP: L-asparaginase
LPL: lysophospholipase Lyso-PtdCho: lyso-phosphatidylcholine
MRI: magnetic resonance imaging
MRS: magnetic resonance spectroscopy
MTT: 3-[4,5-dimethylthiazol-2-yl]-2,5-diphenyltetrazodium bromide
NMR: nuclear magnetic resonance
PA: phospahtidic acid
PBL: peripheral blood lymphocyte
PCho: phosphocholine
PET/CT: positron electron tomography/computed tomography
PHA: phytohematoagglutinin
PI: Propidium iodide
PLA1/PLA2/PLC/PLD: phospholipases A1/A2/C/D
PtdCho: phosphatidylcholine
QSAR: quantitative structure-activity relationship
shRNA: short hairpin RNA
siRNA: small interfering RNA
T-ALL: T acute lymphoblastic leukemia
TNBC: triple-negative breast cancer

BIBLIOGRAPHY

Achuthan, S., Santhoshkumar, T. R., Prabhakar, J., Nair, A. S., and Pillai, R. M. (2011). Drug-induced Senescence Generates Chemoresistant Stemlike Cells with Low Reactive Oxygen Species. Journal of Biological Chemistry *286*, 37813-37829.

Adjei, A. A., and Rowinsky, E. K. (2003). Novel anticancer agents in clinical development. Cancer biology & therapy *2*, 15.

Al-Saffar, N., Troy, H., de Molina, A., Jackson, L. E., Madhu, B., Griffiths, J. R., Leach, M. O., Workman, P., Lacal, J. C., Judson, I. R., and Chung, Y.-L. (2006). Noninvasive Magnetic Resonance Spectroscopic Pharmacodynamic Markers of the Choline Kinase Inhibitor MN58b in Human Carcinoma Models. Cancer research *66*, 427-434.

Aoyama, C., Ishidate, K., Sugimoto, H., and Vance, D. E. (2007). Induction of choline kinase alpha by carbon tetrachloride (CCl 4) occurs via increased binding of c-jun to an AP-1 element. Biochimica et Biophysica Acta (BBA)-Molecular and Cell Biology of Lipids *1771*, 1148-1155.

Aoyama, C., Liao, H., and Ishidate, K. (2004). Structure and function of choline kinase isoforms in mammalian cells. Progress in lipid research *43*, 266-281.

Aoyama, C., Nakashima, K., and Ishidate, K. (1998a). Molecular cloning of mouse choline kinase and choline/ethanolamine kinase: their sequence comparison to the respective rat homologs. Biochimica et biophysica acta *1393*, 179-185.

Aoyama, C., Nakashima, K., Matsui, M., and Ishidate, K. (1998b). Complementary DNA sequence for a 42 kDa rat kidney choline/ethanolamine kinase. Biochimica et biophysica acta *1390*, 1-7.

Aoyama, C., Ohtani, A., and Ishidate, K. (2002). Expression and characterization of the active molecular forms of choline/ethanolamine kinase-alpha and -beta in mouse tissues, including carbon tetrachloride-induced liver. The Biochemical journal *363*, 777-784.

Asim, M., Massie, C. E., Orafidiya, F., Pértega-Gomes, N., Warren, A. Y., Esmaeili, M., Selth, L. A., Zecchini, H. I., Luko, K., Qureshi, A., *et al.* (2016). Choline Kinase Alpha as an Androgen Receptor Chaperone and Prostate Cancer Therapeutic Target. Journal of the National Cancer Institute *108*.

Báñez-Coronel, M. (2004). A novel 4, 4'-bispyridyl-5, 5'-perfluoroalkyl-2, 2'-bisoxazol with antitumoral activity via cell cycle arrest and induction of apoptosis. International ….

Bañez-Coronel, M., Ramírez de Molina, A., Rodríguez-González, A., Sarmentero, J., Ramos, M. A., García-Cabezas, M. A., García-Oroz, L., and Lacal, J. C. (2008). Choline kinase alpha depletion selectively kills tumoral cells. Current cancer drug targets *8*, 709-719.

Bansal, A., Harris, R. A., and DeGrado, T. R. (2011). Choline phosphorylation and regulation of transcription of choline kinase α in hypoxia. Journal of lipid research *53*, 149-157.

Brognard, J., and Hunter, T. (2011). Protein kinase signaling networks in cancer. Current opinion in genetics & development *21*, 4-11.

Cabezon, B., Cao, J., and Raymo, F. M. (2000). Self-Complementary [2] Catenanes and Their Related [3] Catenanes. … A European Journal.

Campos, J. M. M., Núñez, M. C. C., Sánchez, R. M., Gómez-Vidal, J. A. A., Rodríguez-González, A., Báñez, M., Gallo, M. A., Lacal, J. C., and Espinosa, A. (2002). Quantitative structure-activity relationships for a series of symmetrical bisquaternary anticancer compounds. Bioorganic & medicinal chemistry *10*, 2215-2231.

Canino, C., Mori, F., Cambria, A., Diamantini, A., Germoni, S., Alessandrini, G., Borsellino, G., Galati, R., Battistini, L., Blandino, R., *et al.* (2011). SASP mediates chemoresistance and tumor-initiating-activity of mesothelioma cells. Oncogene *31*, 3148-3163.

Cantrill, S. J., Fulton, D. A., Heiss, A. M., Pease, A. R., Stoddart, J. F., White, A. J., and Williams, D. J. (2000). The influence of macrocyclic polyether constitution upon ammonium ion/crown ether recognition processes. Chemistry (Weinheim an der Bergstrasse, Germany) *6*, 2274-2287.

Castro-Navas, F. F., Schiaffino-Ortega, S., Carrasco-Jimenez, M. P. P., Ríos-Marco, P., Marco, C., Espinosa, A., Gallo, M. A., Mariotto, E., Basso, G., Viola, G., *et al.* (2015). New more polar symmetrical bipyridinic compounds: new strategy for the inhibition of choline kinase α1. Future medicinal chemistry *7*, 417-436.

Challapalli, A., Trousil, S., Hazell, S., Kozlowski, K., Gudi, M., Aboagye, E. O., and Mangar, S. (2015). Exploiting altered patterns of choline kinase-alpha expression on human prostate tissue to prognosticate prostate cancer. Journal of Clinical Pathology *68*.

Chou, T. C. (2006). Theoretical basis, experimental design, and computerized simulation of synergism and antagonism in drug combination studies. Pharmacol Rev *58*, 621-681.

Chua, B., Gallego-Ortega, D., de Molina, A., Ullrich, A., Lacal, J., and Downward, J. (2009). Regulation of Akt(ser473) phosphorylation by choline kinase in breast carcinoma cells. Molecular cancer *8*, 131.

Clem, B. F., Clem, A. L., Yalcin, A., Goswami, U., Arumugam, S., Telang, S., Trent, J. O., and Chesney, J. (2011). A novel small molecule antagonist of choline kinase-α that simultaneously suppresses MAPK and PI3K/AKT signaling. Oncogene *30*, 3370-3380.

Conejo-García, A., Campos, J. M., Entrena, A., Sánchez-Martín, R. M., Gallo, M., and Espinosa, A. (2003a). Conformational Dynamics of a Bispyridinium Cyclophane. The Journal of Organic Chemistry *68*, 8697-8699.

Conejo-García, A., Campos, J. M., Sánchez-Martín, R. M., Gallo, M., and Espinosa, A. (2003b). Bispyridinium Cyclophanes: Novel Templates for Human Choline Kinase Inhibitors. Journal of medicinal chemistry *46*, 3754-3757.

Exton, J. H. (2000). Phospholipase D. Annals of the New York Academy of Sciences *905*, 61-68.

Falcon, S. C., Hudson, C. S., Huang, Y., Mortimore, M., Golec, J. M., Charlton, P. A., Weber, P., and Sundaram, H. (2013). A non-catalytic role of choline kinase alpha is important in promoting cancer cell survival. Oncogenesis *2*.

Gallego-Ortega, D., de Molina, A., Ramos, M., Valdes-Mora, F., Barderas, M., Sarmentero-Estrada, J., and Lacal, J. (2009). Differential Role of Human Choline Kinase α and β Enzymes in Lipid Metabolism: Implications in Cancer Onset and Treatment. PLoS ONE *4*.

Gey, C., and Seeger, K. (2013). Metabolic changes during cellular senescence investigated by proton NMR-spectroscopy. Mechanisms of Ageing and Development *134*, 130-138.

Giovannini, E., Lazzeri, P., Milano, A., Gaeta, M., and Ciarmiello, A. (2015). Clinical applications of choline PET/CT in brain tumors. Current pharmaceutical design *21*, 121-127.

Glunde, K., Bhujwalla, Z. M., and Ronen, S. M. (2011). Choline metabolism in malignant transformation. Nature Reviews Cancer *11*, 835-848.

Glunde, K., Raman, V., Mori, N., and Bhujwalla, Z. M. (2005). RNA interference-mediated choline kinase suppression in breast cancer cells induces differentiation and reduces proliferation. Cancer research *65*, 11034-11043.

Glunde, K., Shah, T., Winnard, P. T., Raman, V., Takagi, T., Vesuna, F., Artemov, D., and Bhujwalla, Z. M. (2008). Hypoxia Regulates Choline Kinase Expression through Hypoxia-Inducible Factor-1α Signaling in a Human Prostate Cancer Model. Cancer research *68*, 172-180.

Gomez-Perez, V., McSorley, T., See Too, W. C., Konrad, M., and Campos, J. M. (2012). Novel 4-amino bis-pyridinium and bis-quinolinium derivatives as choline kinase inhibitors with antiproliferative activity against the human breast cancer SKBR-3 cell line. ChemMedChem *7*, 663-669.

Granata, A., Nicoletti, R., Perego, P., Iorio, E., Krishnamachary, B., Benigni, F., Ricci, A., Podo, F., Bhujwalla, Z. M., Canevari, S., *et al.* (2015). Global metabolic profile identifies choline kinase alpha as a key regulator of glutathione-dependent antioxidant cell defense in ovarian carcinoma. Oncotarget *6*, 11216-11230.

Granata, A., Nicoletti, R., Tinaglia, V., Cecco, D. L., Pisanu, M. E., Ricci, A., Podo, F., Canevari, S., Iorio, E., Bagnoli, M., and Mezzanzanica, D. (2014). Choline kinase-alpha by regulating cell aggressiveness and drug sensitivity is a potential druggable target for ovarian cancer. British Journal of Cancer *110*, 330-340.

Gross, S., Rahal, R., Stransky, N., Lengauer, C., and Hoeflich, K. P. (2015). Targeting cancer with kinase inhibitors. The Journal of clinical investigation *125*, 1780-1789.

Gruber, J., Too, W., Wong, M., Lavie, A., McSorley, T., and Konrad, M. (2012). Balance of human choline kinase isoforms is critical for cell cycle regulation. FEBS Journal *279*, 1915-1928.

Guo, L., Xie, B., and Mao, Z. (2012). Autophagy in Premature Senescent Cells Is Activated via AMPK Pathway. International Journal of Molecular Sciences *13*, 3563-3582.

Han, X., Tai, H., Wang, X., Wang, Z., Zhou, J., Wei, X., Ding, Y., Gong, H., Mo, C., Zhang, J., *et al.* (2016). AMPK activation protects cells from oxidative stress-induced senescence via autophagic flux restoration and intracellular NAD+ elevation. Aging Cell *15*, 416-427.

Hanahan, D., and Weinberg, R. A. (2011). Hallmarks of Cancer: The Next Generation. Cell *144*, 646-674.

Hara, T., Kosaka, N., Suzuki, T., Kudo, K., and Niino, H. (2003). Uptake rates of 18F-fluorodeoxyglucose and 11C-choline in lung cancer and pulmonary tuberculosis: a positron emission tomography study. Chest *124*, 893-901.

Hernández-Alcoceba, R., Fernández, F., and Lacal, J. C. (1999). In vivo antitumor activity of choline kinase inhibitors: a novel target for anticancer drug discovery. European Journal of Cancer *35*.

Hong, B. S., Allali-Hassani, A., Tempel, W., Finerty, P. J., Mackenzie, F., Dimov, S., Vedadi, M., and Park, H.-W. W. (2010). Crystal structures of human choline kinase isoforms in complex with hemicholinium-3: single amino acid near the active site influences inhibitor sensitivity. The Journal of biological chemistry *285*, 16330-16340.

Houweling, M., Klein, W., and Geelen, M. J. H. (2002). Regulation of phosphatidylcholine and phosphatidylethanolamine synthesis in rat hepatocytes by 5-aminoimidazole-4-carboxamide ribonucleoside (AICAR). Biochemical Journal *362*, 97-104.

Huai, L., Wang, C., Zhang, C., Li, Q., Chen, Y., Jia, Y., Li, Y., Xing, H., Tian, Z., Rao, Q., *et al.* (2012). Metformin induces differentiation in acute promyelocytic leukemia by activating the MEK/ERK signaling pathway. Biochemical and Biophysical Research Communications *422*, 398-404.

Hui, L., Zheng, Y., Yan, Y., Bargonetti, J., and Foster, D. A. (2006). Mutant p53 in MDA-MB-231 breast cancer cells is stabilized by elevated phospholipase D activity and contributes to survival signals generated by phospholipase D. Oncogene *25*, 7305-7310.

Ido, Y., Duranton, A., Lan, F., Cacicedo, J. M., Chen, T. C., Breton, L., and Ruderman, N. B. (2012). Acute Activation of AMP-Activated Protein Kinase Prevents H2O2-Induced Premature Senescence in Primary Human Keratinocytes. PLoS ONE *7*.

Iorio, E., Mezzanzanica, D., Alberti, P., Spadaro, F., Ramoni, C., D'Ascenzo, S., Millimaggi, D., Pavan, A., Dolo, V., Canevari, S., and Podo, F. (2005). Alterations of Choline Phospholipid Metabolism in Ovarian Tumor Progression. Cancer research *65*, 9369-9376.

Iorio, E., Ricci, A., Bagnoli, M., Pisanu, M., Castellano, G., Vito, M., Venturini, E., Glunde, K., Bhujwalla, Z. M., Mezzanzanica, D., *et al.* (2010). Activation of Phosphatidylcholine Cycle Enzymes in Human Epithelial Ovarian Cancer Cells. Cancer research *70*, 2126-2135.

Ishidate, K. (1997). Choline/ethanolamine kinase from mammalian tissues. Biochimica et biophysica acta *1348*, 70-78.

Jain, A. N. (2007). Surflex-Dock 2.1: robust performance from ligand energetic modeling, ring flexibility, and knowledge-based search. Journal of computer-aided molecular design *21*, 281-306.

Johnstone, C. N., Smith, Y. E., Cao, Y., Burrows, A. D., Cross, R. S., Ling, X., Redvers, R. P., Doherty, J. P., Eckhardt, B. L., Natoli, A. L., *et al.* (2015). Functional and molecular characterisation of EO771.LMB tumours, a new C57BL/6-mouse-derived model of spontaneously metastatic mammary cancer. Disease models & mechanisms *8*, 237-251.

Kamb, A., Wee, S., and Lengauer, C. (2007). Why is cancer drug discovery so difficult? Nature reviews Drug discovery *6*, 115-120.

Kappe, O. C. (2004). Controlled Microwave Heating in Modern Organic Synthesis. Angewandte Chemie International Edition *43*, 6250-6284.

Kennedy, E. P. (1957). Metabolism of lipids. Ann Rev Biochem *26*, 119–148.

Kent, C. (1990). Regulation of phosphatidylcholine biosynthesis. Progress in lipid research *29*, 87-105.

Kishton, R. J., Barnes, C. E., Nichols, A. G., Cohen, S., Gerriets, V. A., Siska, P. J., Macintyre, A. N., Goraksha-Hicks, P., de Cubas, A. A., Liu, T., *et al.* (2016). AMPK Is

Essential to Balance Glycolysis and Mitochondrial Metabolism to Control T-ALL Cell Stress and Survival. Cell Metabolism *23*, 649-662.

Koch, K., Hartmann, R., Schröter, F., Suwala, A., Maciaczyk, D., Krüger, A., Willbold, D., Kahlert, U., and Maciaczyk, J. (2016). Reciprocal regulation of the cholinic phenotype and epithelial-mesenchymal transition in glioblastoma cells. Oncotarget.

Krishnamachary, B., Glunde, K., Wildes, F., Mori, N., Takagi, T., Raman, V., and Bhujwalla, Z. M. (2009). Noninvasive detection of lentiviral-mediated choline kinase targeting in a human breast cancer xenograft. Cancer research *69*, 3464-3471.

Kruse, U., Pallasch, C. P., Bantscheff, M., Eberhard, D., Frenzel, L., Ghidelli, S., Maier, S. K., Werner, T., Wendtner, C. M., and Drewes, G. (2010). Chemoproteomics-based kinome profiling and target deconvolution of clinical multi-kinase inhibitors in primary chronic lymphocytic leukemia cells. Leukemia *25*, 89-100.

Kunz, J. B., Rausch, T., Bandapalli, O. R., Eilers, J., Pechanska, P., Schuessele, S., Assenov, Y., Stutz, A. M., Kirschner-Schwabe, R., Hof, J., *et al.* (2015). Pediatric T-cell lymphoblastic leukemia evolves into relapse by clonal selection, acquisition of mutations and promoter hypomethylation. Haematologica *100*, 1442-1450.

Lacal, J., and Campos, J. M. (2014). Preclinical characterization of RSM-932A, a novel anticancer drug targeting the human choline kinase alpha, an enzyme involved in increased lipid metabolism of cancer cells. Molecular cancer therapeutics *14*, 31-39.

Lacal, J. C. (2001). Choline kinase: a novel target for antitumor drugs. IDrugs : the investigational drugs journal *4*, 419-426.

Lalic, H., Dembitz, V., Lukinovic-Skudar, V., Banfic, H., and Visnjic, D. (2014). 5-Aminoimidazole-4-carboxamide ribonucleoside induces differentiation of acute myeloid leukemia cells. Leukemia & Lymphoma *55*, 2375-2383.

Liao, E. C., Hsu, Y. T., Chuah, Q. Y., Lee, Y. J., Hu, J. Y., Huang, T. C., Yang, P. M., and Chiu, S. J. (2014). Radiation induces senescence and a bystander effect through metabolic alterations. Cell death & disease *5*.

Lloveras, J., Hamza, M., Chap, H., and Douste-Blazy, L. (1985). Action of hemicholinium-3 on phospholipid metabolism in Krebs II ascites cells. Biochemical pharmacology *34*, 3987-3993.

Locatelli, F., Schrappe, M., Bernardo, M. E., and Rutella, S. (2012). How I treat relapsed childhood acute lymphoblastic leukemia. Blood *120*, 2807-2816.

Malito, E., Sekulic, N., Too, W. C., Konrad, M., and Lavie, A. (2006). Elucidation of human choline kinase crystal structures in complex with the products ADP or phosphocholine. Journal of molecular biology *364*, 136-151.

Menendez, J. A., and Lupu, R. (2007). Fatty acid synthase and the lipogenic phenotype in cancer pathogenesis. Nature reviews Cancer *7*, 763-777.

Miyake, T., and Parsons, S. J. (2012). Functional interactions between Choline kinase α, epidermal growth factor receptor and c-Src in breast cancer cell proliferation. Oncogene *31*, 1431-1441.

Mori, N., Glunde, K., Takagi, T., Raman, V., and Bhujwalla, Z. M. (2007). Choline Kinase Down-regulation Increases the Effect of 5-Fluorouracil in Breast Cancer Cells. Cancer research *67*, 11284-11290.

Mori, N., Wildes, F., Kakkad, S., Jacob, D., Solaiyappan, M., Glunde, K., and Bhujwalla, Z. M. (2015). Choline kinase-α protein and phosphatidylcholine but not phosphocholine are required for breast cancer cell survival. NMR in Biomedicine *28*, 1697-1706.

Morrish, F., Isern, N., Sadilek, M., Jeffrey, M., and Hockenbery, D. M. (2009). c-Myc activates multiple metabolic networks to generate substrates for cell-cycle entry. Oncogene *28*, 2485-2491.

Morrish, F., Neretti, N., Sedivy, J. M., and Hockenbery, D. M. (2008). The oncogene c-Myc coordinates regulation of metabolic networks to enable rapid cell cycle entry. Cell cycle (Georgetown, Tex) *7*, 1054-1066.

Nakagami, K., Uchida, T., Ohwada, S., Koibuchi, Y., Suda, Y., Sekine, T., and Morishita, Y. (1999). Increased choline kinase activity and elevated phosphocholine levels in human colon cancer. Japanese journal of cancer research : Gann *90*, 419-424.

Neidle, S., and Thurston, D. E. (2005). Chemical approaches to the discovery and development of cancer therapies. Nature reviews Cancer *5*, 285-296.

Nguyen, K., Devidas, M., Cheng, S. C., La, M., Raetz, E. A., Carroll, W. L., Winick, N. J., Hunger, S. P., Gaynon, P. S., Loh, M. L., and Children's Oncology, G. (2008). Factors influencing survival after relapse from acute lymphoblastic leukemia: a Children's Oncology Group study. Leukemia *22*, 2142-2150.

Panula, S., and Pera, R. A. R. (2008). Preparation of human foreskin fibroblasts for human embryonic stem cell culture. Cold Spring Harbor Protocols.

Peisach, D., Gee, P., Kent, C., and Xu, Z. (2003). The crystal structure of choline kinase reveals a eukaryotic protein kinase fold. Structure (London, England : 1993) *11*, 703-713.

Pérez-Mancera, P. A., Young, A. R. J., and Narita, M. (2014). Inside and out: the activities of senescence in cancer. Nature Reviews Cancer *14*, 547-558.

Porcù, E., Viola, G., Bortolozzi, R., Persano, L., Mitola, S., Ronca, R., Presta, M., Romagnoli, R., Baraldi, P. G., and Basso, G. (2013). TR-644 a novel potent tubulin binding agent induces impairment of endothelial cells function and inhibits angiogenesis. Angiogenesis *16*, 647-662.

Pui, C. H. (2015). Genomic and pharmacogenetic studies of childhood acute lymphoblastic leukemia. Front Med *9*, 1-9.

Ramírez de Molina, A., Báñez-Coronel, M., Gutiérrez, R., Rodríguez-González, A., Olmeda, D., Megías, D., and Lacal, J. C. (2004a). Choline kinase activation is a critical requirement for the proliferation of primary human mammary epithelial cells and breast tumor progression. Cancer research *64*, 6732-6739.

Ramírez de Molina, A., Gutiérrez, R., Ramos, M., Silva, J., Silva, J., Bonilla, F., Sánchez, J., and Lacal, J. (2002a). Increased choline kinase activity in human breast carcinomas: clinical evidence for a potential novel antitumor strategy. Oncogene *21*.

Ramírez de Molina, A., Penalva, V., Lucas, L., and Lacal, J. (2002b). Regulation of choline kinase activity by Ras proteins involves Ral–GDS and PI3K. Oncogene *21*.

Ramírez De Molina, A., Penalva, V., Lucas, L., and Lacal, J. C. (2002c). Regulation of choline kinase activity by Ras proteins involves Ral-GDS and PI3K. Oncogene *21*, 937-946.

Ramírez de Molina, A., Rodríguez-González, A., and Lacal, J. (2004b). From Ras signalling to ChoK inhibitors: a further advance in anticancer drug design. Cancer Letters *206*.

Ramírez de Molina, A., Rodríguez-González, A., Penalva, V., Lucas, L., and Lacal, J. (2001). Inhibition of ChoK Is an Efficient Antitumor Strategy for Harvey-, Kirsten-, and N-ras-Transformed Cells. Biochemical and Biophysical Research Communications *285*.

Ramírez de Molina, A., Rodríguez-González, A. n., Gutiérrez, R., Martínez-Piñeiro, L., Sánchez, J. J., Bonilla, F., Rosell, R., and Lacal, J. (2002d). Overexpression of choline kinase is a frequent feature in human tumor-derived cell lines and in lung, prostate, and colorectal human cancers. Biochemical and Biophysical Research Communications *296*.

Ramírez de Molina, A., Sarmentero-Estrada, J., Belda-Iniesta, C., Tarón, M., de Molina, V., Cejas, P., Skrzypski, M., Gallego-Ortega, D., de Castro, J., Casado, E., *et al.* (2007). Expression of choline kinase alpha to predict outcome in patients with early-stage non-small-cell lung cancer: a retrospective study. The Lancet Oncology *8*.

Reimand, J., Wagih, O., and Bader, G. D. (2013). The mutational landscape of phosphorylation signaling in cancer. Scientific reports *3*, 2651.

Ricoult, S. J. H., Yecies, J. L., Ben-Sahra, I., and Manning, B. D. (2016). Oncogenic PI3K and K-Ras stimulate de novo lipid synthesis through mTORC1 and SREBP. Oncogene *35*, 1250-1260.

Roberts, K. G., Morin, R. D., Zhang, J., Hirst, M., Zhao, Y., Su, X., Chen, S.-C., Payne-Turner, D., Churchman, M. L., Harvey, R. C., *et al.* (2012). Genetic Alterations Activating Kinase and Cytokine Receptor Signaling in High-Risk Acute Lymphoblastic Leukemia. Cancer Cell *22*, 153-166.

Rodriguez-Gonzalez, A., Ramirez de Molina, A., Banez-Coronel, M., Megias, D., and Lacal, J. C. (2005). Inhibition of choline kinase renders a highly selective cytotoxic effect in tumour cells through a mitochondrial independent mechanism. International journal of oncology *26*, 999-1008.

Rodríguez-González, A., Ramírez de Molina, A., Fernández, F., and Lacal, J. (2004). Choline kinase inhibition induces the increase in ceramides resulting in a highly specific and selective cytotoxic antitumoral strategy as a potential mechanism of action. Oncogene *23*.

Rodriguez-Gonzalez, A., Ramirez de Molina, A., Fernandez, F., and Lacal, J. C. (2004). Choline kinase inhibition induces the increase in ceramides resulting in a highly specific and selective cytotoxic antitumoral strategy as a potential mechanism of action. Oncogene *23*, 8247-8259.

Rodríguez-González, A., Ramírez de Molina, A., Fernández, F., Ramos, M., del Núñez, M., Campos, J., and Lacal, J. (2003). Inhibition of choline kinase as a specific cytotoxic strategy in oncogene-transformed cells. Oncogene *22*.

Rubio-Ruíz, B., Conejo-García, A., Ríos-Marco, P., Carrasco-Jiménez, M. P. P., Segovia, J., Marco, C., Gallo, M. A., Espinosa, A., and Entrena, A. (2012). Design, synthesis, theoretical calculations and biological evaluation of new non-symmetrical choline kinase inhibitors. European journal of medicinal chemistry *50*, 154-162.

Rubio-Ruiz, B., Figuerola-Conchas, A., Ramos-Torrecillas, J., Capitán-Cañadas, F., Ríos-Marco, P., Carrasco, M. P., Gallo, M. Á., Espinosa, A., Marco, C., Ruiz, C., *et al.* (2014). Discovery of a new binding site on human choline kinase α1: design, synthesis,

crystallographic studies, and biological evaluation of asymmetrical bispyridinium derivatives. Journal of medicinal chemistry *57*, 507-515.

Rufini, A., Tucci, P., Celardo, I., and Melino, G. (2013). Senescence and aging: the critical roles of p53. Oncogene *32*, 5129-5143.

Sahún-Roncero, M., Rubio-Ruíz, B., Conejo-García, A., Velázquez-Campoy, A., Entrena, A., and Hurtado-Guerrero, R. (2013). Determination of potential scaffolds for human choline kinase α1 by chemical deconvolution studies. Chembiochem : a European journal of chemical biology *14*, 1291-1295.

Sahún-Roncero, M., Rubio-Ruiz, B., Saladino, G., Conejo-García, A., Espinosa, A., Velázquez-Campoy, A., Gervasio, F., Entrena, A., and Hurtado-Guerrero, R. (2013). The Mechanism of Allosteric Coupling in Choline Kinase α1 Revealed by the Action of a Rationally Designed Inhibitor. Angewandte Chemie International Edition *52*, 4582-4586.

Sanchez-Lopez, E., Zimmerman, T., del Pulgar, G. T., Moyer, M. P., Sanjuan, L. J. C., and Cebrian, A. (2013). Choline kinase inhibition induces exacerbated endoplasmic reticulum stress and triggers apoptosis via CHOP in cancer cells. Cell Death & Disease *4*.

Sánchez-Martín, R., Campos, J. M., Conejo-García, A., Cruz-López, O., Báñez-Coronel, M., Rodríguez-González, A., Gallo, M. A., Lacal, J. C., and Espinosa, A. (2005). Symmetrical Bis-Quinolinium Compounds: New Human Choline Kinase Inhibitors with Antiproliferative Activity against the HT-29 Cell Line. Journal of medicinal chemistry *48*, 3354-3363.

Santos, C. R., and Schulze, A. (2012). Lipid metabolism in cancer. FEBS Journal *279*, 2610-2623.

Schiaffino-Ortega, S., Baglioni, E., Mariotto, E., Bortolozzi, R., Serrán-Aguilera, L., Ríos-Marco, P., Carrasco-Jimenez, P. M., Gallo, M. A., Hurtado-Guerrero, R., Marco, C., *et al.* (2016). Design, synthesis, crystallization and biological evaluation of new symmetrical biscationic compounds as selective inhibitors of human Choline Kinase α1 (ChoKα1). Scientific Reports *6*, 23793.

Schiaffino-Ortega, S., López-Cara, L., Ríos-Marco, P., Carrasco-Jimenez, M., Gallo, M. A., Espinosa, A., Marco, C., and Entrena, A. (2013). New non-symmetrical choline kinase inhibitors. Bioorganic & Medicinal Chemistry *21*, 7146-7154.

Schrappe, M., Valsecchi, M. G., Bartram, C. R., Schrauder, A., Panzer-Grumayer, R., Moricke, A., Parasole, R., Zimmermann, M., Dworzak, M., Buldini, B., *et al.* (2011). Late MRD response determines relapse risk overall and in subsets of childhood T-cell ALL: results of the AIEOP-BFM-ALL 2000 study. Blood *118*, 2077-2084.

Serrán-Aguilera, L., Nuti, R., López-Cara, L. C., Mezo, M., Macchiarulo, A., Entrena, A., and Hurtado-Guerrero, R. (2015). Pharmacophore-Based Virtual Screening to Discover New Active Compounds for Human Choline Kinase α1. Molecular Informatics *34*.

Serrán-Aguilera, L., Nuti, R., López-Cara, L. C., Mezo, M., Macchiarulo, A., Entrena, A., and Hurtado-Guerrero, R. (2015). Pharmacophore-Based Virtual Screening to Discover New Active Compounds for Human Choline Kinase α1. Molecular Informatics *34*, 458-466.

Shaw, R. J. (2009). LKB1 and AMP-activated protein kinase control of mTOR signalling and growth. Acta physiologica (Oxford, England) *196*, 65-80.

Shi, W. Y., Xiao, D., Wang, L., Dong, L. H., Yan, Z. X., Shen, Z. X., Chen, S. J., Chen, Y., and Zhao, W. L. (2012). Therapeutic metformin/AMPK activation blocked lymphoma cell growth via inhibition of mTOR pathway and induction of autophagy. Cell death & disease *3*.

Sujobert, P., and Tamburini, J. (2015). Co-activation of AMPK and mTORC1 as a new therapeutic option for acute myeloid leukemia. Molecular & Cellular Oncology *3*.

Tan, H., Chen, L., Guan, Y., and Lin, X. (2011). Comparison of MRI, F-18 FDG, and 11C-Choline PET/CT for Their Potentials in Differentiating Brain Tumor Recurrence From Brain Tumor Necrosis Following Radiotherapy. Clinical Nuclear Medicine *36*, 978.

Tian, M., Zhang, H., Oriuchi, N., Higuchi, T., and Endo, K. (2004). Comparison of 11C-choline PET and FDG PET for the differential diagnosis of malignant tumors. European journal of nuclear medicine and molecular imaging *31*, 1064-1072.

Trousil, S., Carroll, L., Kalusa, A., Aberg, O., Kaliszczak, M., and Aboagye, E. O. (2013). Design of symmetrical and nonsymmetrical N , N -dimethylaminopyridine derivatives as highly potent choline kinase alpha inhibitors. MedChemComm *4*, 693-696.

Trousil, S., Kaliszczak, M., Schug, Z., Nguyen, Q.-D., Tomasi, G., Favicchio, R., Brickute, D., Fortt, R., Twyman, F. J., Carroll, L., *et al.* (2016). The novel choline kinase inhibitor ICL-CCIC-0019 reprograms cellular metabolism and inhibits cancer cell growth. Oncotarget *7*, 37103-37120.

Uchida, T. (1996). Stimulation of phospholipid synthesis in HeLa cells by epidermal growth factor and insulin: activation of choline kinase and glycerophosphate acyltransferase. Biochimica et Biophysica Acta (BBA)-Lipids and Lipid ….

Uchida, T., and Yamashita, S. (1990). Purification and properties of choline kinase from rat brain. Biochimica et biophysica acta *1043*, 281-288.

Wang, T., Jinjun, L. I., Chen, F., Zhao, Y., Xianghuo, H. E., Wan, D., and Jianren, G. U. (2007). Choline Transporters in Human Lung Adenocarcinoma: Expression and Functional Implications. Acta Biochimica et Biophysica Sinica *39*, 668-674.

Wang, W., Yang, X., de Silanes, I., Carling, D., and Gorospe, M. (2003). Increased AMP:ATP Ratio and AMP-activated Protein Kinase Activity during Cellular Senescence Linked to Reduced HuR Function. Journal of Biological Chemistry *278*, 27016-27023.

Warden, C. H., and Friedkin, M. (1985). Regulation of choline kinase activity and phosphatidylcholine biosynthesis by mitogenic growth factors in 3T3 fibroblasts. The Journal of biological chemistry *260*, 6006-6011.

Wu, G., Aoyama, C., Young, S. G., and Vance, D. E. (2008). Early embryonic lethality caused by disruption of the gene for choline kinase alpha, the first enzyme in phosphatidylcholine biosynthesis. The Journal of biological chemistry *283*, 1456-1462.

Xiao, X., Sun, J., Li, X., Li, H., and Wang, Y. (2007). Binuclear titanocenes linked by the bridge combination of rigid and flexible segment: Synthesis and their use as catalysts for ethylene polymerization. Journal of Molecular Catalysis A: Chemical *267*, 86-91.

Xiong, J., Bian, J., Wang, L., Zhou, J. Y., Wang, Y., Zhao, Y., Wu, L. L., Hu, J. J., Li, B., Chen, S. J., *et al.* (2015). Dysregulated choline metabolism in T-cell lymphoma: role of choline kinase-α and therapeutic targeting. Blood Cancer Journal *5*, 287.

Yalcin, A., Clem, B., Makoni, S., Clem, A., Nelson, K., Thornburg, J., Siow, D., Lane, A. N., Brock, S. E., Goswami, U., *et al.* (2010). Selective inhibition of choline kinase simultaneously attenuates MAPK and PI3K/AKT signaling. Oncogene *29*, 139-149.